uOttawa

L'Université canadienne
Canada's university

FACULTÉ DES ÉTUDES SUPÉRIEURES ET POSTOCTORALES

uOttawa

L'Université canadienne
Canada's university

FACULTY OF GRADUATE AND POSDOCTORAL STUDIES

Mélanie Carrière
AUTEUR DE LA THÈSE / AUTHOR OF THESIS

M.Sc. (Earth Sciences)
GRADE / DEGREE

Department of Earth Sciences
FACULTÉ, ÉCOLE, DÉPARTEMENT / FACULTY, SCHOOL, DEPARTMENT

Origins of Martian Valley Networks Based on a Comparative Statistical Analysis of Martian and Terrestrial Basin Shape Functions

TITRE DE LA THÈSE / TITLE OF THESIS

Dr. M. Sawada
DIRECTEUR (DIRECTRICE) DE LA THÈSE / THESIS SUPERVISOR

Dr. D. Fisher
CO-DIRECTEUR (CO-DIRECTRICE) DE LA THÈSE / THESIS CO-SUPERVISOR

EXAMINATEURS (EXAMINATRICES) DE LA THÈSE / THESIS EXAMINERS

Dr. D. King

Dr. B. Lauriol

Gary W. Slater
Le Doyen de la Faculté des études supérieures et postdoctorales / Dean of the Faculty of Graduate and Postdoctoral Studies

Origins of Martian Valley Networks Based on a Comparative Statistical Analysis of Martian and Terrestrial Basin Shape Functions

Mélanie Carrière

Thesis submitted to the
Faculty of Graduate and Postdoctoral Studies
University of Ottawa
in partial fulfillment of the requirements for the
M.Sc. degree in the Earth Sciences

Ottawa-Carleton Geoscience Centre

and

University of Ottawa

Ottawa, Canada

November 2008

© Mélanie Carrière, Ottawa, Canada, 2008

Library and
Archives Canada

Published Heritage
Branch

395 Wellington Street
Ottawa ON K1A 0N4
Canada

Bibliothèque et
Archives Canada

Direction du
Patrimoine de l'édition

395, rue Wellington
Ottawa ON K1A 0N4
Canada

Your file Votre référence
ISBN: 978-0-494-48594-1
Our file Notre référence
ISBN: 978-0-494-48594-1

NOTICE:
The author has granted a non-exclusive license allowing Library and Archives Canada to reproduce, publish, archive, preserve, conserve, communicate to the public by telecommunication or on the Internet, loan, distribute and sell theses worldwide, for commercial or non-commercial purposes, in microform, paper, electronic and/or any other formats.

The author retains copyright ownership and moral rights in this thesis. Neither the thesis nor substantial extracts from it may be printed or otherwise reproduced without the author's permission.

AVIS:
L'auteur a accordé une licence non exclusive permettant à la Bibliothèque et Archives Canada de reproduire, publier, archiver, sauvegarder, conserver, transmettre au public par télécommunication ou par l'Internet, prêter, distribuer et vendre des thèses partout dans le monde, à des fins commerciales ou autres, sur support microforme, papier, électronique et/ou autres formats.

L'auteur conserve la propriété du droit d'auteur et des droits moraux qui protège cette thèse. Ni la thèse ni des extraits substantiels de celle-ci ne doivent être imprimés ou autrement reproduits sans son autorisation.

In compliance with the Canadian Privacy Act some supporting forms may have been removed from this thesis.

While these forms may be included in the document page count, their removal does not represent any loss of content from the thesis.

Conformément à la loi canadienne sur la protection de la vie privée, quelques formulaires secondaires ont été enlevés de cette thèse.

Bien que ces formulaires aient inclus dans la pagination, il n'y aura aucun contenu manquant.

Canada

Abstract

Despite more than 35 years of study since the discovery of the Martian valley networks, questions still exist as to the fluvial process responsible for their origin. As part of the investigation on the relative importance of surface runoff versus groundwater sapping in the formation of the Martian valley networks, morphometric methods provide an objective and quantitative approach. In this study, four shape indices (circularity, elongation, lemniscate index and lemniscate ratio), traditionally used to quantify the planimetric shape of terrestrial drainage basins, are adapted into shape functions to determine the evolution of basin shape with elevation. The shape functions of 39 terrestrial basins of known origins (surface runoff, groundwater sapping, or meltwater) are analyzed to determine their ability to distinguish between different formation processes. Through hierarchical clustering analysis, it is determined that regional slope exerts a stronger control on a basin's internal shape than formation process. Once basins are divided into separate groups based on their regional slope (steep vs. flat), hierarchical clustering analysis is successful at clustering basins with respect to their formation process based on their shape functions. The shape functions are then used to characterize 23 Martian valley networks. Using self-organizing maps and k-nearest neighbour, the shape functions of the Martian basins are classified as most similar to the groundwater sapping basins of Chile's Atacama Desert. However, reasons for this similarity are not limited to groundwater sapping and could also be attributed to, among other possibilities, a combination of intermittent and scarce precipitation, the effects of impact cratering, or differences in the erosional mechanics that formed the Martian valley networks.

Acknowledgements

Je tiens à remercier tous ceux et celles qui m'ont aidée et supportée au long de ces dernières années. Premièrement, je désire remercier mes superviseurs, Dr. Michael Sawada et Dr. David Fisher, pour avoir accepté de s'impliquer et d'avoir pris intérêt dans un projet hors de leur domaine de recherche. L'initiative qu'ils ont démontrée et les conseils pratiques qu'ils m'ont donnés furent énormément appréciés. J'aimerais aussi remercier mes examinateurs, Dr. King et Dr. Lauriol, pour leur contribution indispensable.

Je suis reconnaissante de mes amis, en particulier Denis, pour sa patience, ses nombreux conseils et son optimisme, ainsi qu'Alexandre, pour son support moral et son amitié incessante. De plus, je n'oublie pas mes paires dans le laboratoire LAGGISS qui ont su partager les hauts et les bas de mon cheminement.

Finalement, je tiens à remercier ma famille. En particulier je suis extrêmement reconnaissante de mes parents qui m'ont toujours encouragée à persévérer.

Table of Contents

List of Tables

List of Figures

1. Introduction

Martian valley networks were first observed by the Mariner 9 mission in the early 1970s (McCauley et al., 1972). Their drainage patterns range from quasi-dendritic with integrated branching tributary systems to long, sinuous valleys with few, short tributaries. Their similarity to terrestrial drainage networks provides compelling evidence for the past presence of water on Mars. Although their fluvial origin is widely accepted (Mars Channel Working Group, 1983), there is debate as to the relative importance of surface runoff versus groundwater sapping in their formation. Determining the formation process of valley networks is important as it could have vastly different implications on the reconstruction of ancient climate on Mars. An origin by surface runoff from rainfall requires the Martian paleoclimate to have been warm and wet, whereas a groundwater sapping origin could have taken place under much colder and drier conditions. Arguments in favour of surface runoff from precipitation include their quasi-dendritic drainage patterns, the correlation between the topography and the degree of dissection, and the pluvial style of degradation of craters formed concurrently with the valley networks (Craddock and Howard, 2002). Arguments in favour of groundwater sapping include the non-typical morphology of some valleys, the low drainage densities of the networks and climate models which predict that early Mars was cold and dry (Craddock and Howard, 2002).

Previous studies of Martian valley networks focused mainly on qualitative, valley-scale morphology. However, in morphological studies, the interpretation of the observations is usually constrained by the climatic assumptions made and is affected by any postformational modification that may have altered the original valleys. Since global digital elevation data have become available from the Mars Orbiter Laser Altimeter (MOLA) instrument aboard Mars Global Surveyor in 2003, focus has shifted towards more quantitative approaches. Basin-scale morphometric studies allow for a quantitative analysis of the whole basin and do not depend upon the choice of climatic assumptions. Whereas individual valley-scale features may be obscured by cratering, aeolian, and mass-wasting processes, the overall character of the basin is more likely to have survived.

A number of morphometric methods used in the study of terrestrial basins have been attempted on the Martian valley networks, including measures of drainage densities, hypsometric analysis as well as studies on longitudinal profile and cross-sections. However, the complicated

relationship between the factors that control the character of drainage basins has thus far prevented the determination of the formation process of the Martian valley networks.

In this study, 23 Martian basins are compared to 39 terrestrial basins formed by different processes. Following the methods of Stepinski and Coradetti (2004), Stepinski and Stepinski (2005) and Luo and Howard (2005), elevation data were used to determine the internal change in shape of a basin with elevation. Since a basin's planimetric shape is related to the erosional processes that formed it, measurement of drainage basin shape should therefore be useful as a criterion for distinguishing between regions of different erosional origins (McArthur and Ehrlich, 1977). As such, the primary purpose of this thesis is to characterize Martian valley networks with respect to terrestrial basins using quantitative morphometric descriptors of basin shape.

This thesis is divided as follows: A literature review (Chapter 2) presenting relevant information related to Martian geology and climate, valley networks, surface runoff and groundwater sapping, the factors controlling the characteristics of drainage basins, and morphometric methods that can be used to quantify a drainage basin. The objectives of the thesis are also presented in Chapter 2. Chapter 3 presents the terrestrial analogue sites chosen for the investigation. The data and statistical analysis performed to undertake this study are presented in Chapter 4. The results are presented in Chapter 5, followed by their interpretation and discussion in Chapter 6. Finally, the main conclusions reached from this thesis are given in Chapter 7.

2. Literature Review

2.1 Martian Geology and Climate

The geological history of Mars is divided into three major epochs: the Noachian (~ 4.6 - 3.5 Ga), the Hesperian (~ 3.5 - 1.8 Ga) and the Amazonian (~ 1.8 Ga - present). Noachian terrains are characterized by rugged, heavily cratered material formed during the period of heavy bombardment, a period of high impact cratering rates due to collisions with material left over from the formation of the solar system (Tanaka, 1986). Hesperian terrains are characterized by less cratered, ridged plains material (Tanaka, 1986). Amazonian terrains are characterized by relatively smooth, moderately cratered plains material and polar deposits (Tanaka, 1986). In addition, Mars consists of two major geological provinces: the southern highlands and the northern lowlands. On average, the northern lowlands are 3 km lower in elevation than the southern highlands and are composed of younger (Hesperian to Amazonian in age), smoother plains units covering a Noachian basement (Frey et al. 2002) whereas the southern highlands are mostly composed of ancient, heavily cratered Noachian terrains.

Mars is currently a cold (temperatures average 220K) planet with an atmospheric pressure that averages 6 mbars. As such, under current surface temperature and atmospheric pressure conditions, liquid water is not stable on the Martian surface, except in transient form in valleys near its equator. However, evidence of past fluvial activity, such as channels, putative deltas, terraces and shorelines (Cabrol and Grin, 1999), suggests that the climatic conditions on Mars may have been drastically different in the past. For example, Melosh and Vickery (1989) computed that the primitive Martian atmosphere must have been at least ~ 1 bar, formed in part by volatiles released from impacts during its accretion phase (Boslough et al., 1980) and degassing from large-scale melting following accretion and planetary differentiation (Craddock and Howard, 2002), a condition required for a warm paleoclimate conducive to the formation of precipitation.

2.2 Valley Networks

As determined from morphology and crater counting studies (Baker and Partridge, 1986), Martian valley networks are mostly of Noachian age with formation primarily ceasing near the

end of the period of heavy bombardment. However, a few valley networks continued to form in the Hesperian period in the Tempe, Electris, Casius and Mangala regions (Grant and Schultz, 1989; Chapman and Tanaka, 1990; Scott and Chapman, 1991), along the flanks of some Martian volcanoes (Gulick and Baker, 1990) and even into the Amazonian on Alba Patera (Gulick and Baker, 1990). The valley networks are located almost exclusively (> 99%, (Carr and Clow, 1981)) in the cratered highlands of the southern hemisphere and range in length from <5 km to nearly 1000 km (Mars Channel Working Group, 1983). The valleys themselves have mean widths of a few kilometers and mean depths of ~ 100 m (Williams and Phillips, 2001). Valley preservation ranges from pristine to degraded, with degraded valleys situated mainly in the upper reaches and pristine valley situated in the lower reaches of the networks (Baker and Partridge, 1986). The maximum drainage density (stream length per unit area) is of the order of ~ 0.1 km/km^2 (Hynek and Phillips, 2003), which is at least one order of magnitude smaller than the minimum terrestrial value of ~ 1 km/km^2 (Gregory, 1976). The similarity of their quasi-dendritic planimetric form to that of terrestrial drainage networks appears to indicate a common origin (i.e. precipitation resulting in surface runoff). However, many valleys also have morphological characteristics that are more consistent with a groundwater sapping origin.

2.3 Surface Runoff

Surface runoff, the principal process of drainage formation on Earth, occurs when precipitation exceeds the surface infiltration rate or when the soil is fully saturated. Surface runoff can be generated either by rainfall or by the melting of snow or glaciers; however the erosional mechanics of these two runoff sources are different (Weigert et al. 2003). Terrestrial valleys formed by surface runoff have distinctive morphological characteristics such as V-shaped cross sections, tapered tributary heads that blend into the surrounding terrain, drainage densities greater than 1 km/km^2 and low junction angles (Gulick, 2001). The climatic implications associated with Martian valleys formed by surface runoff from precipitation include a thick atmosphere (~ 1 bar) and a recurringly mild climate (either annual, seasonal or intermittent). Surface runoff from precipitation seemingly explains the spatial distribution of Martian valley networks, as determined by Craddock and Howard (2002) who found that the extent and degree of terrain dissection from valley networks correlated strongly with topography, as would be

expected from fluvial erosion resulting from precipitation. In addition, the Martian southern highlands contain a large population of craters whose extensive modification occurred concurrently with valley network formation. Simulation models by Craddock and Howard (2002) indicate that these craters were most likely modified by surface runoff from precipitation.

However there are several arguments against the formation of Martian valley networks by surface runoff from precipitation under a warm and wet paleoclimate scenario. Firstly, because of Mars' greater distance from the Sun, it only receives 43% as much solar radiation as Earth. In addition, models of the Sun's composition through time suggest that its original luminosity was only 70% of its current value (Gough, 1981). As a result of the faint young Sun hypothesis, climate models of Mars have difficulty generating above freezing surface temperatures (Haberle et al. 1994). Secondly, valley networks tend to form as isolated systems or in clusters as opposed to being uniformly distributed over the terrain like most terrestrial pluvial systems (Gulick, 1993). Gulick (2001) interpreted such a distribution to be suggestive of localized water sources such as that generated from groundwater sapping rather than surface runoff from precipitation. Finally, the apparent low drainage density of Martian valley networks seems to contradict an origin by surface runoff. However, as discussed in section 2.5, interpretation of drainage density values is not straightforward.

2.4 Groundwater Sapping

As defined by Laity and Malin (1985), "groundwater sapping is the process leading to the undermining and collapse of valley head and sidewalls by weakening or removal of basal support as a result of enhanced weathering and erosion by concentrated fluid flow at a site of seepage". Several mechanisms for driving the groundwater flow on Mars have been proposed, including hydrothermal circulation induced by magmatic intrusions (Gulick and Baker, 1990), impact melt (Brakenridge et al., 1985) or a higher primordial heat flux (Squyres and Kasting, 1994). In addition to their low drainage densities, Martian valley networks have many morphological characteristics that are consistent with terrestrial groundwater sapping systems, including: U-shaped cross-sections, amphitheater heads, constant downvalley widths, high and steep sidewalls, numerous hanging valleys, structural control, numerous short first order tributaries, and high junction angles (Carr, 1996; Carr and Malin, 2000; Laity and Malin, 1985; Gulick,

2001). In the past, groundwater sapping has been the favored origin for the Martian valley networks because it is possible for the process to operate under cold and dry climatic conditions not drastically different from those observed on Mars today. However there are several arguments against the formation of Martian valley networks by groundwater sapping driven by hydrothermal circulation in a cold, dry paleoclimate scenario. Firstly, results from climate models remain controversial since they are based in part on "largely untestable assumptions and unconstrained variables" (Craddock and Howard, 2002). For example, the nature of the faint young Sun is still an open question. In fact, computational models concerning the lithium depletion in the solar atmosphere suggest that the young Sun was actually brighter and more massive than present (e.g. Boothroyd et al., 1991; Graedel et al., 1991), contrary to the expectation that the young Sun's luminosity was only 70% of its current value. Modifying the Sun's luminosity in the climate models to reflect these conditions would enable the Martian paleoclimate to achieve above freezing temperatures (Haberle et al., 1994). Secondly, groundwater sapping driven by hydrothermal circulation fails to provide a satisfactory mechanism for sustaining the large amount of recharge required for maintaining valley network systems (see Craddock and Howard, 2001 for discussion) or to explain how the water became initially emplaced in the Martian lithosphere. In addition, common features associated with terrestrial hydrothermal systems have yet to be identified on Mars (e.g. seeps, fumaroles, hot springs, geysers, phreatic explosion craters). Finally, it is often mistakenly assumed that all Martian valleys have U-shaped cross sections and amphitheater heads. In fact, 60% of the valley cross-sections studied by Williams and Phillips (2001) were V-shaped and 41% of the networks contained both U-shaped and V-shaped valleys.

2.5 Factors Controlling Drainage Basin Characteristics

As discussed by Craddock and Howard (2002) and Baker and Partridge (1986), in addition to formation process, several factors influence to varying degrees the characteristic signature of a drainage basin, including vegetation, topography, climate, lithology, maturity and preservation.

- *Vegetation:* For terrestrial basins, the presence of vegetation greatly increases the amount of infiltration of a soil and impedes the surface runoff. However, for Mars, vegetation is not a factor.

- *Topography:* The effect of slope on the character of a drainage basin stems from the fact that there is a critical slope required to initiate channel incision (Horton, 1945). In general, due to the increase in kinetic energy, steeper slopes have lower infiltration rates and in turn produce greater amounts of surface runoff. Thus, steep slopes have a greater potential for erosion. Other topographic factors which have an effect on the character of a drainage basin include relief and contributing area.
- *Climate:* Mean annual precipitation, precipitation intensity and the precipitation effectiveness index are some of the most important factors affecting drainage density. However the relationship is not straightforward. For example, terrestrial drainage density has a bimodal relation with annual rainfall, the highest density being observed in semiarid and superhumid regions (Abrahams, 1984), whereas the drainage density in arid and humid regions is lower due to the lack of runoff and the impeding effect of vegetation, respectively (Abrahams, 1984).
- *Lithology:* Rock type, permeability and stratigraphy all influence the character of a drainage basin. For example, substrates with high permeability and infiltration (e.g. sandstone) will result in networks with low drainage densities. However, while data from the Thermal Emission Spectrometer (THEMIS) and the Mars Orbiter Camera (MOC) aboard the Mars Global Surveyor mission indicate that the Martian southern highlands are layered and composed of fractured basalt or indurated volcanic ash/cinders (Malin and Edgett, 1999; Bandfield et al., 2000), the permeability and stratigraphy of the Martian highlands remain mostly unknown.
- *Maturity:* The character of a drainage basin changes as the system evolves through time. Abrahams (1984) found that terrestrial drainage basins typically tend to reach maturity in less than 10^5 years, with basins forming over resistant substrates taking up to 10^7 years. In comparison to terrestrial systems, the Martian valley networks have often been described as immature due to their low drainage densities (e.g. Stepinski and Collier, 2004; Irwin et al., 2005), despite crater counting data from Baker and Partridge (1986) which suggests they formed over a span of 10^8 years. As such, Martian valley networks may have formed over short or intermittent time periods during that span or, alternatively, the formation of the Martian valley networks occurred at a much slower rate than terrestrial systems.

- *Preservation:* While most terrestrial systems are currently active, the Martian valley networks are billions of years old. The preservation of the Martian systems can be attributed to the absence of tectonic processes and fluvial activity on Mars. However, some of the Martian valley networks have since been subjected to mass wasting, aeolian infilling and impact cratering, which renders the comparison between the basins of both planets more difficult.

2.6 Basin Morphometry

2.6.1 Hortonian drainage basin composition

The foundations for quantitative methods to describe drainage networks were conceived by Horton (1932; 1945), who developed a set of rules for assigning stream orders. Horton also demonstrated that the composition of drainage networks formed by surface runoff, expressed in terms of stream order, bifurcation ratio and stream length ratio, follows a number of laws. These include the law of streams numbers and the law of stream lengths. Horton (1945) noted that the bifurcation ratio, the ratio of the number of streams of a given order to the number of streams of the next higher order, is approximately constant for all orders of streams in a given basin. This is the basis for the law of stream numbers, which relates the number of streams of a given order to the stream order. On a semi-logarithmic scale, the relation between these is linear, with the slope associated to the bifurcation ratio. Similarly, the stream length ratio, the ratio of the average length of streams of a given order to the average length of streams of the next lower order, is approximately constant for all orders of streams in a given basin (Horton, 1945). The law of stream lengths thus relates the average length of streams of a given order to the stream order. On a semi-logarithmic scale, the relation between these is linear, with the slope associated to the stream length ratio.

Since Horton (1945) proposed that the composition of a drainage network is related to its geomorphic factors, this method has been frequently used to analyze terrestrial basins, with deviations from these laws (i.e. non-linear relationships) or non-typical bifurcation or stream length ratios used to infer the geomorphic properties of a basin. This method was adapted to the study of pristine Martian valley networks by Cabrol (2001), who noted that the networks have high bifurcation ratios and a lack of 2^{nd} order streams compared to terrestrial systems and that the

relation between the number of streams of a given order and the stream order showed limited variation from one valley network to another. Due to the limited variation in composition, Cabrol (2001) hypothesized that the Martian valley network systems in their study were probably all formed under similar conditions, attributing the high number of 1^{st} order streams with respect to 2^{nd} order streams to formation by groundwater sapping rather than by surface runoff.

Although these laws have been tested by a number of studies and found satisfactory (Milton, 1966), the semi-logarithmic form of the equations, the typical form of probability functions, led some researchers to investigate the appropriateness of using these laws to infer geomorphic factors. Leopold and Langbein (1962) and Milton (1966), found that both the law of stream numbers and the law of stream lengths hold when applied to random walk networks. They concluded that these are simply a statistical probability function that apply equally well to any branching system. As an example, Milton (1966) demonstrated that the law of stream numbers could be fitted to the branches of a plum tree with a standard error of estimate similar to the one obtained by fitting the equation to the Miller Basin, Victoria, Australia. As such, the adhesion of drainage networks to these laws can not be used to infer their geomorphic properties, leaving open the question of their effect on the values of the bifurcation ratio and stream length ratio. In random walk networks, there is no restraint on the direction of stream flow, but in the case of real drainage networks, streams must follow the gradient of the topography. This results in a more frequent union of stream channels and smaller values for both ratios. For example, Horton (1945) found that typical bifurcation ratios for terrestrial basins formed by surface runoff had values of ~ 2 to 4, whereas Milton (1966) found that the bifurcation ratio of five random walk networks ranged from 3.9 to 5.9. As such, the effect of a basin's geomorphic properties is expected to be reflected in the magnitude of a basin's bifurcation and stream length ratios.

For the purposes of this study, in order to use drainage network composition to investigate the origins of the Martian valley networks, it must first be determined if this method can successfully distinguish between terrestrial basins formed by different processes. For these purposes, a two tailed t-Test of the bifurcation ratios and stream length ratios of 5 runoff basins and 6 groundwater sapping basins was performed. The two-tailed t-statistic results (see Appendix A) indicate that, at the 95% confidence level, there is insufficient evidence to reject the null hypothesis. That is to say that the bifurcation and stream length ratios of the groundwater sapping basins are not statistically different from those of the surface runoff basins.

As such, it was determined that Horton's drainage network composition is not a viable method for evaluating the relative importance of surface runoff and groundwater sapping in the formation of the Martian valley networks.

2.6.2 Drainage density

A second common morphometric method used to study Martian valley networks is drainage density, which is defined as the total length of a basin's streams divided by the area of the basin. Because very low terrestrial drainage densities usually only occur in extremely arid regions due to a lack of surface runoff, the low drainage density values of Martian valley networks is the most frequently used argument to support formation by groundwater sapping under a cold and dry Martian climate (Craddock and Howard, 2002). However, difficulties in calculating Martian drainage densities arise because of low image resolution and the degraded nature of many of the valley networks. There is also the possibility that the lower order streams may be obscured by aeolian sediments or impact ejecta filling the valleys. In addition, considering the complicated relation between drainage density and climate discussed section 2.5 and the fact that there is no critical drainage density value that can be used to distinguish between networks formed by surface runoff and groundwater sapping, using the value of a basin's drainage density to infer its past climate or formation process is questionable (Stepinski and Stepinski, 2005).

2.6.3 Hypsometric analysis

Another morphometric method, developed by Langbein (1947) for terrestrial basin analysis that has recently been used to analyze Martian valley networks is hypsometric analysis. This method plots the distribution of the basin's area with respect to elevation and has been demonstrated to be sensitive to processes responsible for the landform (Willgoose and Hancock, 1998; Hurtrez et al., 1999) and basin maturity (Strahler, 1952). Since typical terrestrial basins formed by surface runoff display concave upward profiles, most of their surface area is located at lower elevations, yielding a characteristic hypsometric curve that is expected to be able to distinguish between different styles of fluvial erosion. As a result, Luo (2002) attempted to apply this method to determine the formation process of the Martian valley networks. His results suggested a complicated mixture of both groundwater sapping and surface runoff processes was

responsible for the formation of the Martian valley networks. However, Fortezzo and Grant (2004) pointed out that the profiles of Martian basins have a natural tendency to be concave upwards because of impact cratering, placing in doubt the reliability of hypsometric analysis as a morphometric method for determining the style of erosion on Mars (Stepinski and Stepinski, 2005).

2.6.4 Basin shape functions

Noting that there is a non-conformance between topography and drainage of some Martian valley networks when compared to terrestrial basins formed by surface runoff (Figure 1), Stepinski and Coradetti (2004) adapted the concept of drainage basin shape via the circularity ratio to study the internal morphometry of terrestrial and Martian drainage basins. The circularity ratio, introduced by Miller (1953), compares the area of a drainage basin to that of a circle of the same perimeter. Since the planimetric shape is related to the erosional processes of a drainage basin, measurement of the drainage basin shape should therefore be useful as a criterion for distinguishing between regions of different erosional origins (McArthur and Ehrlich, 1977). Taking inspiration from hypsometric analysis, Stepinski and Coradetti (2004) introduced a circularity shape function which computes the circularity ratio at a range of different elevations within the basin. Thus, the circularity shape function is a quantitative measure of the change in circularity of a basin with elevation. Similarly to the circularity ratio, the elongation ratio, introduced by Schumm (1956), compares the length of a basin to the diameter of a circle of the same perimeter. However, the ideal steady state basin shape of terrestrial systems is more closely approximated by a lemniscate loop (tear-shape) than by a circle, which led Chorley et al. (1957) to use the lemniscate loop as the figure of reference. The lemniscate index describes the rotundity of a basin whereas the lemniscate ratio compares the perimeter of a basin to that of a lemniscate loop of the same rotundity. The advantages to using shape functions derived from shape indices as morphometric parameters to study drainage basins is that they are dimensionless and, due to the fractal nature of drainage basins (Rodriguez-Iturbe and Rinaldo, 1997), scale-independent. In this study, four shape indices were adapted into shape functions: the circularity ratio, the elongation ratio, the lemniscate index, and the lemniscate ratio.

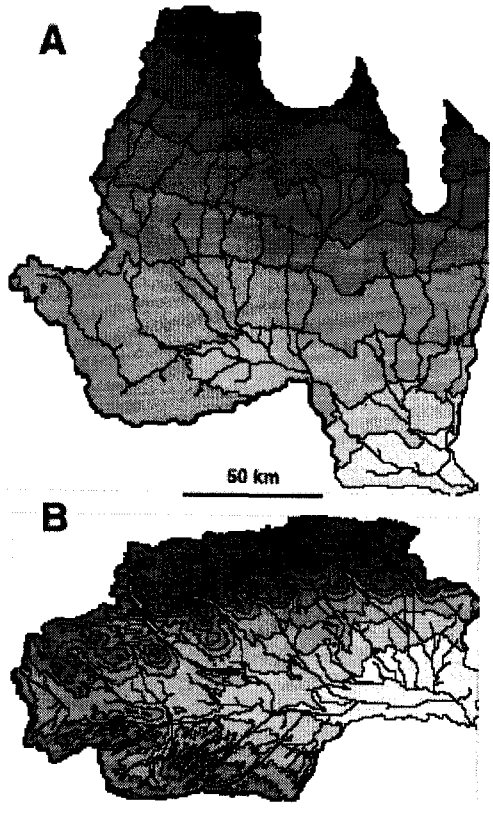

Figure 1: Topography and drainage map of (A) Warrego Valles, Mars and (B) Green River, Utah. The topography of the Green River basin follows the drainage network, whereas the drainage network of Warrego Valles appears to be disconnected from the basin's topography. Lighter shades indicate areas of lower elevation and darker shades indicate areas of higher elevation. (From Stepinski and Coradetti, 2004)

2.7. Thesis Objectives

The objectives of this thesis are to: i) investigate the role of formation process and other control factors (e.g. slope) on the internal shape of drainage basins; ii) assess the efficiency of four shape functions (circularity, elongation, lemniscate index, and lemniscate ratio) as criteria for distinguishing between terrestrial drainage basins formed by different processes (surface runoff from precipitation, surface runoff from meltwater and groundwater sapping); iii) characterize Martian basins using shape functions; and iv) determine which terrestrial site is the best analogue for Mars based on shape functions. These objectives will be addressed by computing and comparing the shape functions of basins formed by different processes situated in the United States (Utah, Florida, Arizona, Oklahoma, Hawaii), Canada (Nunavut) and Chile to the shape functions of 23 Martian basins using digital elevation models.

3. Study Sites

To compare the shape functions of Martian basins and terrestrial basins formed by different processes, 23 Martian basins were selected from 18 locations as well as 39 basins from 7 terrestrial sites (Figure 2): Utah, Florida, Arizona, Oklahoma, Hawaii, Nunavut and Chile. Except for Oklahoma and Arizona, these sites are commonly used as terrestrial analogues for Martian valley networks. Table 1 summarizes the formation process, the average regional slope of the sites (calculated from the minimum and maximum elevation of the longitudinal profile of a basin's main stream), climate and location of the terrestrial sites.

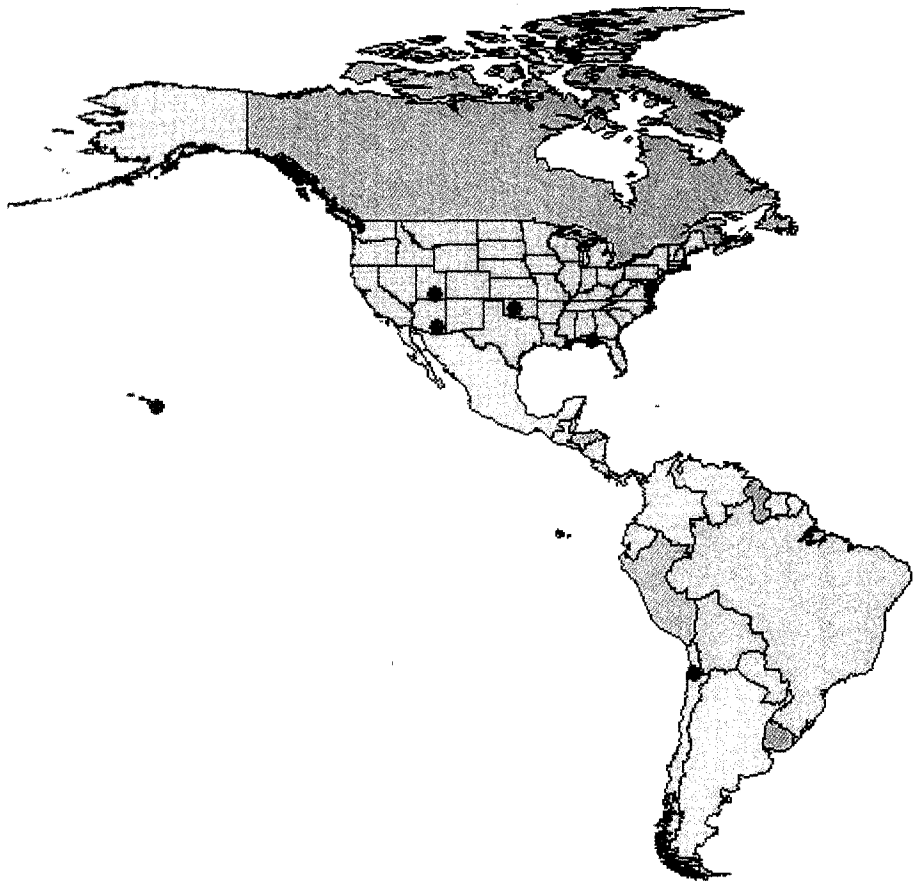

Figure 2: Location of the 7 terrestrial sites used in this study.

Table 1: Summary of the formation process, regional slope, climate and location of the terrestrial analogue sites

Sites	Formation Process	Average Slope (°)	Climate Region	Latitude	Longitude
Florida	Sapping	0.2	Temperate Forest	30.6°N	86.4°W
Oklahoma	Runoff	0.3	Grassland	20.1°N	155.7°W
Arizona	Runoff	1.1	Grassland	31.7°N	110.0°W
Devon Island	Meltwater	1.2	Polar Desert	89.1°N	75.3°W
Utah	Sapping	1.7	Desert	37.4°N	111.0°W
Utah	Runoff	3.2	Desert	37.4°N	111.0°W
Chile	Sapping	3.5	Desert	20.4°S	69.2°W
Hawaii	Sapping	6.5	Tropical Rainforest	34.9°N	98.1°W
Hawaii	Runoff	9.5	Tropical Rainforest	34.9°N	98.1°W

3.1 Utah, USA

Eleven basins, 4 formed by groundwater sapping and 7 formed by surface runoff, were selected from the Glen Canyon region, Colorado Plateau, of southeastern Utah (Figure 3). The region receives ~ 150 mm of precipitation annually (Western Regional Climate Centre, 2008) and has an arid to semiarid desert climate. Both groundwater sapping and surface runoff systems are found within the same region as tributaries to the lower Escalante River and Colorado River. Because the valleys have developed under the same lithologic, stratigraphic and climatic conditions, the differences in form are attributed primarily to the dip direction of the geologic units with respect to the valley heads as well as the permeability of the exposed geologic units and the amount of relief (Laity and Malin, 1985). Surface runoff plays a greater role in the formation of the tributaries southwest of the lower Escalante River because of the greater topographic relief and less permeable exposed geologic units (San Rafael Group and cretaceous rocks) in the upper reaches of the basins, whereas the northeast tributaries receive less surface runoff because of the lower topographic relief and the less permeable units have been stripped away leaving behind the highly permeable Navajo Sandstone (Laity and Malin, 1985). In

addition, the Navajo Sandstone is underlain by the Kayenta Formation, formed of interbedded silt and clay, which acts as an impermeable layer to concentrate groundwater flow at the interface of the two layers (Laity and Malin, 1985). Since the geologic units dip in a general southwest direction, the northeast tributaries receive greater amounts of groundwater than the southwest tributaries as the groundwater flows towards the valley heads of the northeast tributaries and away from the valley heads of the southwest tributaries (Figure 4) (Laity and Malin, 1985). Due to the low amount of surface runoff and high amount of groundwater, the northeast streams flow directly on the Kayenta bedrock as the groundwater exits the Navajo Sandstone at the unit interface and causes the headward erosion of the valley heads and Navajo Sandstone through groundwater sapping (Laity and Malin, 1985). In contrast, because the southwest tributaries receive higher amounts of surface runoff and lower amounts of groundwater sapping, the southwest streams are able to form directly on the Navajo Sandstone (Laity and Malin, 1985).

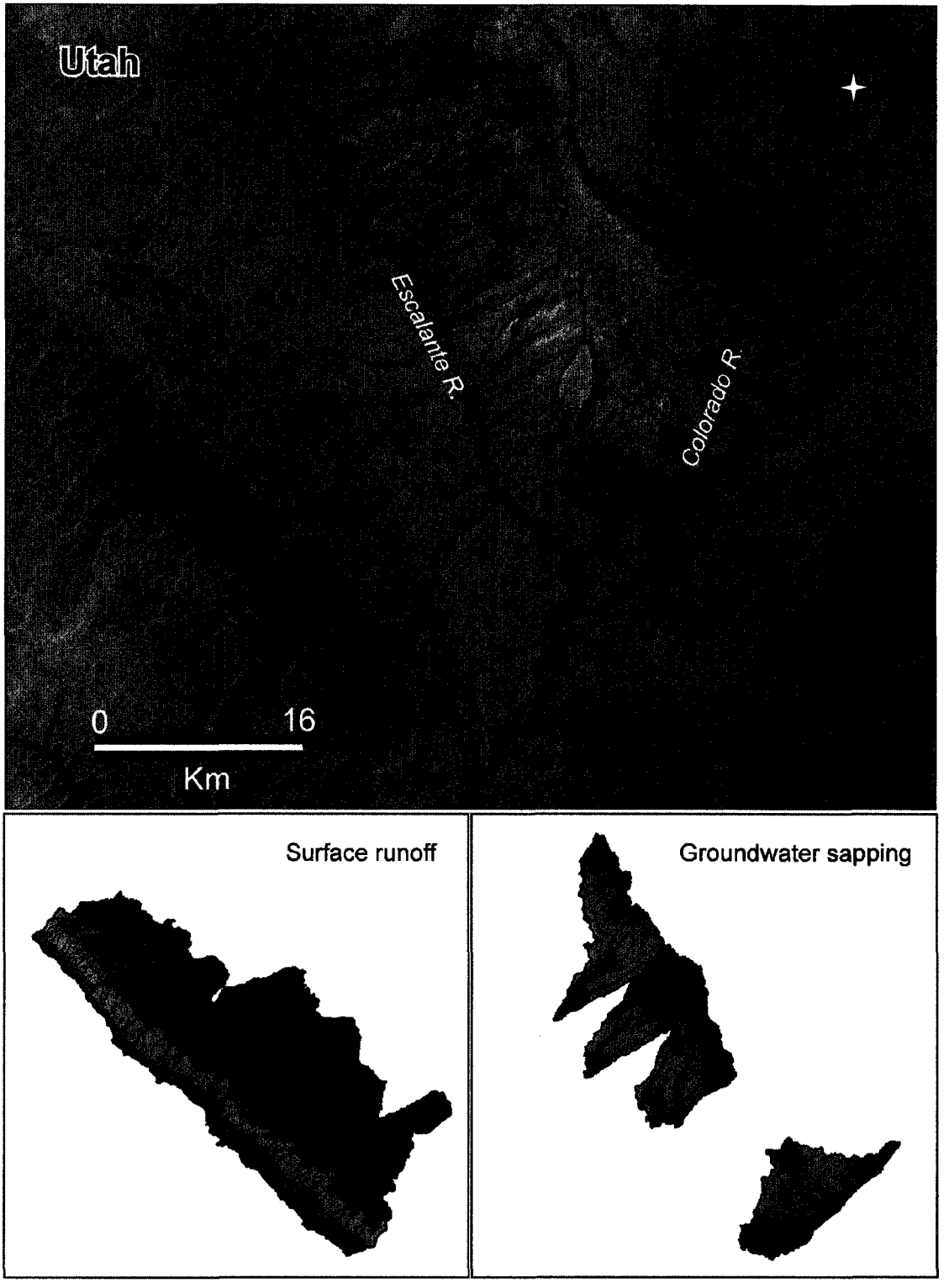

Figure 3: Upper panel: 30 m Landsat image of the Glen Canyon region of the Colorado Plateau, southeastern Utah, showing the location of the drainage basins examined. Lower two panels: Relative topography and drainage network of each basin. Blue shades indicate areas of lower elevation and red shades indicate areas of higher elevation.

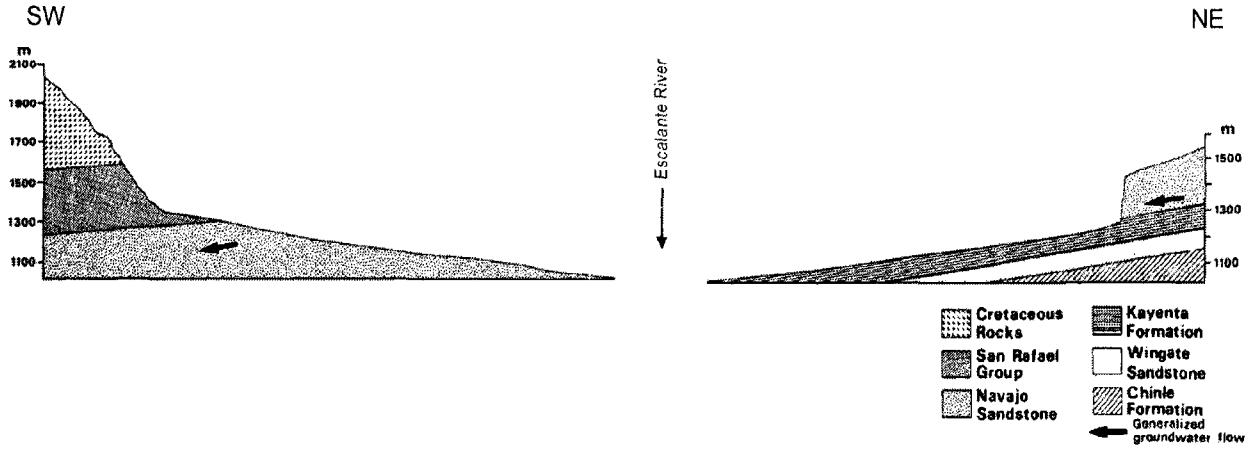

Figure 4: Typical geology and longitudinal profiles of tributaries to the Escalante River, Utah. The southwestern tributaries have less permeable geologic units exposed in the headwater regions, greater relief, and groundwater flowing away from the valley heads, resulting in the dominance of surface runoff processes. The northeastern tributaries have highly permeable geologic units exposed, lesser relief and groundwater flowing towards the valley heads resulting in the dominance of groundwater sapping processes. (Adapted from Laity and Malin, 1985)

3.2 Florida, USA

Two groundwater sapping basins were selected from the Eglin Air Force Base area in the Florida Panhandle region of northern Florida (Figure 5). The area receives ~ 1750 mm of precipitation annually (Southeast Regional Climate Centre, 2008) and has a humid temperate forest climate. The main geologic unit of the area is the highly permeable Citronelle Formation which consists of unconsolidated, non marine quartz sands that contain discontinuous layers of clay and gravel (Schumm et al., 1995). Due to the high permeability of the Citronelle Formation, groundwater sapping processes dominate the Eglin Air Force Base landscape, although surface runoff does occur during periods of high intensity precipitation (Schumm et al., 1995). Unlike the Navajo Sandstone in southeastern Utah, the Citronelle Formation is not underlain by an impermeable layer. As a result, the groundwater sapping systems of the Florida Panhandle are not formed by concentrated groundwater flow at the interface of two geologic units. Instead, groundwater sapping in the Florida Panhandle is attributed to a high, stable water table (Schumm et al., 1995).

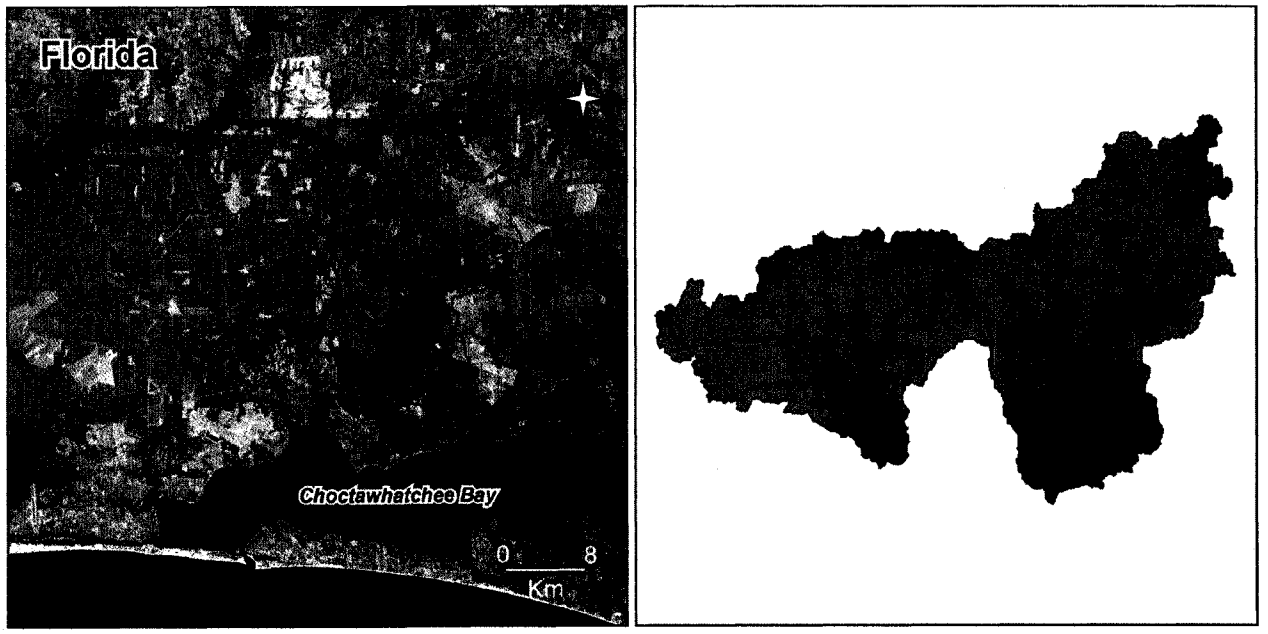

Figure 5: Left panel: 30 m Landsat image of the Florida Panhandle region of northern Florida showing the location of the drainage basins examined. Right panel: Relative topography and drainage network of each basin. Blue shades indicate areas of lower elevation and red shades indicate areas of higher elevation.

3.3 Atacama Desert, Chile

Five groundwater sapping basins were selected from the Atacama Desert on the western slope of the Central Andes in northern Chile (Figure 6). The region receives ~ 1 mm of precipitation annually (Houston and Hartley, 2003), making the hyperarid Atacama Desert one of the driest regions on Earth. The headwaters of the valleys have formed in the Huasco Ignimbrite Formation with the lower reaches transitioning into the El Diablo Formation, formed of coarse andesitic conglomerates (Farias et al., 2005). The groundwater is recharged from precipitation at higher elevations in the Western Altiplano (Hoke et al., 2004). Due to the ubiquitous presence of precipitation on Earth, most terrestrial groundwater sapping systems are actually composite systems where groundwater sapping dominates over surface runoff processes. However, the hyperaridity of the Atacama Desert marks the Chilean basins as almost pure groundwater sapping endmembers.

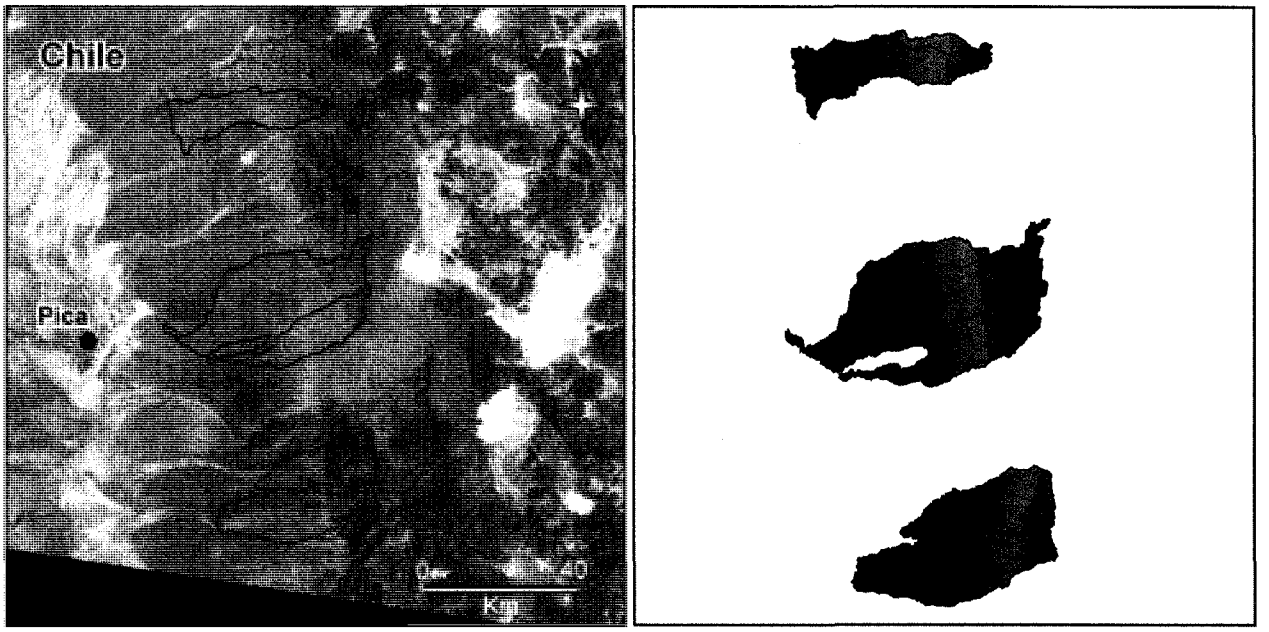

Figure 6: Left panel: 30 m Landsat image of the Atacama Desert region of Chile showing the location of the drainage basins examined. Right panel: Relative topography and drainage network of each basin. Blue shades indicate areas of lower elevation and red shades indicate areas of higher elevation.

3.4 Hawaii, USA

Nine basins, 4 formed by groundwater sapping and 5 formed by surface runoff, were selected from the northeastern slope of Kohala Volcano on the island of Hawaii (Figure 7). The northeastern flank of Kohala receives on average ~ 2500 mm of precipitation annually while the summit receives ~ 5000 mm (Stearns and MacDonald, 1946), reflective of the region's humid tropical rainforest climate. The geology of the area consists of highly permeable layered basalt flows that dip seaward (Kochel and Baker, 1990) overlain by an ash mantle which reduces the surface permeability enough to allow small, shallow surface runoff valleys to form (Gulick and Baker, 1990). In addition, the presence of local impermeable dike swarms permits groundwater to become perched at high elevations (Figure 8) (Stearns, 1966). As the surface runoff valleys incise through the basalt, some breach into the perched aquifers, initiating the formation of large, deep groundwater sapping valleys (Kochel and Baker, 1990).

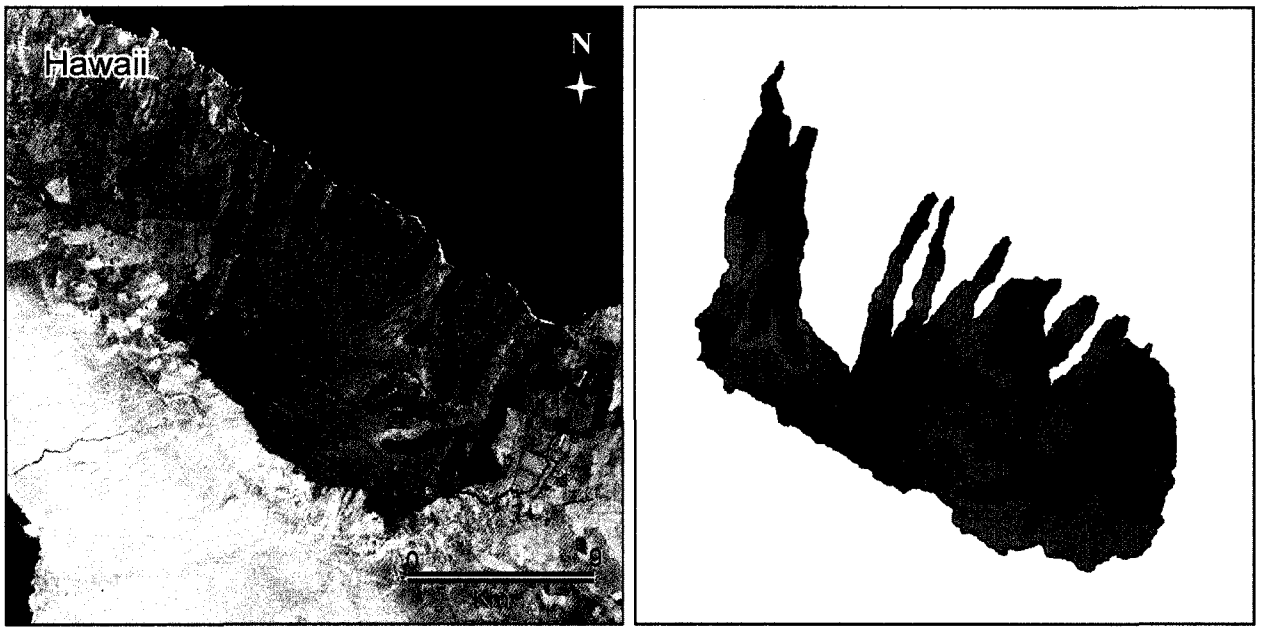

Figure 7: Left panel: 30 m Landsat image of the Kohala Volcano region of the Island of Hawaii showing the location of the drainage basins examined. Right panel: Relative topography and drainage network of each basin. Blue shades indicate areas of lower elevation and red shades indicate areas of higher elevation.

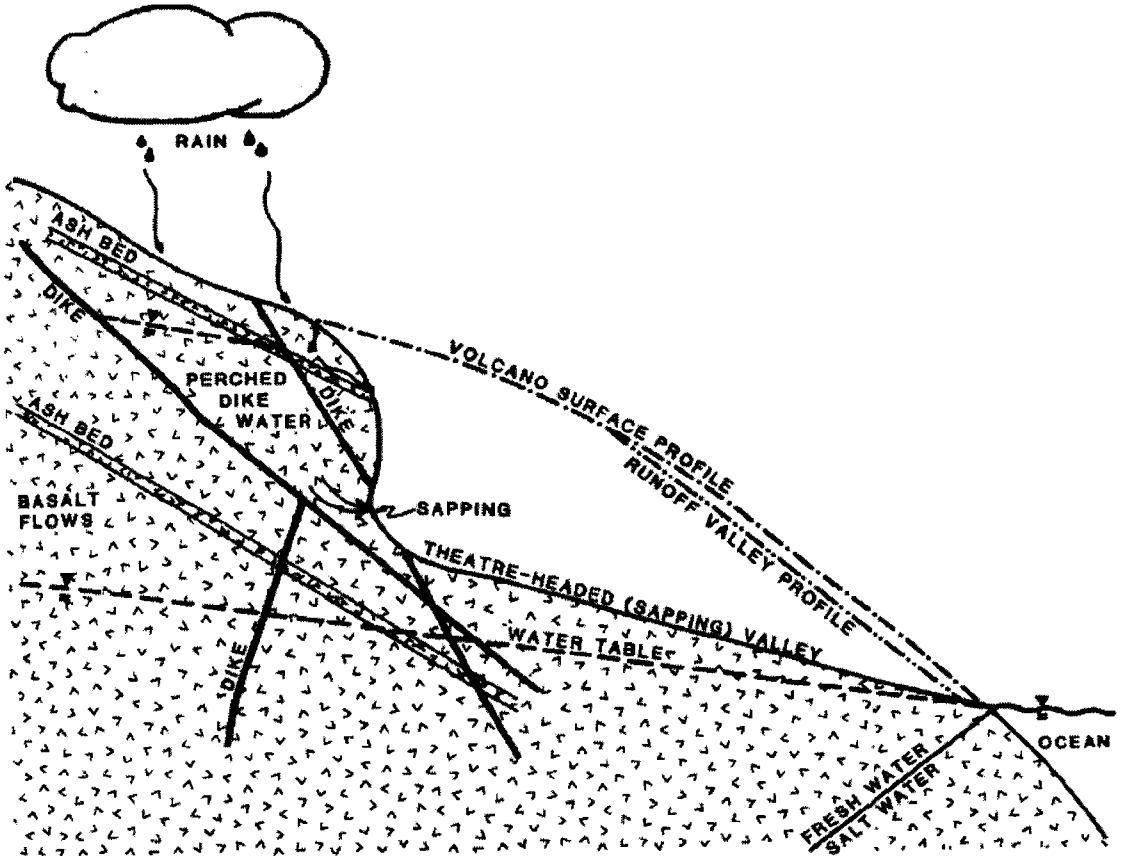

Figure 8: Schematic of location of perched groundwater caused by impermeable dike swarms resulting in groundwater sapping systems on Kohala Volcano, Hawaii. (From Kochel and Baker, 1990)

3.5 Oklahoma, USA

Four surface runoff basins were selected from the Little Washita Experimental Watershed in southwestern Oklahoma (Figure 9). This agricultural watershed is used to model the response of surface runoff to precipitation. The region receives ~ 795 mm of precipitation annually (Van Liew and Garbrecht, 2003) and has a semiarid to subhumid grassland climate. The geology of the watershed consists mainly of sandy alluvial deposits that overlay the Rush Springs Formation, formed of fine grained sandstone and siltstone (Van Liew and Garbrecht, 2003).

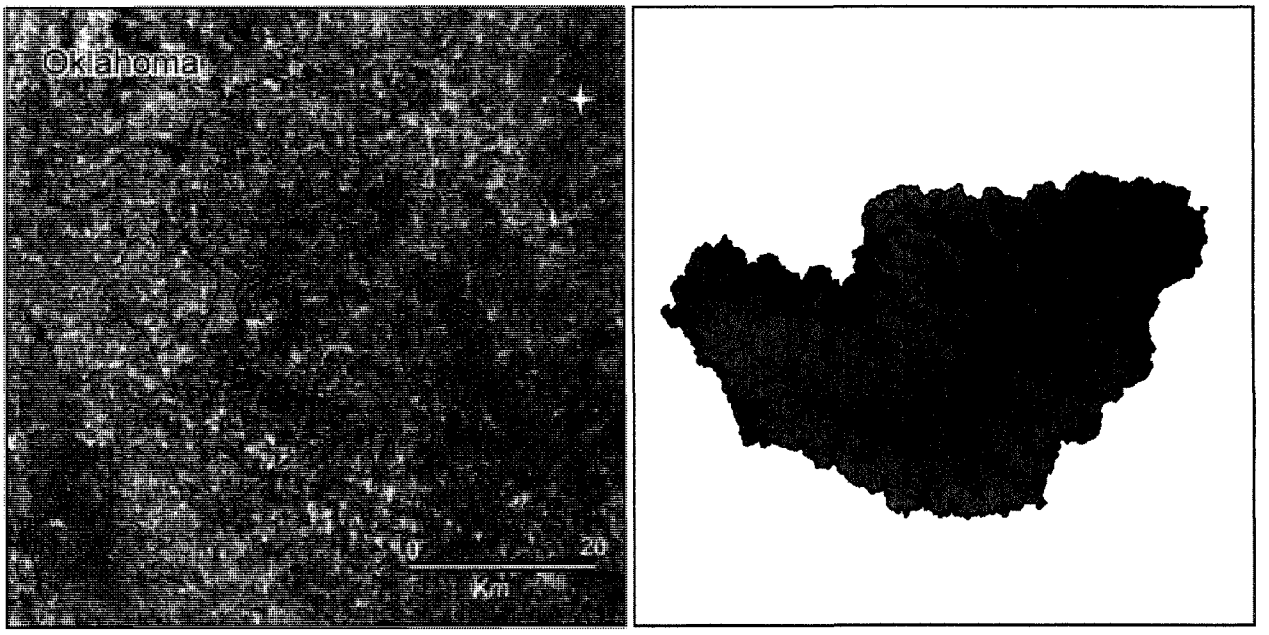

Figure 9: Left panel: 30 m Landsat image of the Little Washita Experimental watershed of southwestern Oklahoma showing the location of the drainage basins examined. Right panel: Relative topography and drainage network of each basin. Blue shades indicate areas of lower elevation and red shades indicate areas of higher elevation.

3.6 Arizona, USA

Four surface runoff basins were selected from the Walnut Gulch Experimental Watershed in southeastern Arizona (Figure 10), which is also used to model the response of surface runoff to precipitation. The watershed is a tributary to the San Pedro River and receives the majority of its runoff from localized thunderstorms (Michaud and Sorooshian, 1994). The region receives ~ 310 mm of precipitation annually (Goodrich et al., 2008) and has a semiarid grassland climate. The geology of the watershed consists mainly of alluvial deposits ranging from clays and silts to well-cemented boulder conglomerates that overlay bedrock formed of limestone and weathered granite intrusions (Renard et al., 1993).

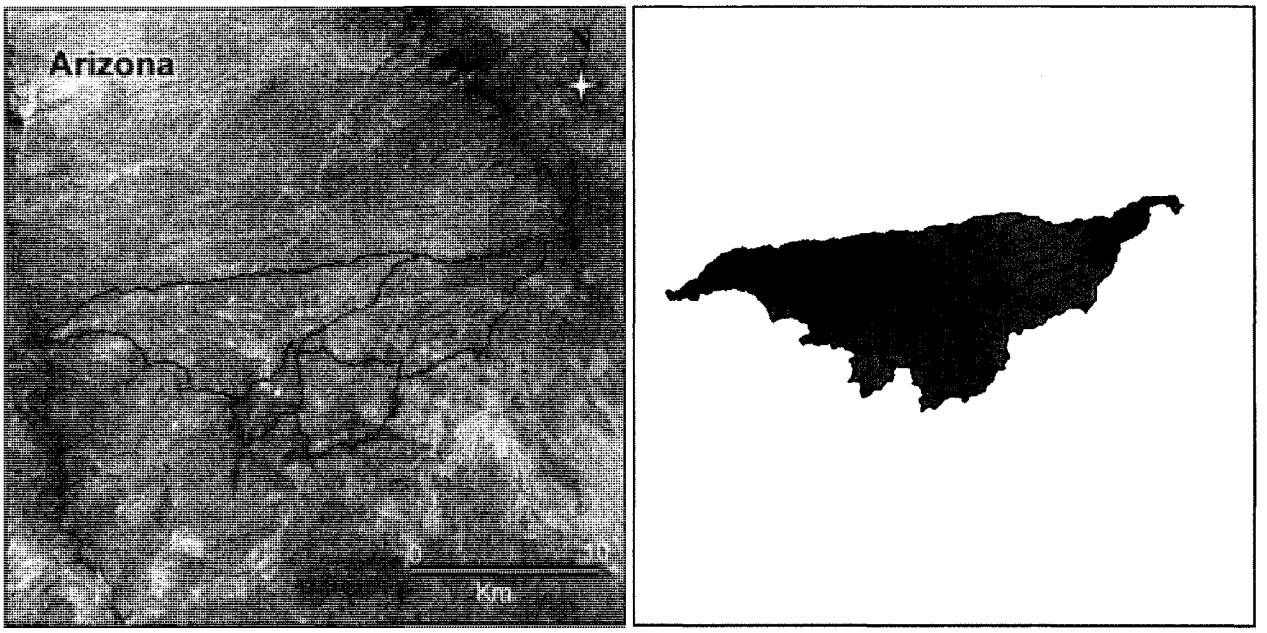

Figure 10: Left panel: 30 m Landsat image of the Walnut Gulch Experimental Watershed of southeastern Arizona showing the location of the drainage basins examined. Right panel: Relative topography and drainage network of each basin. Blue shades indicate areas of lower elevation and red shades indicate areas of higher elevation.

3.7 Devon Island, Canada

Four glacial meltwater basins a few kilometers east of Haughton Crater were selected from Devon Island, Nunavut (Figure 11). The climate on Devon Island is part of the polar desert regime, receiving ~ 150 mm of precipitation annually (Environment Canada, 2004). The valleys have formed in the Lower Allen Bay Formation, which consists of dolimitic limestone (Osinski, 2005). Lee et al. (1999) interpreted the networks to have been formed by glacial meltwater as a result of the decay and retreat of an ice cover with possible intervals of glacial reoccupation.

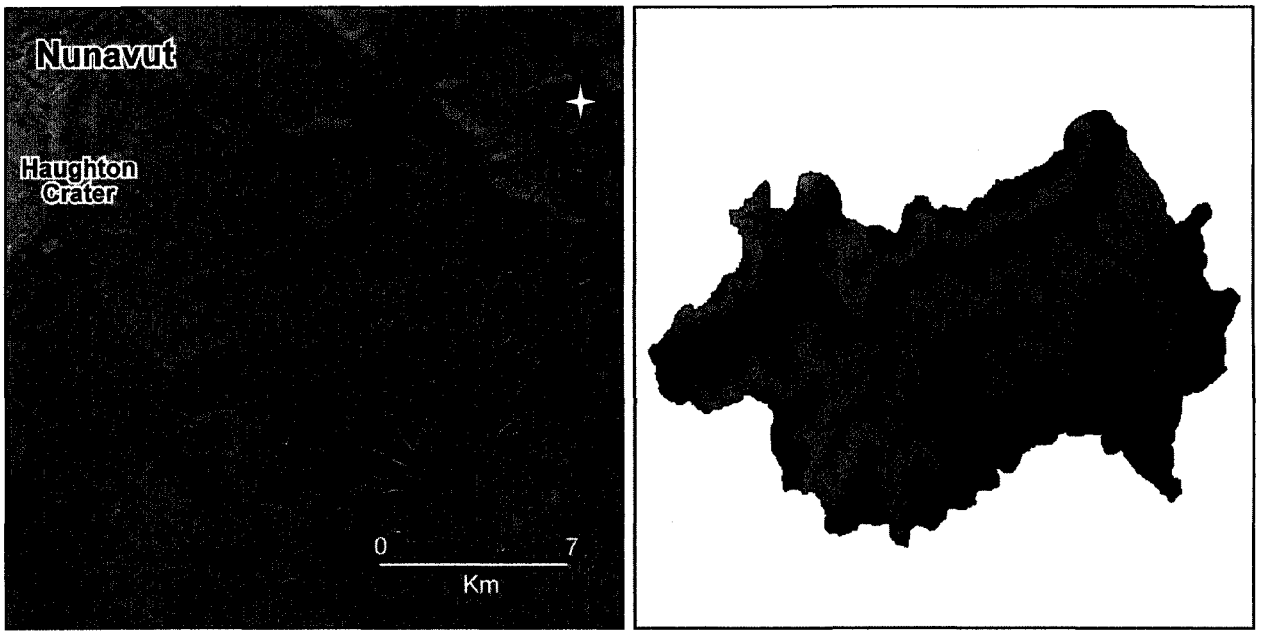

Figure 11: Left panel: 30 m Landsat image of the Haughton Crater region of Devon Island, Nunavut showing the location of the drainage basins examined. Right panel: Relative topography and drainage network of each basin. Blue shades indicate areas of lower elevation and red shades indicate areas of higher elevation.

3.8 Mars

Twenty-three Martian valley networks, as described in section 2.2, were selected from 18 locations (Figure 12). All of the named networks, except for Locras, have been previously studied by Stepinski and Coradetti (2004) and Stepinski and Stepinski (2005). Additionally, all of the networks, except for Locras and Unnamed 2, are located in the southern hemisphere. Table 2 summarizes the average regional slope and location of the Martian sites. The individual basins are outlined in Figure 13.

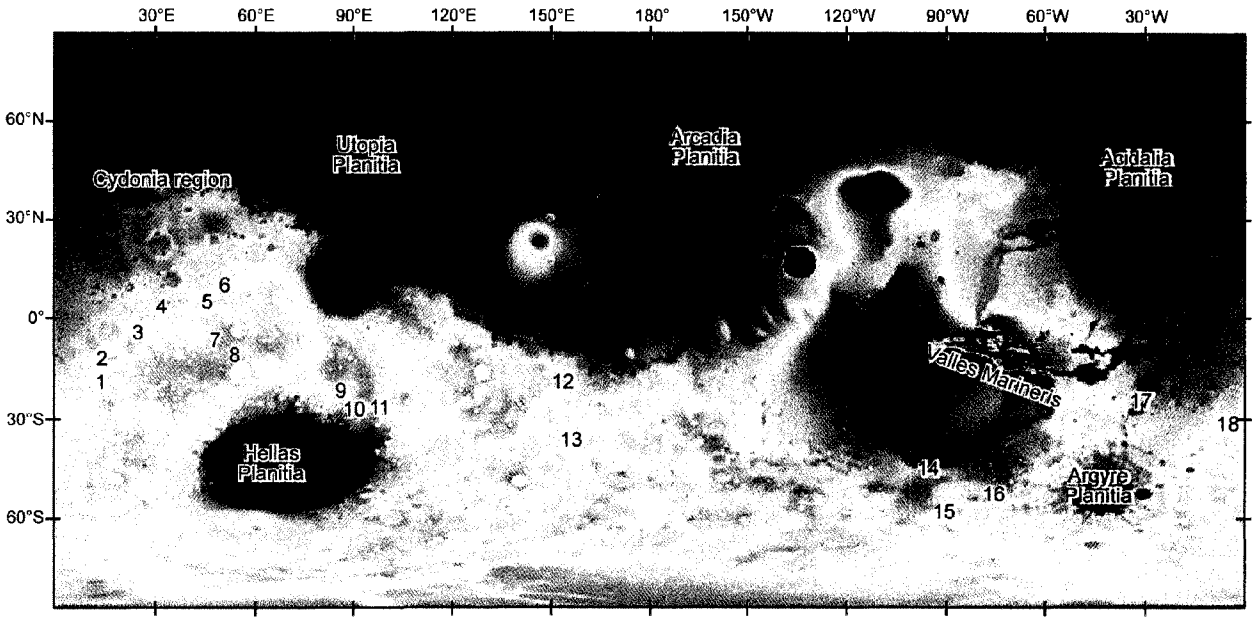

Figure 12: Digital elevation data of Mars with the location of the valley networks used in this study. Blue shades indicate areas of lower elevation and red shades indicate areas of higher elevation. 1: Evros Vallis West; 2: Evros Vallis North; 3: Schiaparelli; 4: Naktong Vallis; 5: Locras; 6: Unnamed 2; 7: Dawes East; 8: Unnamed 1; 9: Millochau West; 10: Millochau South; 11: Millochau East; 12: Unnamed 3; 13: Unnamed 4; 14: Warrego Vallis; 15: Unnamed 5; 16: Douglass; 17: Arda Valles; 18: Unnamed 6

Table 2: Summary of the regional slope and location of the Martian valley networks

Site	Average Slope (°)	Latitude	Longitude
Arda Valles	0.7	20.6°S	-31.8°E
Dawes East	0.2	5.5°S	45.0°E
Douglass	0.2	47.5°S	-75.7°E
Evros Vallis North	0.6	7.9°S	14.8°E
Evros Vallis West	0.2	13.1°S	13.7°E
Locras	0.3	9.1°N	47.4°E
Millochau East	1.0	23.4°S	94.1°E
Millochau South	0.7	22.5°S	89.9°E
Millochau West	0.3	18.6°S	88.0°E
Naktong Vallis	0.2	0.8°S	34.8°E
Schiaparelli	0.4	0.4°S	23.6°E
Warrego Vallis	1.3	42.2°S	-92.1°E
Unnamed 1	0.4	9.1°S	53.9°E
Unnamed 2	0.3	13.1°N	51.0°E
Unnamed 3	0.4	14.0°S	153.8°E
Unnamed 4	0.3	33.7°S	155.6°E
Unnamed 5	0.4	53.4°S	-91.3°E
Unnamed 6	0.3	25.8°S	-3.3°E

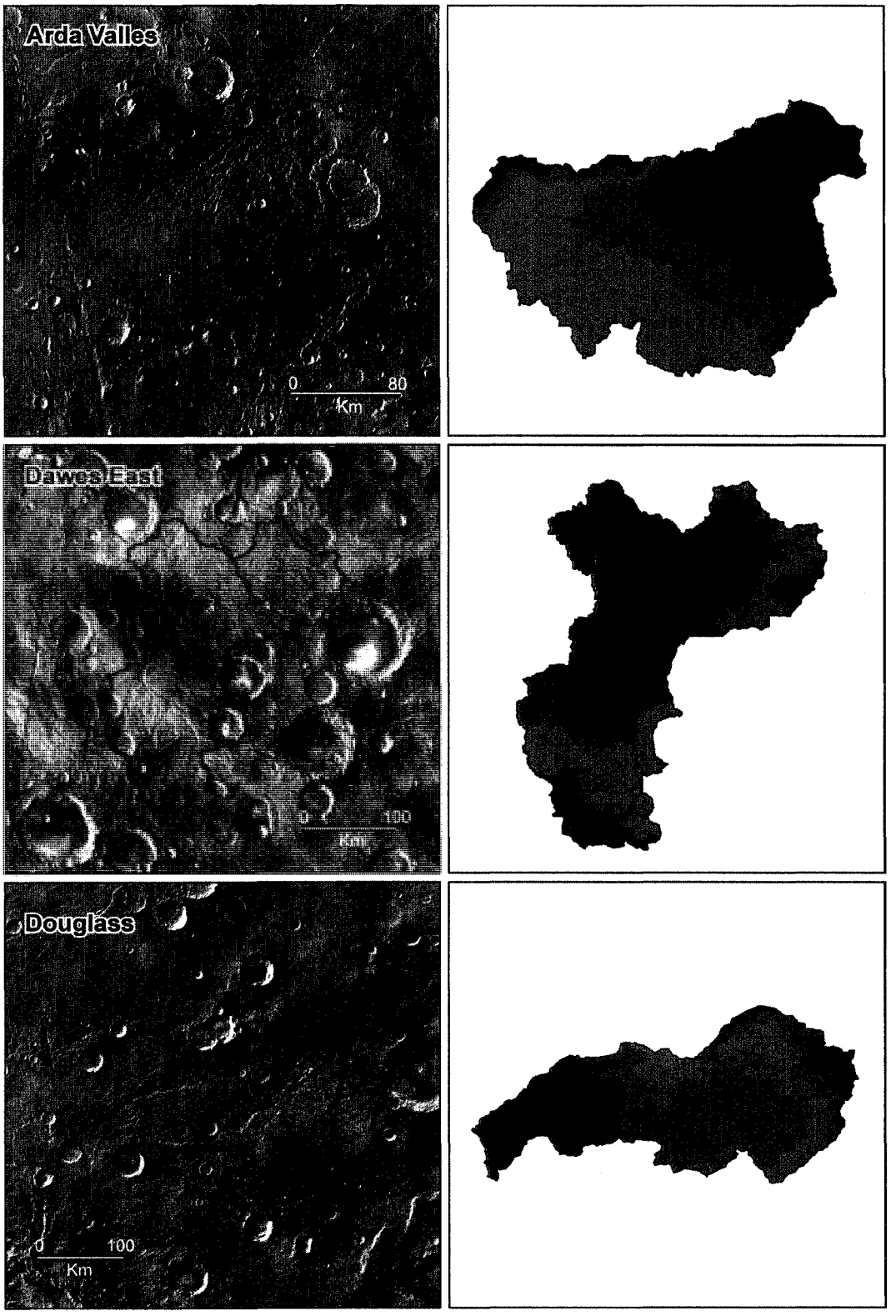

Figure 13: Left column: 230 m THEMIS image of the location of the valley networks examined. Right column: Relative topography and drainage network of each basin. Blue shades indicate areas of lower elevation and red shades indicate areas of higher elevation.

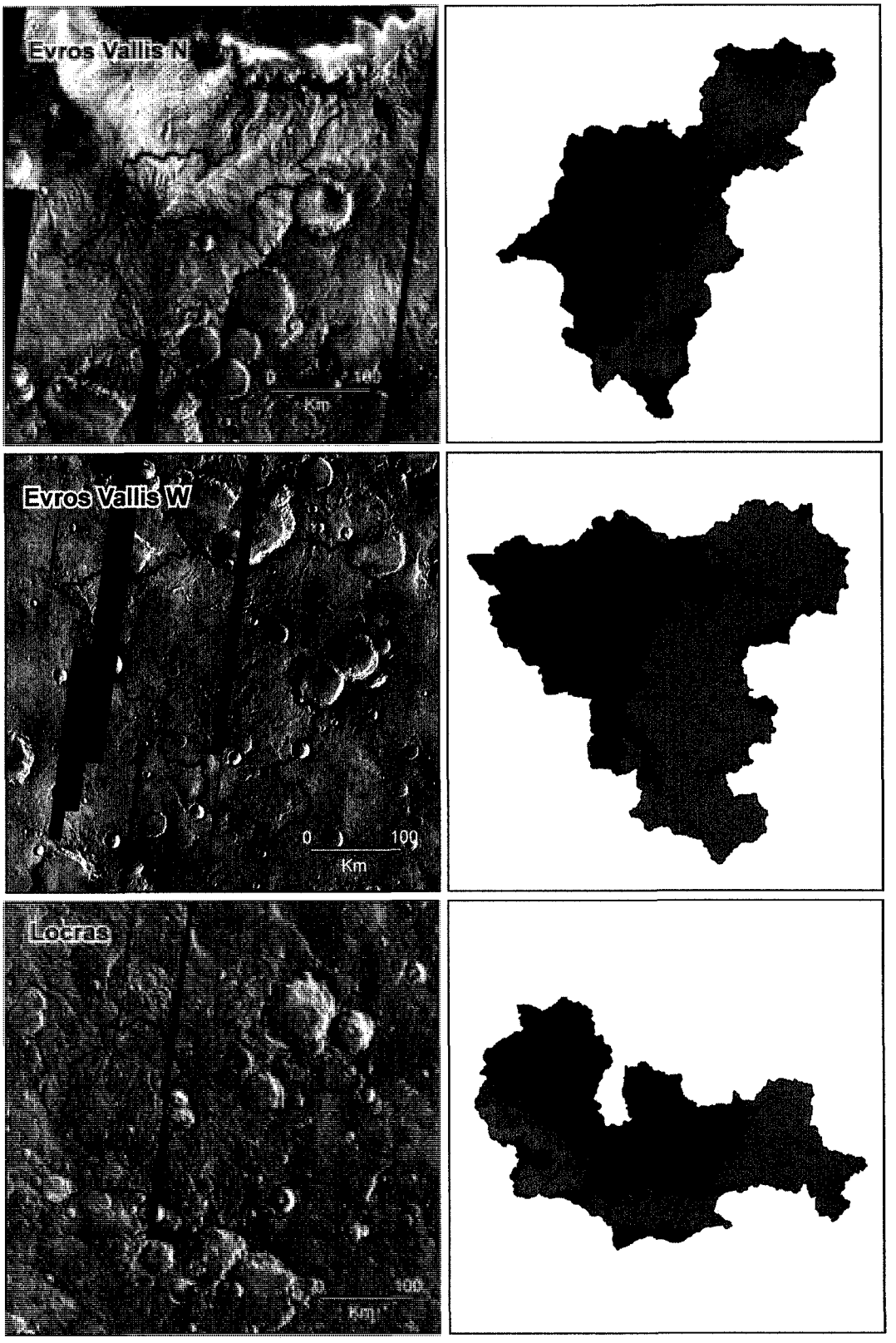

Figure 13: *(Continued).*

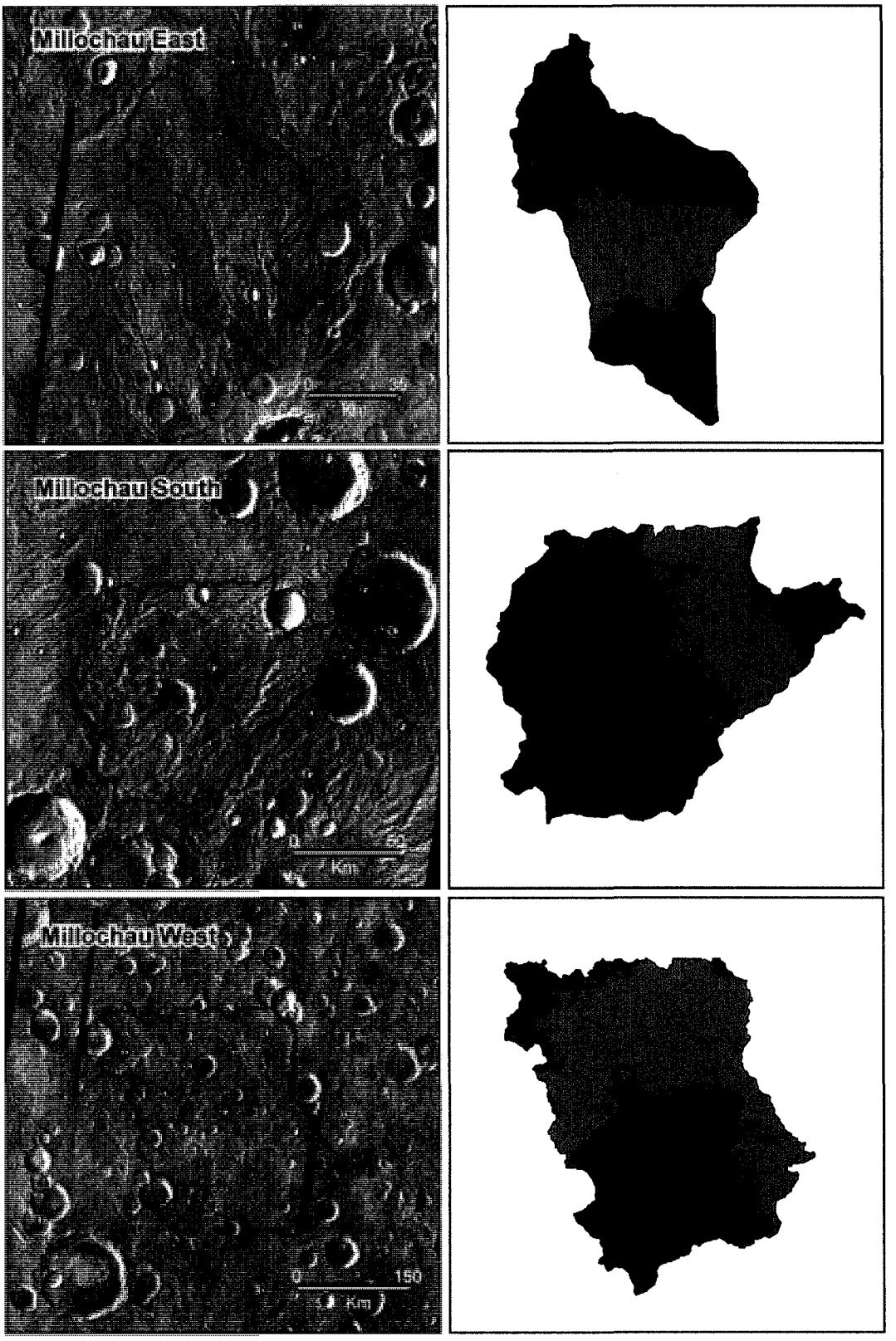

Figure 13: *(Continued).*

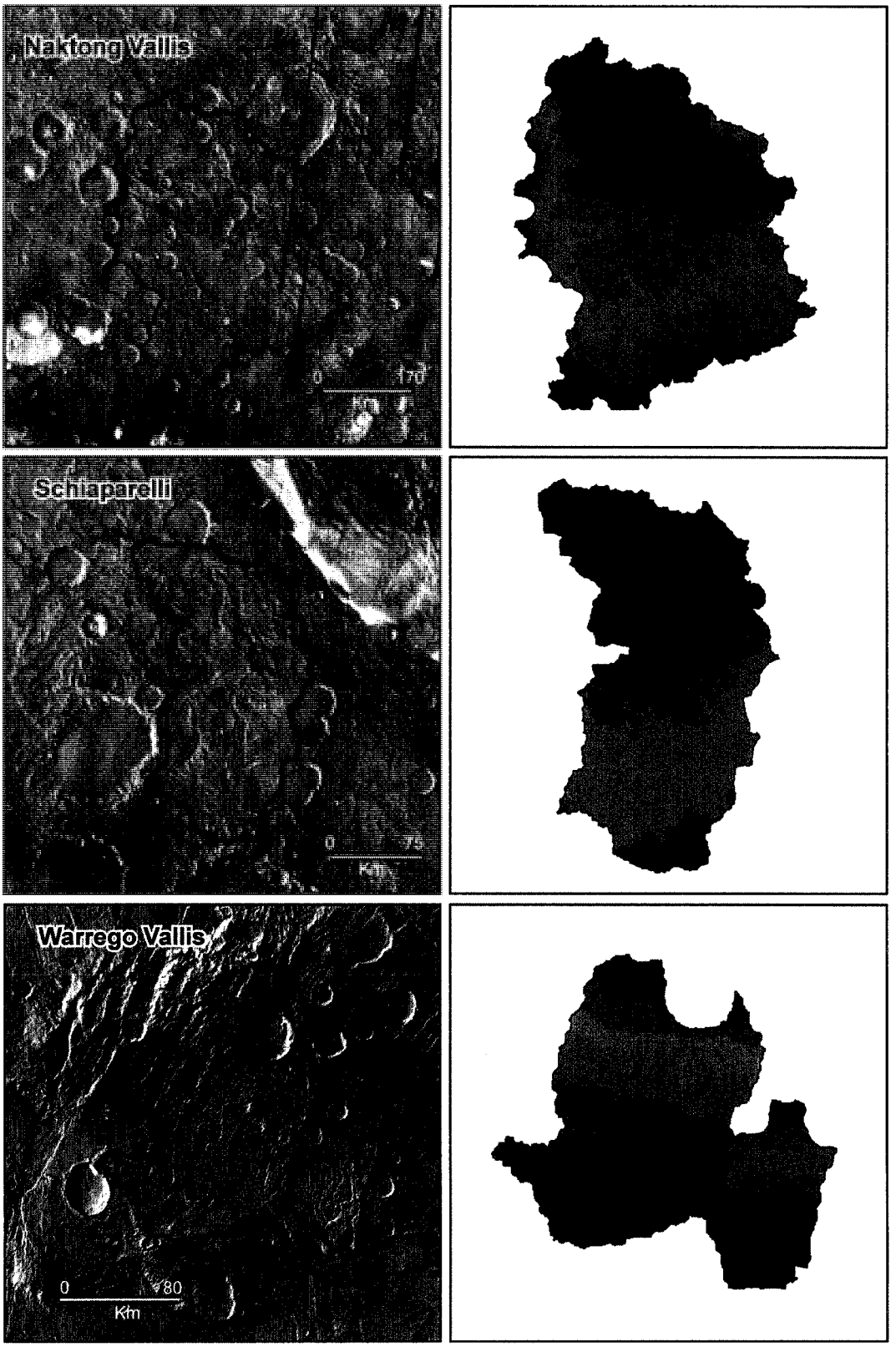

Figure 13: *(Continued).*

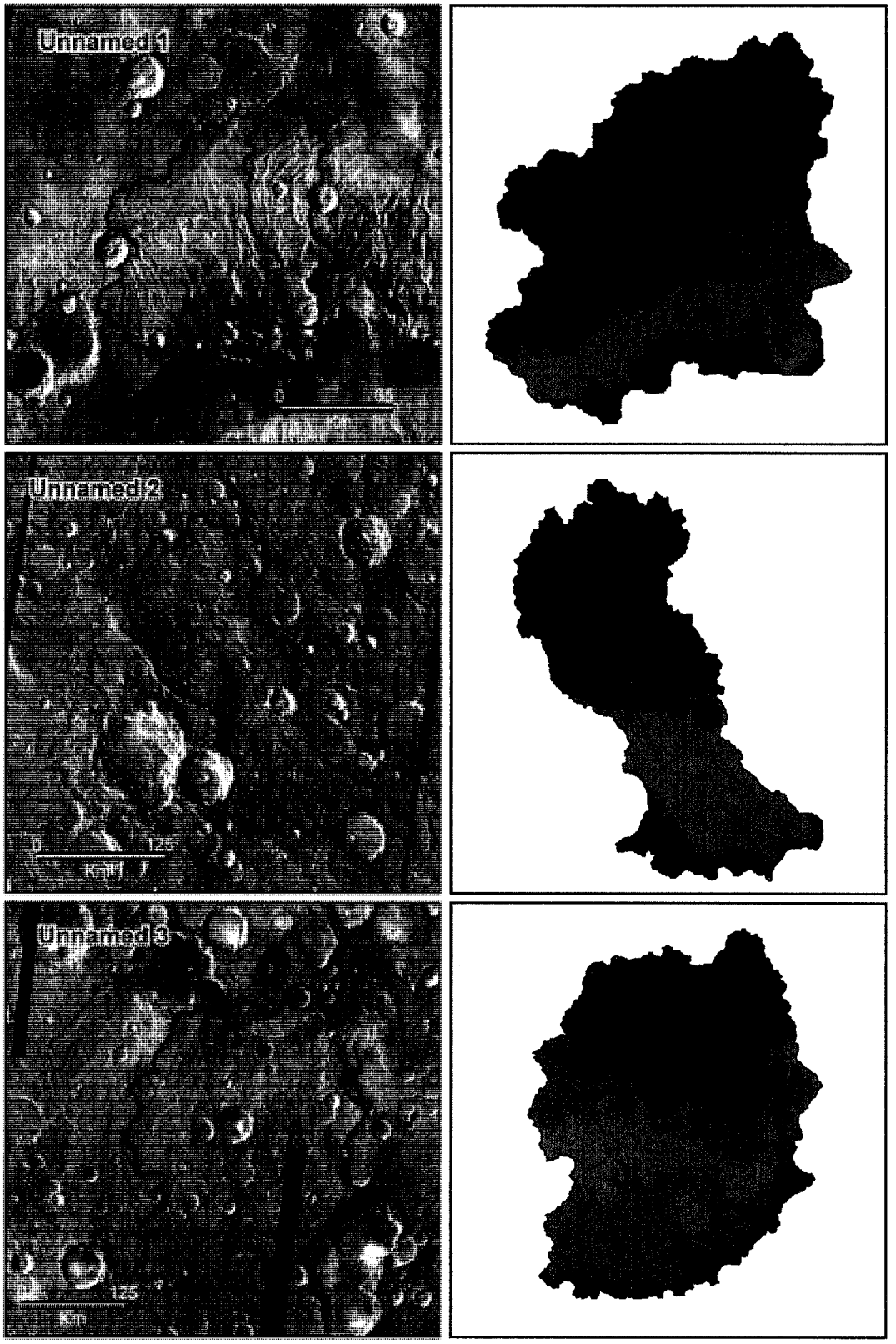

Figure 13: *(Continued).*

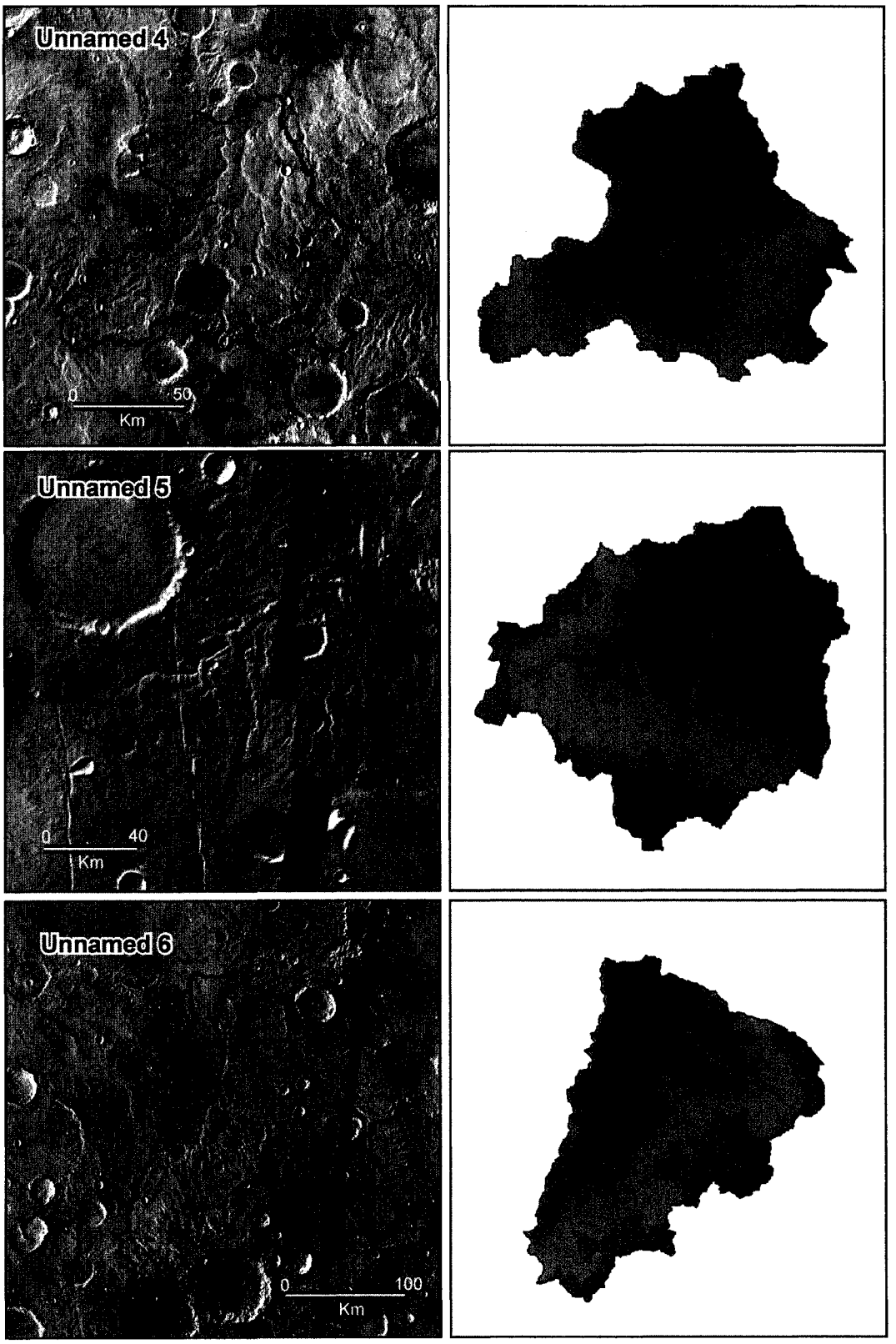

Figure 13: *(Continued)*

4. Methodology

4.1 Data and Image Processing

4.1.1 Terrestrial

Visual assessment of the terrestrial study sites was undertaken using Landsat 7 imagery. Landsat 15 m panchromatic scenes were obtained from the University of Maryland Institute for Advanced Computer Studies (UMIACS). For the analysis of the drainage basin morphometry, digital elevation models (DEMs) and hydrography data were used. Available hydrography data were obtained from the National Topographic Data Base (NTDB) at a scale of 1:50,000 for the Canadian site, from the National Hydrographic Database (NHD) at a scale of 1:24,000 for the American sites and from the Environmental Systems Research Institute (ESRI) Digital Chart of the World at a scale of 1:1,000,000 for the Chilean site. For the Canadian site, DEMs were obtained at a scale of 1:50,000 (~ 30 m) from GeoBase. For the American sites, 1 arcsecond (~ 30 m) National Elevation Data (NED) were obtained from the US Geological Survey (USGS). For the Chilean site, 30 m Advanced Spaceborne Thermal Emission and Reflection Radiometer (ASTER) DEMs were obtained from NASA's Earth Observing System Data Gateway. To preserve scale along the central meridian of each site, all datasets were reprojected using a modified transverse Mercator projection with a scale factor of 0.9996 at the central meridian of each 6 degree zone.

4.1.2 Martian

For visual assessment of the Martian study sites, a 256 pixels/degree (~ 230 m) daytime thermal infrared (12.57 μm) global mosaic, released November 16th 2006, from the Thermal Emission Imaging System (THEMIS) aboard Mars Odyssey was used. The analysis of the valley network morphometry was performed using 128 pixels/degree (~ 460 m) global digital elevation data released in 2003 from the Mars Orbiter Laser Altimeter (MOLA) aboard Mars Global Surveyor. This is the highest resolution global digital elevation data currently available for Mars. Both of these datasets were obtained from the USGS Planetary GIS Web Server (PIGWAD) and were also reprojected to a modified transverse Mercator projection and predefined Mars 2000 datum in ArcGIS.

4.2 Drainage Basin and Network Extraction

The drainage basins and drainage network of each study site were extracted from the digital elevation data through a standard series of processing steps using ArcHydro tools (ESRI, 2002), an ArcGIS-based suite of tools designed for water resources applications. Starting from the DEM, these tools generate raster grids of adjusted elevation, flow direction, flow accumulation, stream definition, stream segmentation, and watershed delineation, from which the vector representation of the drainage catchments and network are obtained (Figure 14). If prior vector data of the drainage network are available (NHD data, for example), the first step is to recondition the surface of the DEM using the AGREE surface reconditioning system. This algorithm adjusts the surface elevation to be consistent with the vector data by dropping/raising the elevation of the cells within a given buffer distance of the identified streams (Figure 15) to ensure drainage continuity in flat areas (Hellweger and Maidment, 1997). This method is an improvement from previous methods, such as "burning in the streams", that only decreased the elevation of the cells directly identified as a stream. Because the buffer enables the AGREE algorithm to adjust the elevation of all the cells within a given distance of the stream, discrepancies between the stream vector data and the exact location of the streams on the DEM are tolerable (Hellweger and Maidment, 1997). In contrast, with the "burning in the streams" method, discrepancies would result in the creation of two nearly parallel drainage troughs, the original stream and the one burned in by the algorithm (Hellweger and Maidment, 1997).

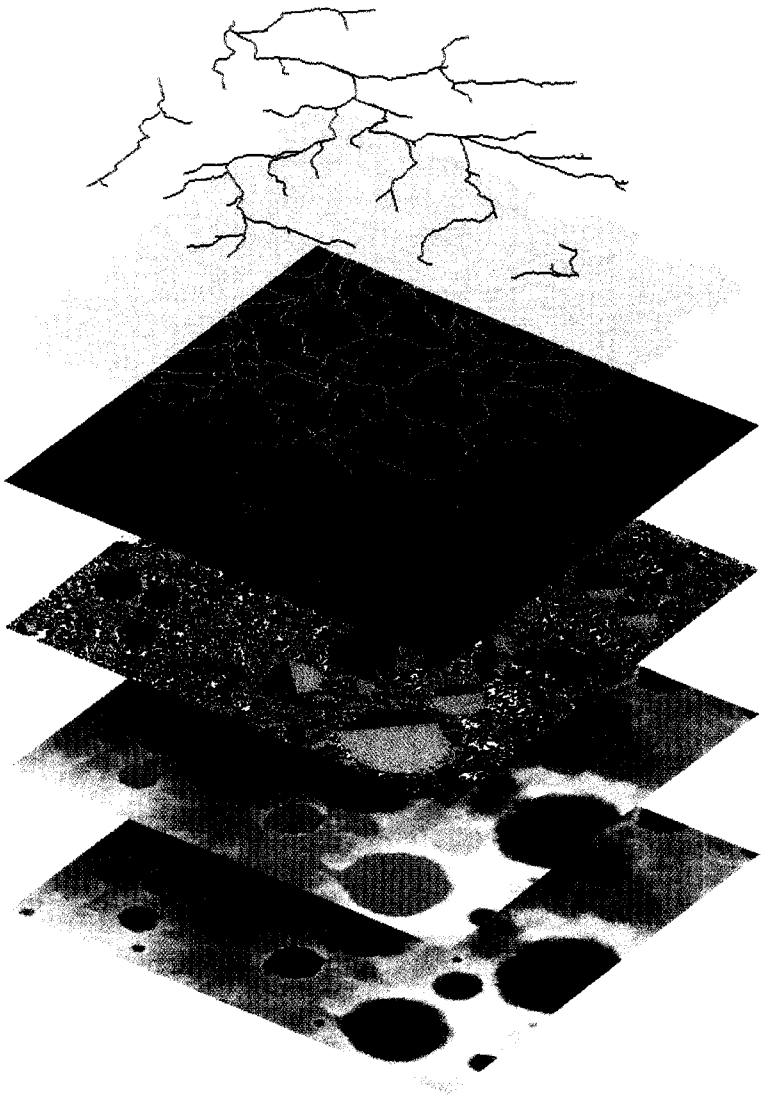

Figure 14: Arc Hydro processing steps. The bottom layer is the original DEM. The second layer is the grid of adjusted elevations. The third layer is the flow direction grid. The fourth layer is the flow accumulation grid. The fifth layer is the extracted vector representation of the drainage catchments. The uppermost layer is the extracted vector representation of the drainage network.

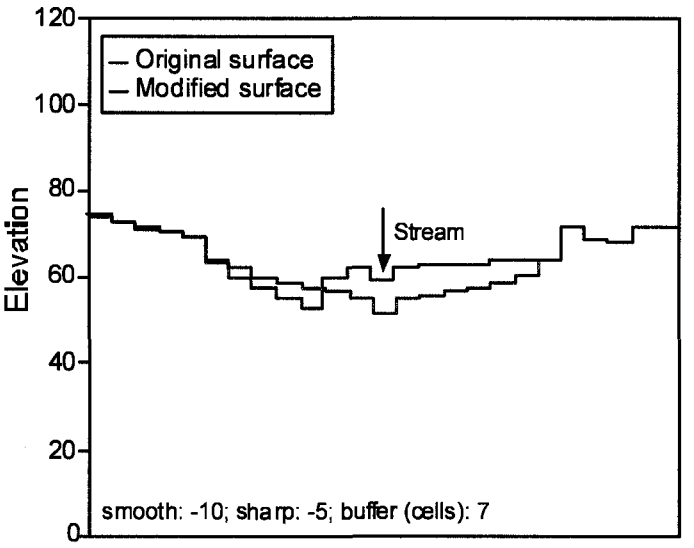

Figure 15: The AGREE algorithm adjusts the surface elevation to be consistent with the stream vector data by dropping/raising the elevation of the cells within a given buffer distance of the identified streams. The smooth distance specifies the elevation drop over the specified range of cells within the buffer distance of the stream vector whereas the sharp distance specifies the elevation drop of the cell containing the stream vector. (Adapted from Hellweger and Maidment, 1997)

If prior hydrography data are unavailable, as is the case for Mars, then it is possible to start with the second step: filling the sinks in the DEM. The Fill Sinks tool raises pit cell elevations (artifacts in the DEM) and levels them with the surrounding terrain. Although this tool was developed to handle artificial sinks, it is an important step in the preparation of the Martian elevation data for hydrological analysis. Due to the emplacement of craters subsequent to the formation of the valley networks, the Martian terrain contains numerous natural closed depressions which interfere with the drainage network continuity. Filling sinks converts craters into lakes by raising the elevation values within a crater to the lowest point of the crater's rim, thus rendering the surface drainable and ensuring drainage continuity. The downside to this is that the algorithm is unable to detect centripetal drainage patterns, such as drainage networks that form closed lake systems.

The third step is to compute the flow direction grid using the D8 algorithm (O'Callaghan and Mark, 1984). The flow from a particular cell is directed to a single downslope neighbour (one of eight surrounding cells). The flow direction is determined based on the direction of the largest distance weighted drop, calculated by taking the difference in elevation values and

dividing by $\sqrt{2}$ for a diagonal cell and 1 for a non-diagonal cell. As a result, each cell is assigned one of 8 possible flow directions values: East = 1; Southeast = 2; South = 4; Southwest = 8; West = 16; Northwest = 32; North = 64; Northeast = 128.

The next step is to compute the flow accumulation grid. Flow accumulation is simply the total number of cells that drain into a given cell, as determined from the flow direction grid. Finally, a threshold value is chosen from the flow accumulation grid such that cells with flow accumulation above the threshold are defined as belonging to a stream. The threshold is thus the minimum flow required to initiate a stream. Once the drainage network is delineated, drainage catchments are identified as the contributing area draining to each stream segment. Whereas the default threshold value is set to 1% of the maximum flow accumulation, a choice of a smaller threshold will result in the production of drainage networks with higher drainage densities and a greater number of catchments. In the case of Mars, by reducing the threshold it is thus possible to create catchments the size of individual craters. This property was utilized to delineate and remove large, "contaminant" craters from the periphery of the drainage basins. Otherwise, a threshold was carefully selected to create catchments that, when merged together, produce a single drainage basin that properly encompasses the entire drainage network.

4.3 Calculation of Basin Shape Functions

Once a drainage basin has been outlined from the merged catchments, a horizontal plane at relative elevation $z = h/H$ slices the basin into two parts (Figure 16). The area (A), perimeter (P) and basin length (L) of the planar projection of the part of the basin located below z (from now on referred to as a basin "slice") are determined using basic ArcGIS functionality and then used to compute the four shape indices:

Circularity Ratio:

$$C = \frac{A}{A_C(P)} = \frac{4\pi A}{P^2} \qquad (1)$$

The circularity of a basin is the ratio of the area of the basin slice to the area of a circle of perimeter P. Thus, the value of C ranges between 0 to 1 such that, for a perfectly circular basin, C equals 1, and for an elongated basin, $C < 1$.

Elongation Ratio:

$$E = \frac{d_C(A)}{L} = \frac{2\sqrt{A}}{L\sqrt{\pi}} \qquad (2)$$

The elongation of a basin is the ratio of the diameter of a circle of area A to the basin length (the distance from the mouth to the most distant point on the perimeter). Thus, for a circular basin, E equals 1.

Lemniscate Index:

$$k = \frac{\pi L^2}{4A} \qquad (3)$$

As shown in Figure 17, the lemniscate index is a coefficient whose value influences the width of the lemniscate loop. Thus, for a circular basin, k equals 1.

Lemniscate Ratio:

$$L_R = \frac{P(k)}{P} = \frac{2LE(\mathrm{K})}{P} \qquad (4)$$

The lemniscate ratio of a basin is the ratio of the perimeter of a lemniscate loop of lemniscate index k to the perimeter of the basin, where $E(K)$ is an elliptic integral solvable through the use of integral tables (see Appendix B for derivation). For basins of perfect lemniscate shape, L_R equals 1.

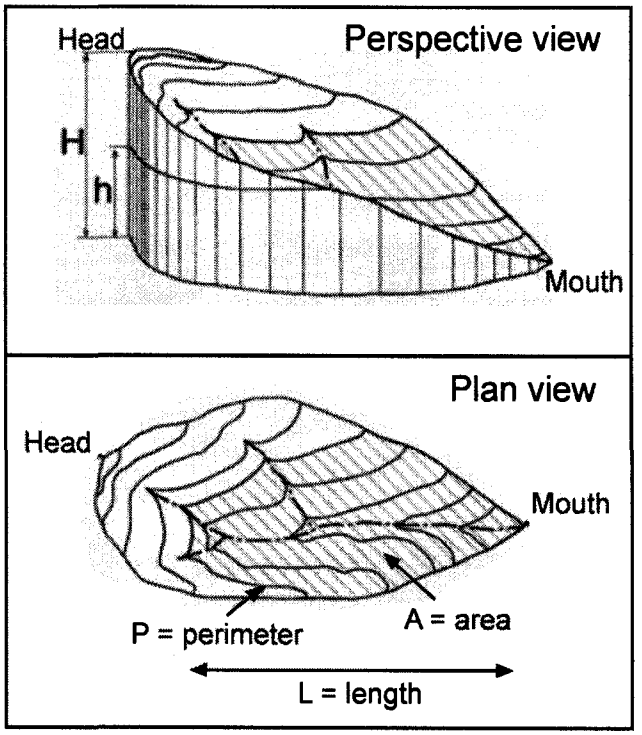

Figure 16: Schematic of the basin parameters used to compute the shape indices. The relative elevation, z, is given by $z = h/H$, H is the total relief, h is the elevation of the horizontal plane slicing the basin, A, is the area of the shaded area, L is the length of the shaded area and P is the perimeter of the shaded area. (Adapted from Luo and Howard, 2005)

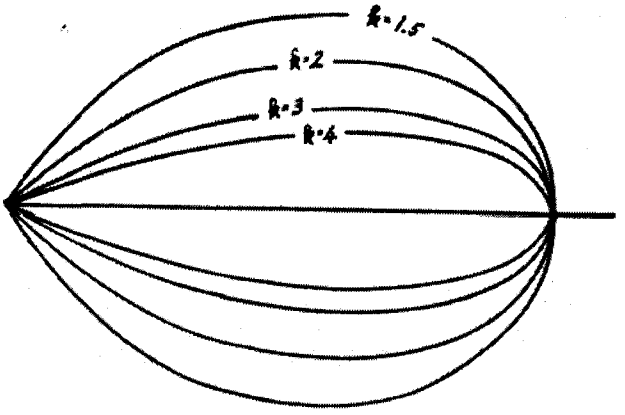

Figure 17: The effect of the lemniscate index, k, on the width of the lemniscate loop. (From Chorley, 1957)

Following the method of Luo and Howard (2005), 25 slices at equal intervals of elevation were obtained from each basin and their area, perimeter and basin length determined. These

were used to construct the four basic shape functions, such that the circularity function is given by $C(z) = [C(z_1), C(z_2), \ldots C(z_{25})]$, where $C(z_1)$ is the circularity of basin slice 1. Furthermore, the shape functions were normalized by dividing each shape function by the overall shape of the basin (shape function value at $z = 1$). Due to external geological factors, two basins with the same internal evolution of shape with elevation will have shape functions of different magnitudes if the overall shape of the two basins is different. Thus, the purpose of normalizing the basin shape functions is to "disengage the internal basin morphometry from the external basin shape" (Stepinski and Coradetti, 2004). Finally, the first and second derivatives with respect to z of the shape functions were also calculated, as it was recognized that these may contain some measure of information on a basin's structure capable of distinguishing between formation processes. The first derivative represents the slope of a given shape function and the second derivative represents the concavity, although these do not have any actual physical significance with respect to the basin. Consequently, a total of 16 shape function variables were used in subsequent statistical analyses: circularity, normalized circularity, 1st derivative of circularity, 2nd derivative of circularity, elongation, normalized elongation, 1st derivative of elongation, 2nd derivative of elongation, lemniscate index, normalized lemniscate index, 1st derivative of lemniscate index, 2nd derivative of lemniscate index, lemniscate ratio, normalized lemniscate ratio, 1st derivative of lemniscate ratio and 2nd derivative of lemniscate ratio.

4.4 Statistical Analysis of Shape Functions

4.4.1 Unsupervised classification: hierarchical clustering analysis

The statistical analysis was performed within the R-language (R Project for statistical computing, 2008), a commonly used statistical programming language based on the S syntax. To identify which shape function is best able to distinguish between the different formation processes (surface runoff from precipitation, surface runoff from meltwater, groundwater sapping), an unsupervised classification of the terrestrial basins' shape functions was performed. In unsupervised classification, the algorithm searches for natural statistical groupings in the data and the analyst must then examine the resulting classes for meaningful attributes connecting the objects in a given cluster in order to identify the classes. Although different methods of unsupervised classification exist, such as clustering (e.g. hierarchical and non-hierarchical),

neural networks and decision trees, hierarchical clustering was used in this study since the output dendrograms (binary, hierarchical trees where observations form the leaves and the two most similar observations are linked through a hypothetical common ancestor, which forms a node in the tree) facilitate the interpretation of the resulting classes. Hierarchical clustering determines successive clusters using previously established clusters. The desired outcome is for the algorithm to naturally partition the basins' shape functions based on their formation processes.

Both types of hierarchical algorithms, agglomerative and divisive (Figure 18), were used to ensure consistency in the results. Agglomerative hierarchical algorithms begin by assigning each terrestrial site to a separate cluster then successively merge the closest pair of clusters, based on a similarity criterion, until all of the sites have been grouped together (Kaufman and Rousseeuw, 2005). Of the many possible choices of similarity criteria, such as "centroid-linkage", the two similarity criteria used in this analysis were "single-linkage", where the distance between two clusters is defined as the distance between the two closest elements in each cluster, and "complete-linkage", where the distance between two clusters is defined as the distance between the two furthest elements in each cluster (Kaufman and Rousseeuw, 2005). In contrast, divisive hierarchical algorithms begin with the sites grouped as a single cluster then successively split it into smaller clusters, based on a minimum diameter criterion, until only clusters consisting of individual sites remain (Kaufman and Rousseeuw, 2005).

In summary, the output dendrograms of three hierarchical clustering algorithms available from R were compared: a complete-linkage agglomerative hierarchical clustering algorithm; a single-linkage agglomerative hierarchical clustering algorithm; and a divisive hierarchical clustering algorithm. Furthermore, the distance between clusters can be computed using several different metrics. Three metrics were compared: Euclidean, Manhattan and Maximum. As a result, 9 dendrograms (3 metrics x 3 clustering algorithms) were produced for each of the 16 shape functions. These were examined in order to determine which of the shape functions generate the best clustering based on formation process.

Given that each observation (i.e. basin shape function) is a combination of 25 individual shape index values, principal components analysis was performed to examine the effects of reducing the dimensionality of the shape functions on the hierarchical clustering results. Principal components analysis transforms (translates and/or rotates) the vector space such that the first principal component accounts for the maximum proportion of the variance and

subsequent components account for the maximum proportion of the remaining variance (Jensen, 2005). As a result, the first few principal components can be used to replace the original 25 shape index values, where each principal component is an orthogonal, uncorrelated and linear combination of the original dataset (Jensen, 2005).

In a similar spirit as principal components analysis, combinations of different shape functions were created, using the individual shape functions which produced formation process-based clusters with high overall accuracies, to determine the effects of increasing the dimensionality on the hierarchical clustering results. As long as the correlation between the shape functions is not too great (up to r = 0.9 (Tabachnick and Fidell, 1996; Hair et al., 1998)), combining them may provide additional information useful for distinguishing between basins formed by different processes. A number of different combinations were created by directly attaching shape functions together. For example, the combination of circularity and elongation is given by $CE(z) = [C(z_1), C(z_2), \ldots C(z_{25}), E(z_1), E(z_2), \ldots E(z_{25})]$. Combinations using two, three, and four shape functions were attempted as well as a combination of all sixteen shape functions. The hierarchical clustering results of the principal components and the combination of shape functions were compared to the hierarchical clustering results of the original sixteen shape functions.

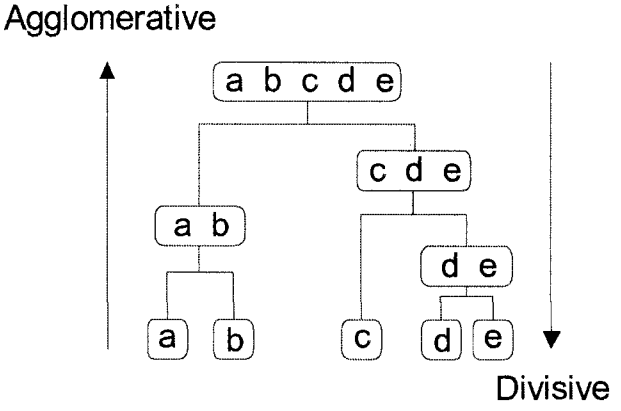

Figure 18: Schematic of the difference between agglomerative and divisive hierarchical clustering algorithms. Agglomerative algorithms begin by assigning each observation to a separate cluster then successively merge the closest pair of clusters until all observations have been grouped together into a single cluster. Divisive algorithms begin with a single cluster then successively split it into smaller clusters until each observation belongs to a separate cluster.

4.4.2 Supervised classification: k-nearest neighbour and self-organizing maps

The second step in the statistical analysis was to perform a supervised classification of the Martian basins using the shape function, principal components or combination of shape functions that generated the best formation process-based clustering of the terrestrial sites during the unsupervised classification portion of the analysis. The purpose of this step is to identify the terrestrial sites and formation processes most analogous to Mars valley networks. In supervised classification, the analyst "trains" the algorithm by specifying sample observations (i.e. shape function of a given basin) of known classes (i.e. formation process). In this case, the terrestrial basins, with their classes specified based on their known formation processes, were used as training sites. The algorithm then determines which class other observations (i.e. shape functions of the Martian basins) belong to according to a criterion determined from the classifier. For example, the maximum likelihood classifier determines the probability of an observation belonging to a given class by computing the probability density functions of the training observations and then assigns it to the class of highest probability. In summary, supervised classification determines which formation process was most likely to have created the Martian valley networks based on the similarity of the shape functions of the Martian basins to the shape functions of terrestrial basins formed by known processes.

Different methods of supervised classification include parametric (e.g. maximum likelihood), non-parametric (e.g. minimum distance to mean) and non-metric (e.g. rule-based decision trees). Parametric methods rely on the assumption that the underlying data are drawn from a Gaussian probability distribution whereas non-parametric methods make no such assumptions (Duda et al., 2001). Non-parametric methods are thus more universally applicable, whereas parametric methods have the potential of performing better when assumptions are met.

Although the distribution of the training data was expected to be normal, this could not be verified due to the statistically small sample sizes. Consequently, two non-parametric methods were used: k-nearest neighbour (KNN) and supervised self-organizing maps (SOM). The k-nearest neighbour classifier assigns the observation to the most common class of the k nearest neighbours, based on Euclidean distance, where k is a positive integer, typically small (Duda et al., 2001). The determination of the optimal value for k is essential for KNN because it should be the maximum number of neighbours with the minimum possible error (Ruiz-Jimenez et al.,

2004). Thus, k was selected based on the highest overall accuracy achieved in the validation analysis.

A self-organizing map is an unsupervised neural network technique for mapping high-dimensional data to 2D that can also be adapted and trained as a supervised classification method (Kohonen, 2005). The 2D map itself consists of a grid of nodes to which observations are mapped such that similar observations are assigned to neighbouring nodes. However, it is important to note that self-organizing maps are non-linear, that is to say, "the distance between adjacent nodes is not constant" (Stepinski and Stepinski, 2005). Additionally, the grid size is one of the most important factors in detecting the differences in the data (Scholz, 2006). If the grid size is too small, it might not explain some important differences. Conversely, if the grid size is too large, the differences will be too small (Wilppu, 1997). Thus, the SOM was trained using different grid sizes, and the optimal grid size (based on the validation analysis) was selected to perform the supervised classification of the Martian basins.

For both KNN and supervised SOM, all of the terrestrial basins were used as training sites to classify the Martian basins. Given the small sample size, a leave-one-out cross-validation was performed to evaluate the performance of both classifiers. Leave-one-out cross-validation leaves out a single observation from the original sample for validation purposes, and repeats the process for every observation in the sample. The results of the supervised Self-organizing map were compared to the results of k-nearest neighbour in order to identify the most likely formation process for the Martian valley networks based on the formation process class most often assigned to them by the supervised classification process.

5. Results

5.1 Basin Shape Functions

Sixteen shape functions, representing the change of a basin's shape with respect to elevation, were produced for each terrestrial and Martian basin (Appendix C). Qualitatively, the change in shape with elevation can be observed from the relative elevation data of each site presented in section 4. As discussed in section 6.2, regional slope has an important effect on a basin's shape function. Consequently, Figure 19 compares the four basic shape functions of the Martian basins (averaged from the 23 Martian sites) to five terrestrial classes: steep sapping, flat sapping, steep runoff, flat runoff and flat meltwater.

The circularity function of flat sapping, flat runoff and flat meltwater basins is concave upwards with an inflexion point near the higher reaches of the basin leading to a flattening in the curve (Figure 19,). This type of curve describes a "mature fluvial landscape with topography conforming to the drainage" (Stepinski and Stepinski, 2005), where the basin is very elongated in the lower reaches, becomes more circular as the intensity of erosion diminishes with lower-order streams, then maintains a near-constant shape beyond the reaches of the streams until the edge of the drainage basin. In contrast, the circularity function of steep sapping and steep runoff basins is nearly linear, increasing with relative height, z, indicating that steep basins gradually become more circular with elevation.

The elongation function has a similar character to the circularity function (Figure 19). As with the circularity function, the elongation function of flat basins is concave upwards in the lower reaches of the basin then flattens out in the upper reaches, whereas the elongation of steep basins is nearly constant throughout the range of elevations. This similarity is expected since both circularity and elongation compare certain basin parameters to those of a circle (area in the case of circularity and diameter in the case of elongation).

The lemniscate index function indicates that flat basins are initially much narrower than steep basins (Figure 19). The high lemniscate index values are once again due to the topography conforming to the drainage.

Figure 19 shows that the lemniscate ratio function for flat basins is concave upwards with a defined minimum near $z = 0.3$ for runoff and sapping basins and near $z = 0.7$ for meltwater basins. Flat basins are initially similar in shape to a lemniscate loop, becoming less so in the

middle reaches, then returning to a lemniscular shape in the upper reaches. The lemniscate ratio function for steep basins on the other hand is nearly linear, increasing with z, indicating that the basins steadily become more lemniscular in shape at progressively higher elevations.

Overall, the distinction between flat terrestrial basins and steep terrestrial basins is noticeable for all four shape functions, although the distinction between the various formation processes is not clear. Qualitatively, it appears that the shape functions of the Martian basins are most similar to steep terrestrial basins.

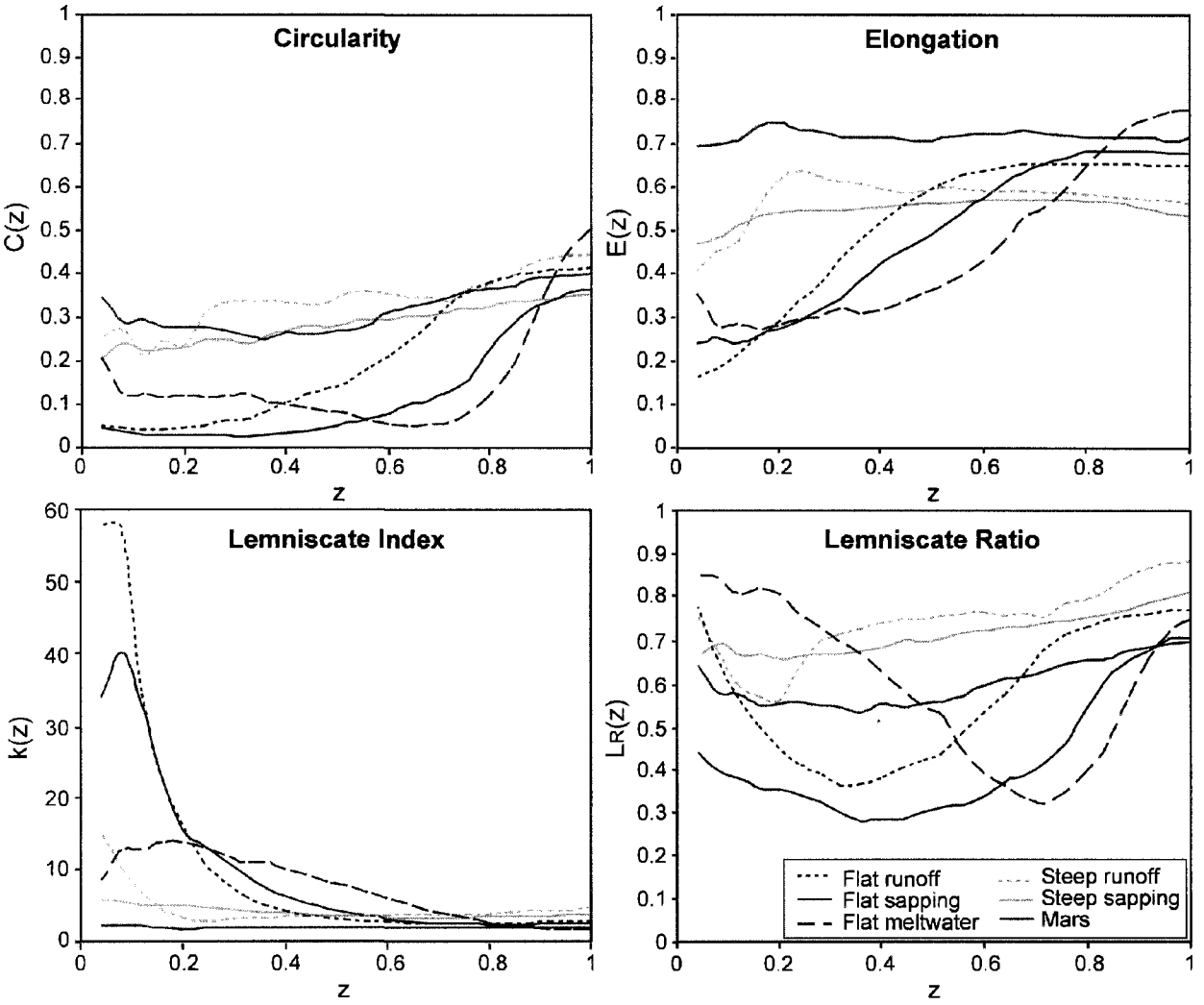

Figure 19: Four basic shape functions (circularity, elongation, lemniscate index and lemniscate ratio) of 6 classes: Flat surface runoff basins, flat groundwater sapping basins, flat meltwater basins, steep surface runoff basins, steep groundwater sapping basins and Martian basins.

5.2 Hierarchical Clustering Analysis

Hierarchical clustering of the terrestrial basins was performed using each of the 16 shape functions. For a given shape function, the algorithm outputs a dendrogram, clustering together similar basins. The resulting clusters were examined in order to identify meaningful attributes connecting the basins within a cluster. In this case, the dendrogram for each of the shape function variables were examined to determine their ability to cluster the basins according to their formation processes. Three clustering algorithms and three distance metrics were compared to ensure that the clustering results were consistent.

When all of the terrestrial basins were entered into the hierarchical clustering algorithms, the primary observation from the majority of the shape functions was that the basins were being clustered based on the regional slope of the sites (i.e. steep vs. flat), rather than by the formation process of the basins (Figure 20: for simplicity, a single representative dendrogram for each of the four basic shape functions is shown). None of the 16 shape functions were able to successfully cluster the basins according to their formation process. Even the normalized shape functions were unable to correct for the differences in shape due to slope. Of the 16 shape functions, the circularity function proved to be the most effective at separating flat and steep basins, based on the three clustering algorithms and the three metrics used (Table 3). The circularity function generally produced two to three clusters separating flat basins from steep basins with an average overall accuracy (percentage of properly classified observations) of 91.7 $\pm$ 1.2 % and an average Kappa coefficient of 0.83 $\pm$ 0.02. The Kappa coefficient represents the proportion of agreement obtained after accounting for the proportion of agreement that could be expected to occur by chance (Foody, 1992).

In accordance with Table 1, the first order effects of regional slope in the clustering results were removed by separating the terrestrial basins into flat ($< 3°$) and steep ($> 3°$) sites for subsequent analysis.

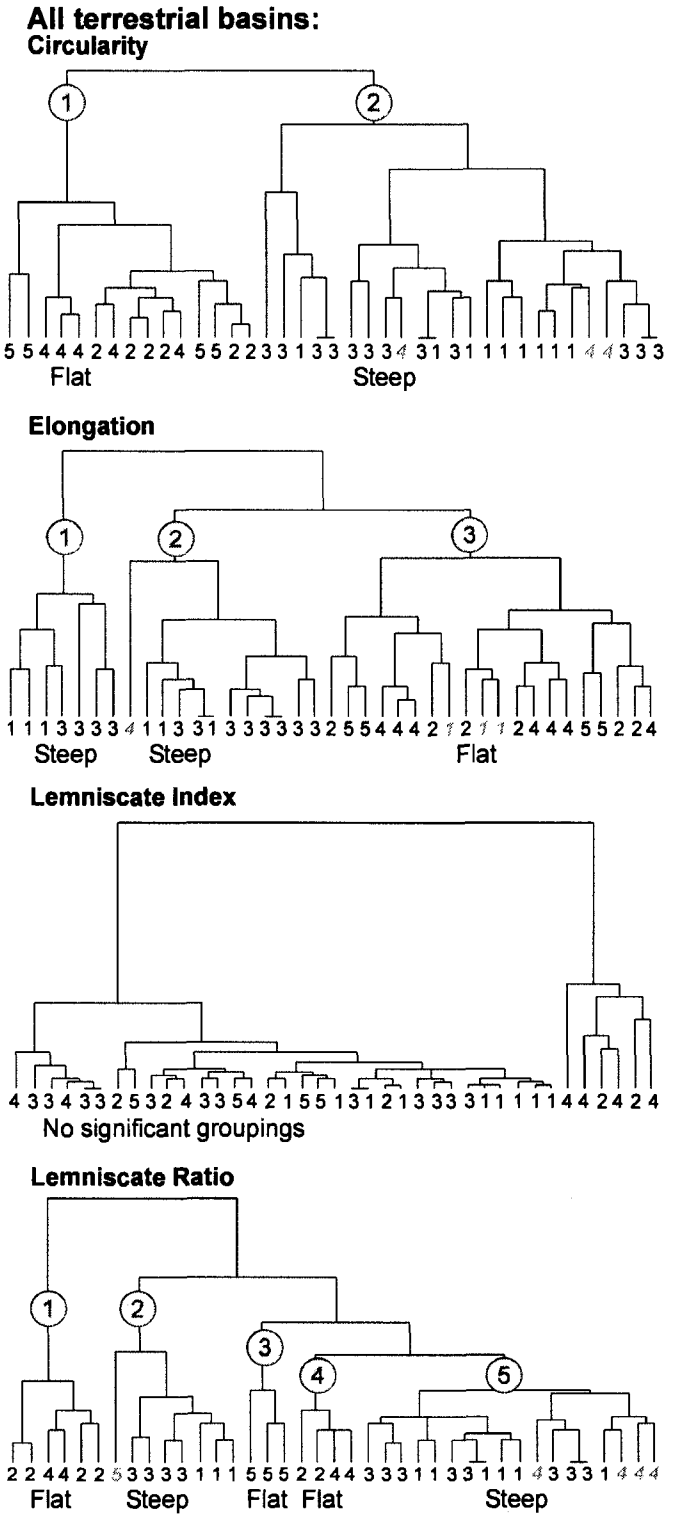

Figure 20: Unsupervised hierarchical clustering of the shape functions of all of the terrestrial basins. The basins are clustered primarily based on the regional slope of the sites. 1: steep groundwater sapping; 2: flat groundwater sapping; 3: steep surface runoff; 4: flat surface runoff; 5: flat meltwater

Table 3: Average overall accuracy and Kappa coefficient of the 16 shape functions for classifying basins into steep vs. flat classes

Shape Function	Average Overall Accuracy (%)	Average Kappa Coefficient
Circularity		
Basic	91.7 ± 1.2	0.83 ± 0.02
Normalized	88.9 ± 1.8	0.77 ± 0.04
1st derivative	75.8 ± 2.5	0.52 ± 0.05
2nd derivative	NA	NA
Elongation		
Basic	88.3 ± 3.2	0.77 ± 0.07
Normalized	86.9 ± 2.7	0.73 ± 0.05
1st derivative	79.5 ± 3.1	0.59 ± 0.06
2nd derivative	NA	NA
Lemniscate Index		
Basic	NA	NA
Normalized	NA	NA
1st derivative	NA	NA
2nd derivative	NA	NA
Lemniscate Ratio		
Basic	86.5 ± 1.2	0.73 ± 0.03
Normalized	89.9 ± 4.1	0.79 ± 0.08
1st derivative	88.1 ± 6.1	0.76 ± 0.12
2nd derivative	NA	NA

Once the terrestrial basins were divided into two separate groups based on their regional slope (flat vs. steep), some shape functions were able to successfully cluster the basins according to their formation process (Figure 21). In the case of flat basins, the first derivative of the lemniscate ratio function proved to be the most effective at distinguishing between basins formed by different processes, based on the three clustering algorithms and the three metrics used (Table 4). The first derivative of the lemniscate ratio function generally produced three clusters separating flat basins formed by surface runoff, groundwater sapping and meltwater with an average overall accuracy of 85.7 ± 3.0% and an average Kappa coefficient of 0.78 ± 0.04. In the case of steep basins, the circularity shape function proved to be the most effective at distinguishing between basins formed by different processes, based on the three clustering algorithms and the three metrics used (Table 5). The circularity shape function generally produced three to five clusters separating steep basins formed by surface runoff and groundwater sapping with an average overall accuracy of 85.2 ± 1.6% and an average Kappa coefficient of 0.69 ± 0.03.

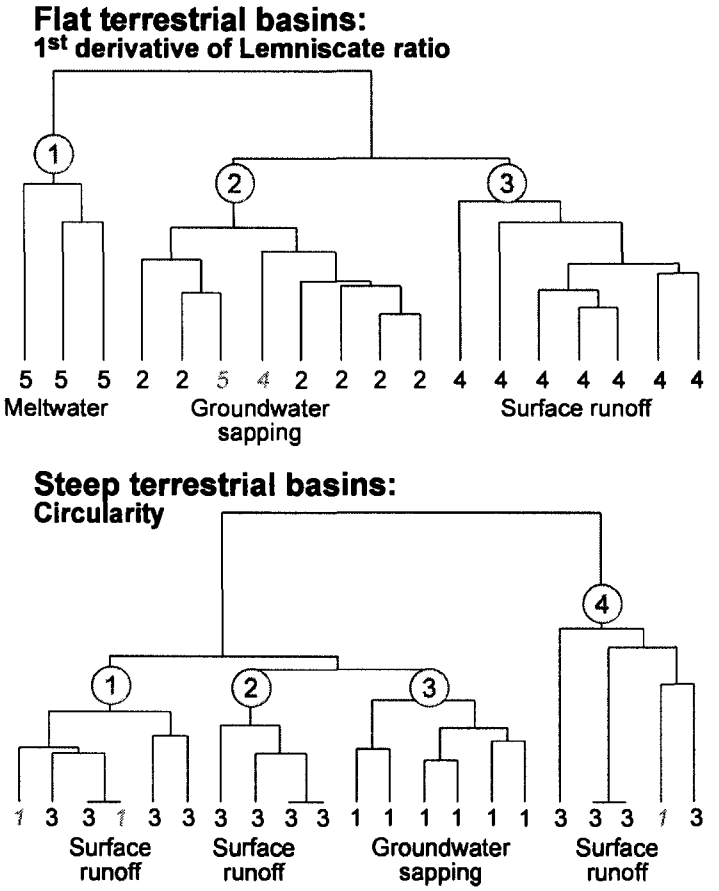

Figure 21: Unsupervised hierarchical clustering of the shape functions of flat and steep terrestrial basins. The basins are successfully clustered based on formation process. 1: steep groundwater sapping; 2: flat groundwater sapping; 3: steep surface runoff; 4: flat surface runoff; 5: flat meltwater

Table 4: Average overall accuracy and Kappa coefficient of the 16 shape functions for classifying flat basins based on formation process

Shape Function	Average Overall Accuracy (%)	Average Kappa Coefficient
Circularity		
Basic	NA	NA
Normalized	NA	NA
1st derivative	NA	NA
2nd derivative	NA	NA
Elongation		
Basic	NA	NA
Normalized	NA	NA
1st derivative	NA	NA
2nd derivative	NA	NA
Lemniscate Index		
Basic	NA	NA
Normalized	NA	NA
1st derivative	NA	NA
2nd derivative	NA	NA
Lemniscate Ratio		
Basic	75.0 ± 3.0	0.61 ± 0.05
Normalized	76.9 ± 5.5	0.64 ± 0.09
1st derivative	85.7 ± 3.0	0.78 ± 0.04
2nd derivative	NA	NA

Table 5: Average overall accuracy and Kappa coefficient of the 16 shape functions for classifying steep basins based on formation process

Shape Function	Average Overall Accuracy (%)	Average Kappa Coefficient
Circularity		
Basic	85.2 ± 1.6	0.69 ± 0.03
Normalized	83.9 ± 2.5	0.67 ± 0.05
1st derivative	NA	NA
2nd derivative	NA	NA
Elongation		
Basic	NA	NA
Normalized	NA	NA
1st derivative	79.8 ± 5.5	0.58 ± 0.11
2nd derivative	NA	NA
Lemniscate Index		
Basic	79.4 ± 2.4	0.58 ± 0.04
Normalized	NA	NA
1st derivative	NA	NA
2nd derivative	NA	NA
Lemniscate Ratio		
Basic	NA	NA
Normalized	NA	NA
1st derivative	NA	NA
2nd derivative	NA	NA

Using principal components analysis, the dimensionality of the shape functions was reduced from 25 slices to 3 principal components representing more than 90% of the total variance. However, based on the three clustering algorithms and the three metrics used, hierarchical clustering of the principal components was essentially identical to the original classification using the full dimensionality of the shape functions. The principal components of the circularity function for all of the terrestrial basins generally produced two to four clusters separating flat basins from steep basins with an average overall accuracy of 91.7 ± 4.2 % (no change relative to the original classification using the circularity function) and an average Kappa coefficient of 0.83 ± 0.08 (Figure 22). The principal components of the 1st derivative of the lemniscate ratio function for the flat terrestrial basins subset generally produced three clusters separating basins formed by surface runoff, groundwater sapping and meltwater with an average overall accuracy of 84.6 ± 5.4% (decrease of 1.1% relative to the original classification using the first derivative of the lemniscate ratio function) and an average Kappa coefficient of 0.76 ± 0.08 (Figure 22). The principal components of the circularity function for the steep terrestrial basins subset

generally produced three to five clusters separating basins formed by surface runoff, groundwater sapping and meltwater with an average overall accuracy of 84.7 ± 2.1% (decrease of 0.5% relative to the original classification using the circularity function) and an average Kappa coefficient of 0.67 ± 0.04 (Figure 22).

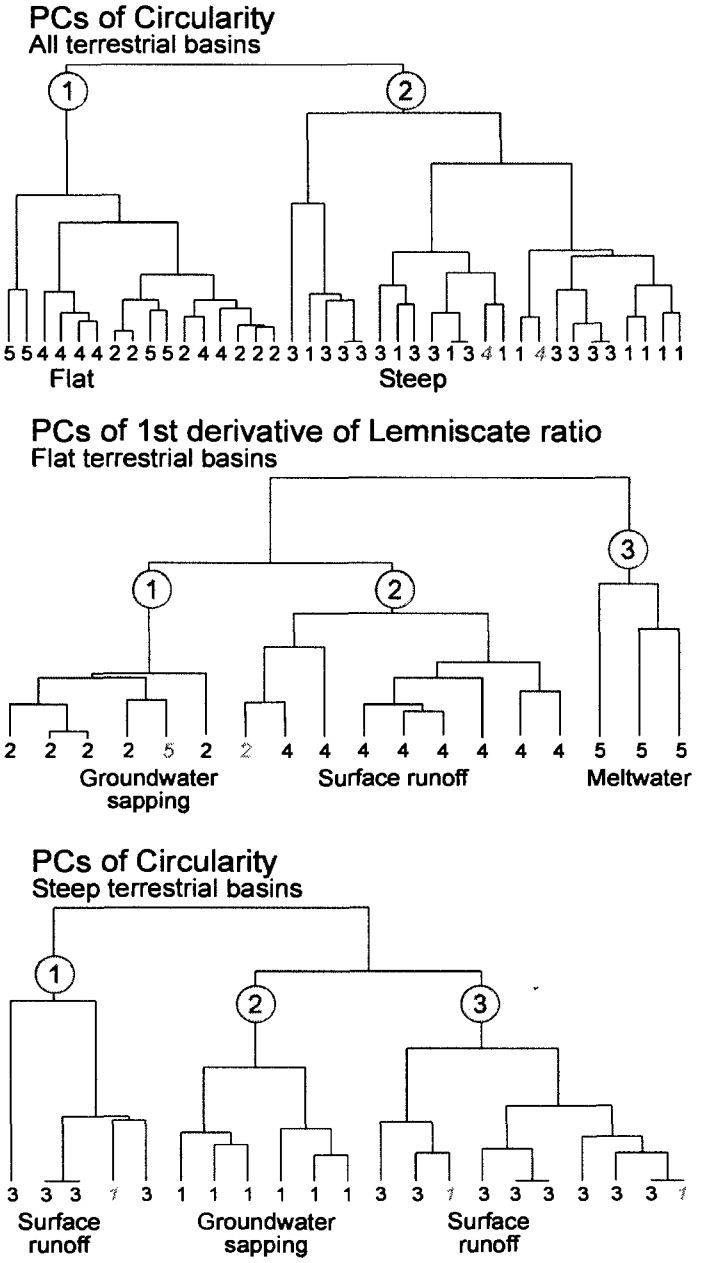

Figure 22: Unsupervised hierarchical clustering of the principal components of the shape functions of terrestrial basins. The basins are clustered similarly to the original shape functions. 1: steep groundwater sapping; 2: flat groundwater sapping; 3: steep surface runoff; 4: flat surface runoff; 5: flat meltwater

Since more than one shape function originally showed promising clustering results, it was expected that combining these shape functions could result in higher accuracy clusters. However, increasing the dimensionality of the shape functions also produced essentially identical results to the original classification. In the case of all the terrestrial basins (both steep and flat), the combination of the circularity and elongation functions ($r = 0.65$, p-value $< 2.2 \times 10^{-16}$) proved to be the most effective and produced three clusters separating steep basins and flat basins with an average overall accuracy of 92.0 ± 2.4% (increase of 0.3% relative to the original classification using the circularity function) and an average Kappa coefficient of 0.84 ± 0.05 (Figure 23). In the case of flat basins, the combination of the first derivative of the lemniscate ratio and the first derivative of elongation functions ($r = 0.13$, p-value = 0.01) proved to be the most effective and produced three clusters separating flat basins formed by surface runoff, groundwater sapping and meltwater with an average overall accuracy of 86.8 ± 7.2% (increase of 1.1% relative to the original classification using the first derivative of the lemniscate ratio function) and an average Kappa coefficient of 0.80 ± 0.11 (Figure 23). In the case of steep basins, the combination of the circularity and the first derivative of the lemniscate ratio functions ($r = 0.23$, p-value = 4×10^{-7}) proved to be the most effective and produced three to five clusters separating steep basins formed by surface runoff and groundwater sapping with an average overall accuracy of 85.7 ± 0.0% (increase of 0.5% relative to the original classification using the circularity function) and an average Kappa coefficient of 0.7 ± 0.0 (Figure 23).

The classification accuracy for both PCA and the shape function combinations did not significantly change compared to the accuracy of the original classification. As a result, the most effective shape functions from the original unsupervised classification (all terrestrial basins: circularity; flat terrestrial basins: 1st derivative of lemniscate ratio; and steep terrestrial basins: circularity) were used for the supervised classification portion of the analysis.

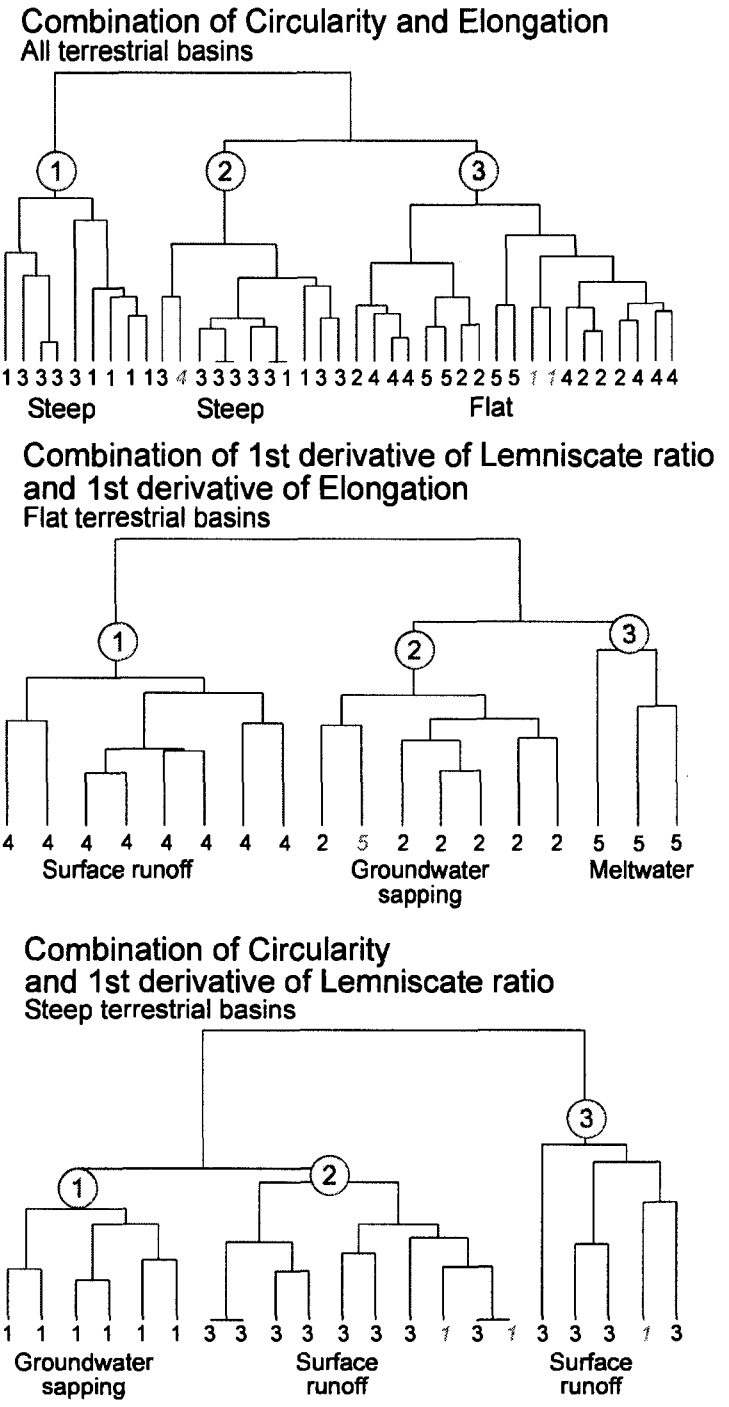

Figure 23: Unsupervised hierarchical clustering of the combinations of the shape functions of terrestrial basins. The basins are clustered similarly to the original shape functions. 1: steep groundwater sapping; 2: flat groundwater sapping; 3: steep surface runoff; 4: flat surface runoff; 5: flat meltwater

5.3 k-Nearest Neighbour and Supervised Self-Organizing Maps

The k-nearest neighbour (KNN) and supervised self-organizing map (SOM) classifiers were used to classify the Martian basins using the terrestrial basins as training sites. A number of classifications were performed and evaluated using leave-one-out cross-validation to determine the optimal number of neighbours for KNN and the optimal grid size for supervised SOM. For the k-nearest neighbour classifier, the optimal number of neighbours was $k = 3$. For supervised SOM, since the number of grid nodes cannot exceed the number of observations, the grid size was set to the maximum allowable square grid (dependant upon the number of training sites).

To determine whether Martian valley networks can be classified as either steep or flat, the circularity shape functions of all of the terrestrial basins were used as training for the supervised classification. For both classifiers, the majority of the Martian valley networks were classified as steep (Table 6). The overall accuracy for both classifiers was 92.3% and the Kappa coefficient was 0.85.

Since the Martian valley networks were classified as steep, the circularity function of the steep terrestrial basins subset was used as training to determine whether Martian valley networks are more similar to the terrestrial groundwater sapping basins or the surface runoff basins. In both KNN and supervised SOM, the majority of the Martian basins were assigned to the groundwater sapping class (Table 6). For KNN, the overall accuracy was 76.2% and the Kappa coefficient was 0.51, whereas for supervised SOM, the overall accuracy was 81.0% and the Kappa coefficient was 0.61.

Table 6: KNN and supervised SOM of Martian valley networks using terrestrial basins as training sites. GW: groundwater sapping; R: surface runoff

Shape function:	**Circularity**		**Circularity**	
Training Sites:	**all terrestrial basins**		**steep terrestrial basins**	
Method:	**KNN, k=3**	**SOM, 6x6 grid**	**KNN, k=3**	**SOM, 6x6 grid**
Leave-one-out	**Acc=92.3%**	**Acc=92.3%**	**Acc=76.2%**	**Acc=81.0%**
cross-validation:	**Kappa=0.85**	**Kappa=0.85**	**Kappa=0.51**	**Kappa=0.61**
Mars basin				
1	Steep	Steep	GW	GW
2	Steep	Steep	GW	GW
3	Steep	Steep	GW	GW
4	Steep	Steep	GW	GW
5	Steep	Steep	GW	GW
6	Flat	Flat	R	GW
7	Steep	Steep	GW	GW
8	Steep	Steep	GW	GW
9	Steep	Steep	R	R
10	Flat	Steep	GW	GW
11	Steep	Steep	R	R
12	Flat	Flat	GW	GW
13	Steep	Steep	GW	GW
14	Steep	Steep	GW	GW
15	Steep	Steep	GW	GW
16	Steep	Steep	GW	GW
17	Steep	Steep	R	R
18	Steep	Steep	GW	GW
19	Steep	Steep	GW	GW
20	Steep	Steep	R	R
21	Steep	Steep	GW	GW
22	Steep	Steep	R	R
23	Steep	Steep	R	R

Furthermore, using the unsupervised self-organizing map itself, the individual terrestrial basins most similar to the Martian basins can be identified by comparing their ensemble of shape functions. The unsupervised self-organizing map in Figure 24 was constructed using a combination of all four of the basic shape functions (circularity, elongation, lemniscate index and lemniscate ratio) so that the entire character of the basins could be compared. The results of both the supervised and unsupervised classifications are reflected in this map. For example, the division between flat terrestrial basins and steep terrestrial basins is evident. Also, due to their proximity, the Martian basins appear to be most similar to the steep terrestrial basins, in particular the steep groundwater sapping basins of Chile.

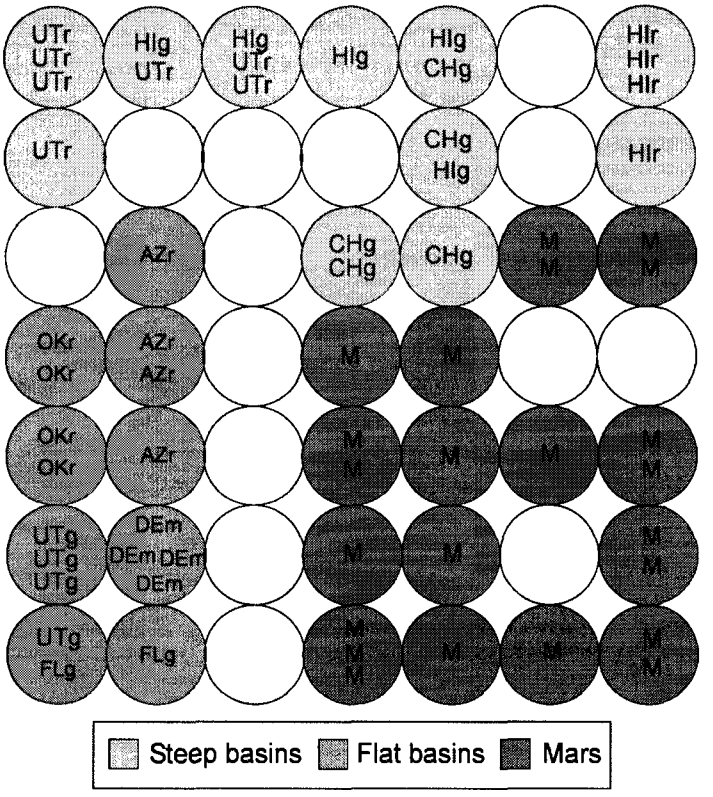

Figure 24: Unsupervised SOM map similarity of study basins using a combination of the four basic shape functions (circularity, elongation, lemniscate index, lemniscate ratio). AZr: Arizona surface runoff; CHg: Chile groundwater sapping; DEm: Devon meltwater; FLg: Florida groundwater sapping; HIg: Hawaii groundwater sapping; HIr: Hawaii surface runoff; M: mars; OKr: Oklahoma surface runoff; UTg: Utah groundwater sapping; UTr: Utah surface runoff

6. Discussion

6.1 Controls on Basin Morphometry

The results of the hierarchical clustering of the terrestrial basins corroborate with the findings of Luo and Howard (2005) who showed that it is possible to distinguish between basins formed by different processes on the basis of their normalized circularity shape functions. However, this study indicates that the regional slope of a basin exerts a stronger control on a basin's internal shape than the formation process itself. This can be seen qualitatively from the shape function curves (Figure 19), where the terrestrial basins can be more easily distinguished based on the steepness of the site than by their formation process. It is only once the terrestrial basins are separated into steep and flat groups that the formation process becomes distinguishable via the use of their shape functions. The effect of regional slope on the shape of a basin is understandably significant because basins that evolve along steep slopes do not have as many lateral degrees of freedom and tend to be narrower than basins that evolve along flat slopes. Consequently, the differences in basin shape due to various formation processes (e.g. surface runoff vs. groundwater sapping) tend to be more evident in flat basins than in steep basins.

The controlling effect of slope and formation process on the shape of a basin is complementary to the findings of Stepinski and Stepinski (2005) who showed that terrestrial basin morphometry (based on the normalized circularity function) correlates with climate (based on annual precipitation rates (mm/year)). Using hierarchical clustering and a self-organizing map, Stepinski and Stepinski (2005) classified 46 Andean basins as wet, moderate or dry. The basins used in their study were mainly formed by surface runoff (with the exception of three Atacama Desert basins that were formed by groundwater sapping) and all have similar steep regional slopes and lithology. It is therefore suggested that the slope, formation process and annual precipitation rates, respectively, each contribute a diminishing amount of control on a basin's morphometry. Future studies should investigate the effect of lithology on basin shape as rock type, permeability, and stratigraphy all influence drainage basin development (Craddock and Howard, 2002).

6.2 Statistical Analysis of Basin Shape Functions

The most effective shape function for describing basin morphometry is dependent upon the purpose. For example, the circularity and elongation shape functions were the most effective at clustering basins according to the steepness of the site; whereas the lemniscate ratio shape function and the circularity and lemniscate index shape functions were the most effective at clustering flat and steep basins, respectively, according to their formation process.

In the case of all the terrestrial basins, the Hawaii surface runoff basins had the tendency to form a third cluster, visible in the dendrograms and unsupervised SOM, and separate from the main clusters that divide the steep and flat basins. This third cluster may be due to the much higher regional slope of the Hawaiian basins (6.5° and 9.5°, Table 1), thus clustering them into their own individual slope class. For the flat basins subset, the number of clusters (3) is consistent with the number of classes (i.e. meltwater, surface runoff and groundwater sapping). The number of clusters for the steep basins (3 to 5), on the other hand, is inconsistent with the number of classes (i.e. surface runoff and groundwater sapping). The average overall accuracy for the classification of the flat and steep basins may be similar; however, considering that steep basins tend to form a series of small clusters, the formation process-based classification of the steep basins is not as clear as it is for the flat basins.

Following the work of Stepinski and Coradetti (2004), Stepinski and Stepinski (2005) and Luo and Howard (2005) who used normalized circularity functions in their studies, the shape functions in this study were also normalized to remove the differences in shape function magnitude due to a basin's overall shape. In theory, normalization should allow for a direct comparison of the internal evolution of the shape of a basin due to the formation process. However, in many cases, the overall accuracy of the hierarchical clustering of the non-normalized shape functions was higher than that of the normalized ones. As such, it appears that normalizing the shape functions may not always be the best approach. For example, depending on the shape function and the formation processes in question, the difference between the shape functions of basins with different overall shapes may be smaller than the difference between the shape functions of basins formed by different processes. In these situations, normalization actually prevents the detection of the inherent differences due to the formation processes.

In addition to the normalized shape functions, the 1st and 2nd derivatives were computed to determine if these contained additional information that could be used to identify a basin's formation process. This proved to be the case, since the 1st derivative of the lemniscate ratio was the most effective shape function for distinguishing between the formation processes of the flat terrestrial basins. It is also feasible to expect that other such transformations may provide favorable results. For example, the elongation shape function was effective at separating flat and steep basins, but was not able to distinguish between the formation processes of steep basins. On the other hand, the lemniscate index shape function was unable to adequately distinguish between flat and steep basins, but was effective at distinguishing between the formation processes of steep basins. Yet, it should be pointed out that these two functions are merely squared reciprocals of each other.

Reducing the dimensionality of the shape functions using PCA did not produce any significant changes in the classification accuracy and no additional information was gained. However, considering the statistically small dataset used in the analysis, this is not surprising. In PCA, an insufficient sample size results in unstable loadings (Cliff, 1970), random, non-replicable factors (Aleamoni, 1976; Humphreys et al., 1969), and lack of generalizability to the population (Osborne and Costello, 2004). Several studies have reviewed the effect of sample size on PCA. Recommendations for the absolute minimum sample size may range from 50 (Barrett and Kline, 1981) to 400 (Aleamoni, 1976). Alternatively, some authors focus on the ratio of the number of observations to the number of variables. Nunnally (1978) recommends a minimum observation to variable ratio of at least 10:1 in exploratory factor analysis (EFA) (Osborne and Costello (2004) note that EFA results should be generalizable to PCA). "Although the ratio of observations to variables is an important predictor of the goodness of a PCA, it appears that as the total number of observations increases, this ratio becomes less important (the converse is also true: as the ratio of observations to variables increases, the total number of observations becomes less important) (Osborne and Costello, 2004)". In light of these studies, PCA may have proven useful if a larger number of basins had been included in the analysis, although undertaking this analysis with hundreds of basins would be very time-consuming.

Similarly, increasing the dimensionality of the shape functions by combining different shape functions did not produce any significant changes in the classification accuracy of the hierarchical clustering analysis. The slight increase in the accuracy came at the cost of an

increase in the standard deviation of the overall accuracy because the clustering results were less consistent. In some cases (e.g. for a given clustering algorithm), the combination of certain shape functions produced a much higher accuracy than the original classification, but this was not consistent across the three algorithms and the three metrics used. Several combinations of variables were tested, including double, triple and quadruple combinations of the individual shape functions that produced high overall accuracies, as well as a combination of all 16 of the shape functions. However, combinations of two shape function variables proved to be the best approach.

For the supervised classification portion of the analysis, the accuracy was determined using leave-one-out cross-validation. This method is computationally expensive but supplies an almost unbiased estimate of the true classification error (Sommer and Golz, 2005). However, considering that the classifier was trained from a small sample using several basins from the same terrestrial sites as the basin left out for validation, the classification accuracy is expected to be somewhat inflated. For a true representation of the classification accuracy, it would be necessary to use a larger and more diversified set of terrestrial basins. In this case, the supervised SOM and KNN were both equally effective at classifying terrestrial basins into their respective steep and flat classes (Table 1). Additionally, although the supervised SOM appears to have out-performed the KNN classifier in classifying steep terrestrial basins according to their formation process, the difference in accuracy is due to a single basin. Overall, the performance of both classifiers was very similar and the conclusions from the classification of the Martian valley networks were the same.

6.3 Origins of Martian Valley Networks

From the supervised classification of the shape functions (Table 6), it appears that the Martian valley networks are most similar to steep terrestrial groundwater sapping basins. In particular, as seen from the unsupervised SOM (Figure 24) Stepinski and Coradetti (2004) and Stepinski and Stepinski (2005), Martian valley networks are most similar to the Chilean Atacama Desert basins. However, a few problems arise from these results. Firstly, although the Martian basins were classified as steep, the regional slope of all the Martian basins in this study is in actuality very low ($\leq 1.3°$; Table 1). Secondly, as seen from the SOM and the studies of

Stepinski and Coradetti (2004) and Stepinski and Stepinski (2005), the Martian basins do not intermingle with the terrestrial basins, suggesting that there is a fundamental difference between the shape functions of terrestrial and Martian basins. These discrepancies can not be attributed to the use of shape functions to identify the formation process of the Martian valley networks, as it was demonstrated in this study that shape functions are able to distinguish between the formation processes of terrestrial basins. Since the interpretation of the origins of the valley networks is conditioned by the choice of training sites, it is possible that the Martian valley networks were formed by a different process not considered in this study. However, the formation processes included in this study make up the most widely held hypotheses on the origins of valley networks. The most likely explanation is that additional factors may have exerted a stronger control on the shape of the Martian valley networks than either formation process or slope. These factors may play a role in the case of the Martian basins but not in the terrestrial basins or simply might not have been present in the investigated terrestrial sites (e.g. cratering, differences in lithology). Consequently, the direct use of terrestrial shape functions to identify the origins of Martian valley networks might produce misleading results. However, the investigation into the similarity of the shape functions of the Martian basins to those of the Chilean Atacama Desert basins and the environment under which they were formed might shed some light into the origins of the Martian valley networks.

The Chilean Atacama Desert groundwater sapping basins and Martian basins both have shape functions that "do not display any systematic behaviour and stay approximately constant for the entire range of z" (Stepinski and Coradetti, 2004). This is a result of the topography's non-conformance with the drainage. Since, the longitudinal profiles of the Chilean and Martian basins are nearly linear (with the slope indicated in Table 1), as opposed to the more typical concave upwards profiles of terrestrial drainage basins, this suggests that erosion was restricted to the channels themselves and did not impact the rest of the basins' topography. For the Chilean basins, this may be attributed to a combination of the intermittent and scarce precipitation (Stepinski and Coradetti, 2004), the groundwater sapping, and the steepness of the regional slope. Stepinski and Coradetti (2004) and Stepinski and Stepinski (2005) postulated that the similarity of the shape functions of the Martian basins to those of the Atacama Desert basins might have been due to a similarity in climate (scarce, intermittent precipitation). However, the reasons for the similarity between the shape functions of the basins of these two sites essentially

come down to two options: 1) considering the age of the Martian valley networks, the topography may have been modified since their formation (i.e. the topography was initially conformant with the drainage) or 2) the Martian valley networks formed under conditions such that there was little erosion of the topography of the surrounding basin. In the first scenario, the topography of the Martian basins may have been eroded by mass wasting, cratering, and/or cryogenic processes. Additionally, the deposition of impact ejecta, volcanic and/or aeolian sediments may have smoothed the relief of the basins. However, studies by Williams and Philips (2001) showed that infilling and mass wasting processes have not greatly altered the original shape of Martian valleys, consistent with the < 20 m of infill in Martian valleys estimated by Goldspiel et al. (1993) and ~ 10 m of infill in topographic lows in the Martian highlands estimated by Craddock et al. (1997). As such, future work should investigate the effects of post-formational impact cratering on basin shape. In the second scenario, the implications are that the erosional mechanics that formed the Martian valley networks were different from those that formed typical terrestrial basins. This could be the result of different geological or climate conditions. It could also be the result of cratering processes occurring simultaneously with valley network formation as "simulation modeling shows that impact events could have frustrated valley network development as the drainage area was constantly evolving" (Craddock and Howard, 2002). Therefore, future studies should investigate the effect of basin formation in cratered terrain on basin shape, the effect of lithology on basin shape, and "whether intermittency of precipitation alone is sufficient to account for the anomalous morphometry of the Martian basins" (Stepinski and Coradetti, 2004) or "whether aridity is a dominant factor" (Stepinski and Stepinski, 2005).

Finally, recent findings from the Microscopy, Electrochemistry and Conductivity Analyzer (MECA) instrument onboard NASA's Phoenix Mars Lander (NASA, 2008a) have revealed the presence of substantial amounts of perchlorate in the soil of the northern polar region of Mars. Perchlorate is a highly reactive hydrophilic salt that, when dissolved in water, increases its density to as high as ~ 1.7 g/cm^3 (Besley and Bottomley, 1969) and reduces its freezing point to as low as 205K (Pestova et al., 2005). Of notable interest, because perchlorate is so soluble in water, on Earth it is found most abundantly in the surface soils of Chile's hyperarid Atacama Desert (NASA, 2008b). If the discovery of ~ 1% perchlorate by Phoenix is representative of all of Mars, or at least a significant portion, then it could have important implications on the past

Martian climate and valley network formation. The need for warm conditions to form Martian valley networks by certain processes would no longer be necessary if water containing dissolved perchlorate with a freezing point of as low as 205K was made available. In addition, given that bedrock erosion is generally assumed to be proportional to stream power (Ω), which is expressed by:

$$\Omega = \rho g Q S \qquad (5)$$

where ρ is the density of water, g is the acceleration due to gravity, Q is the discharge and S is the channel slope (Carter and Anderson, 2006), the power of a stream to erode into bedrock is directly proportional to the density of water. Consequently, the high density of water containing dissolved perchlorate would be much more effective at carving out deep channels, even given a water source with a lower availability. As such, future studies on the erosional mechanics of Martian valley networks would need to take into account the possibility that the eroding fluid might have been denser and possessed a lower freezing point than pure water.

7. Conclusions

In this study, it was shown that shape functions are useful morphometric parameters for distinguishing between some of the geomorphic properties of basins. In particular, the analysis showed that it is possible to use basin shape functions to distinguish between basins formed by groundwater sapping, surface runoff and meltwater. However, the first-order effect on the shape functions of basins was attributed to regional slope, as it appears that slope exerts a stronger control on a basin's shape than other factors, such as climate and formation process.

Secondly, the shape functions of Martian basins were characterized using the shape functions of terrestrial basins formed by known processes. The Martian basins were classified as steep groundwater sapping basins. However, a few caveats must be considered with regard to extending the use of shape functions to characterize Martian valley networks. Firstly, despite the first order effect of slope on terrestrial basin shape and the low regional slope of the Martian basins considered in this study, the Martian valley networks were classified as "steep". In addition, in the unsupervised self-organizing map of the Martian and terrestrial basins, the Martian basins do not intermingle with the terrestrial basins. This lack of interaction suggests that there are fundamental differences between the shape functions of terrestrial and Martian basins that have not been considered. Consequently, the direct use of terrestrial shape functions to identify the origins of Martian valley networks should be undertaken with care.

Despite these caveats, the similarity between the shape functions of the Martian valley networks and those of the Atacama Desert basins of Chile may shed some light onto the origins of the Martian systems. Both of these sites have linear longitudinal profiles and shape functions that stay approximately constant throughout the basin, suggesting that erosion was restricted to the channels themselves. As such, possible reasons for the character of the Martian valley network shape functions include groundwater sapping, a combination of intermittent and scarce precipitation, impact cratering, differences in geologic setting and differences in the erosional mechanics that formed the Martian valley networks due to the possible effects of perchlorate on the freezing point and density of water on Mars.

Consequently, future studies should investigate the effect of lithology, climate, cratering processes (both concurrent with and post valley network formation), and the erosional mechanics of a fluid denser and with a lower freezing point than pure water.

References

Abrahams, A.D., 1984, Channel Networks: A geomorphological perspective, Water Resources Research, Vol. 20, pp. 161-168

Aleamony, L.M., 1976, The relation of sample size to the number of variables in using factor analysis techniques, Educational and Psychological Measurement, Vol. 36, pp. 879-883

Baker, V.R., and J.B. Partridge, 1986, Small Martian valleys: Pristine and degraded morphology, Journal of Geophysical Research, Vol. 91, pp. 3561-3572

Bandfield, J.L., Hamilton, V.E., and P.R. Christensen, 2000, A global view of Martian surface compositions for MGS-TES, Science, Vol. 287, pp. 1626-1630

Barrett, P.T., and P. Kline, 1981, The observation to variable ratio in factor analysis, Personality Study and Group Behavior, Vol. 1, pp. 23-33

Besley, L.M., and G.A. Bottomley, 1969, The water vapour equilibria over magnesium perchlorate hydrates, Journal of Chemical Thermodynamics, Vol. 1, pp. 13-19

Boothroyd, A.I., Sackman, I.J., and F.A. Fowler, 1991, Our Sun, II, early mass loss of 0.1 solar mass and the case of the missing lithium, Astrophysical Journal, Vol. 377, pp. 318-329

Boslough, M.B., Weldon, R.J., and T.J. Ahrens, 1980, Impact-induced water loss from serpentine, nontronite, and kernite, Proceedings of the 11th Lunar Planetary Science Conference, pp. 2145-2158

Brakenridge, G.R., Newsom, H.E., and V.R. Baker, 1985, Ancient hot springs on Mars: Origins and paleoenvironmental significance of small Martian valleys, Geology, Vol. 13, pp. 859-862

Cabrol, N.A., and E.A., Grin, 1999, Distribution, classification, and ages of Martian impact crater lakes, Icarus, Vol. 142, pp. 160-172

Cabrol, N.A., and E.A. Grin, 2001, Composition of the drainage network on early Mars, Geomorphology, Vol. 37, pp. 269-287

Carr, M.H., 1996, Water on Mars, New York: Oxford University Press, 248 p.

Carr, M.H., and G.D. Clow, 1981, Martian channels and valleys: Their characteristics, distribution, and age, Icarus, Vol. 48, pp. 91-117

Carr, M.H., and M.C. Malin, 2000, Meter-scale characteristics of Martian channels and valleys: Their characteristics, distribution and age, Icarus, Vol. 146, pp. 366-386

Carter, C.L., and R.S. Anderson, 2006, Fluvial erosion of physically modeled abrasion-dominated slot canyons, Geomorphology, Vol. 81, pp. 89-113

Chapman, M.G., and K.L. Tanaka, 1990, Small valleys and hydrologic history of the lower Mangala Valles region, Mars, Proceedings of the 20th Lunar Planetary Science Conference, pp. 531-539

Chorley, R.J., Malm, D.E.G., and H.A. Pagorzelski, 1957, A new standard for estimating drainage basin shape, American Journal of Science, Vol. 255, pp. 138-141

Cliff, N., 1970, The relation between sample and population characteristic vectors, Psychometrika, Vol. 35, pp. 163-178

Craddock, R.A., and A.D. Howard, 2002, The case for rainfall on a warm, wet early Mars, Journal of Geophysical Research, Vol. 107, No. E11, doi: 10.1029/2001JE001505

Craddock, R.A., Maxwell, T.A., and A.D. Howard, 1997, Crater morphometry and modification in the Sinus Sabaeus and Margaritifer Sinus regions of Mars, Journal of Geophysical Research, Vol. 102, pp. 13,321-13,340

Duda R.O., Hart, P.E., and D.G. Stork, 2001, Pattern Classification, New York: John Wiley & Sons, 654 p.

Environment Canada, 2004, Canadian climate normals 1971-2001, Resolute Bay, Canada Atmospheric Environment Service, Minister of Supply and Services Canada, Ottawa, ON, Canada

ESRI, 2002, ArcHydro tools v.1.0 Beta2, http://www.crwr.utexas.edu/giswr

Farias, M., Charrier, R., Comte, D., Martinod, J., and G. Herail, 2005, Late Cenozoic deformation and uplift of the western flank of the Altiplano: Evidence from the depositional, tectonic, and geomorphic evolution and shallow seismic activity (northern Chile at 19°30'S), Tectonics, Vol. 24, TC4001, doi: 10.1029/2004TC001667

Foody, G.M., 1992, On the compensation for chance agreement in image classification accuracy assessment, Photogrammetric Engineering and Remote Sensing, Vol. 58, No. 10, pp. 1459-1460

Fortezzo, C. and J.A. Grant, 2004, Hypsometric analyses of Martian basins: A comparison to terrestrial, lunar and Venusian hypsometry, 35th Lunar and Planetary Science Conference, abstract 1647

Frey, H.V., Roark, J.H., Shockey, K.M., Frey, E.L., and S.E.H. Sakimoto, 2002, Ancient lowlands on Mars, Geophysical Research Letters, Vol. 29, No. 10, 1384, doi: 10.1029/2001GL013832

Goldspiel, J.M., Squyres, S.W. and D.G. Jankowski, 1993, Topography of small Martian valleys, Icarus, Vol. 105, pp. 479-500

Goodrich, D.C., Keefer, T.O., Unkrich, C.L., Nichols, M.H., Osborn, H.B., Stone, J.J. and J.R., Smith, 2008, Long-term precipitation database, Walnut Gulch Experimental Watershed, Arizona, United States, Water Resources Research, Vol. 44, W05S04, doi: 10.1029/2006WR005782

Gough, D.O., 1981, Solar interior structure and luminosity variations, Solar Physics, Vol. 74, pp. 21-34

Graedel, T.E., Sackman, I.J., and A.I. Boothroyd, 1991, Early solar mass loss: A potential solution to the weak sun paradox, Geophysical Research Letters, Vol. 18, pp. 1881-1884

Grant, J.A., and P.M. Schultz, 1989, Gradational epochs on Mars: evidence from West-Northwest of Isisdis Basin and Electris, Icarus, Vol. 84, pp. 166-195

Gregory, K.J., 1976, Drainage networks and climate. In Derbyshire, E. (Editor), Geomorphology and climate, London: Wiley, pp. 289-315

Gulick, V.C., and V.R. Baker, 1990, Origin and evolution of valleys on Martian volcanoes, Journal of Geophysical Research, Vol. 95, pp. 14325-14344

Gulick, V.C., 1993, Magnetic intrusions and hydrothermal systems: Implications for the formation of small Martian valleys, PhD thesis, University of Arizona, Tucson, 146 p.

Gulick, V.C., 2001, Origin of the valley networks on Mars: a hydrological perspective, Geomorphology, Vol. 37, pp. 241-268

Haberle, R.M., Tyler, D., McKay, C.P., and W.L. Davis, 1994, A model for the evolution of CO_2 on Mars, Icarus, Vol. 109, pp. 102-120

Hair, J.F., Anderson, R.E., Tatham, R.L. and W.C. Black, 1998, Multivariate Data Analysis, 5th edition, Upper Saddle River, NJ: Prentice Hall, 768 p.

Hellweger, F. and D. Maidment, 1997, AGREE – DEM Surface Reconditioning System, http://www.ce.utexas.edu/prof/maidment/gishydro/ferdi/research/agree/agree.html

Hoke, G.D., Isaks, B.L., Jordan, T.E., and J.S. Yu, 2004, Groundwater-sapping origin for the giant quebradas of northern Chile, Geology, Vol. 32, pp. 605-608, doi: 10.1130/G20601.1

Horton , R.E., 1932, Drainage basin characteristics, Transactions American Geophysical Union, Vol. 13, pp. 350-361

Horton, R.E., 1945, Erosional development of streams and their drainage basins; Hydrophysical approach to quantitative morphology, Geological Society of America Bulletin, Vol. 56, pp. 275-370

Houston, J., and A.J. Hartley, 2003, The Central Andean west-slope rainshadow and its potential contribution to the origin of hyper-aridity in the Atacama Desert, International Journal of Climatology, Vol. 23, pp. 1453-1464, doi: 10.1002/joc.938

Humphreys, L.G., Ilgen, D., McGrath, D., and P. Montanelli, 1969, Capitalization on chance in rotation of factors, Educational and Psychological Measurement, Vol. 29, pp. 259-271

Hurtrez, J.E., Sol, C., and F. Lucazeau, 1999, Effect of drainage area on hypsometry from an analysis of small-scale drainage basins in the Siwalik Hills (central Nepal), Earth Surface Processes and Landforms, Vol. 24, No. 9, pp. 799-808

Hynek, B.M., and R.J. Phillips, 2003, New data reveal mature, integrated drainage systems on Mars indicative of past precipitation, Geology, Vol. 31, No. 9, pp. 757-760

Irwin, R.P., III, Howard, A.D., Craddock, R.A., and J.M. Moore, 2005, An intense terminal epoch of widespread fluvial activity on early Mars: 2. Increased runoff and paleolake development, Journal of Geophysical Research, Vol. 110, E12S15, doi: 10.1029/2005JE002460

Jensen, J.R., 2005, Introductory digital image processing: A remote sensing perspective, 3rd edition, Upper Saddle River, NJ: Prentice-Hall, 526 p.

Kaufman, L., and P.J., Rousseeuw, 2005, Finding groups in data: An introduction to cluster analysis, New Jersey: Wiley Interscience, 342 p.

Kochel, R.C., and V.R. Baker, 1990, Case Study: Ground-water sapping and the geomorphic development of large Hawaiian valleys, In: Higgins, C.G., and D.R. Coates (Editors), Geological Society of America Special Paper 252, pp. 245-257

Kohonen, T., 2001, Self-Organizing Maps, 3rd edition, New York: Springer, 501 p.

Laity, J.E., and M.C. Malin, 1985, Sapping processes and the development of theater-headed valley networks on the Colorado Plateau, Geological Society of America Bulletin, Vol. 96, pp. 203-217

Langbein, W.B., 1947, Topographic characteristics of drainage basins, U.S. Geological Survey Water-Supply Paper, 968-C

Lee, P., Rice, J.W. Jr., Bunch, T.E., Grieve, R.A., McKay, C.P., Schutt, J.W., and Zent, A.P., 1999, Possible analogs for small valleys on Mars at the Haughton Impact Crater site, Devon Island, Canadian High Arctic, 30th Lunar and Planetary Science Conference, Abstract 2033

Leopold, L.B., and W.B. Langbein, 1962, The concept of entropy in landscape evolution, U.S. Geological Survey Professional Paper, 500-A

Luo, W., 2002, Hypsometric analysis of Margaritifer Sinus and origin of valley networks, Journal of Geophysical Research, Vol. 107, E10, 5071, doi: 10.1029/2001JE001500

Luo, W., and A.D. Howard, 2005, Morphometric analysis of Martian valley network basins using a circularity function, Journal of Geophysical Research, Vol. 110 E12S13, doi: 10.1029/2005JE002506

Malin, M.C., and K.E. Edgett, 1999, MGS MOC the first year; Geomorphic processes and landforms, Proceedings of the 30th Lunar Planetary Science Conference, abstract 1028

Mars Channel Working Group, 1983, Channels and valleys on Mars, Geological Society of America Bulletin, Vol. 94, pp. 1035-1054

McArthur, D.S., and R. Ehrlich, 1977, An efficiency evaluation of four drainage basin shape ratios, The Professional Geographer, Vol. 29, No. 3, pp. 290-295

McCauley, J.F., Carr, M.H., Cutts, J.A., Hartmann, W.K., Masursky, H., Milton, D.J., Sharp, R.P., and D.E. Wilhelms, 1972, Preliminary Mariner 9 report on the geology of Mars, Icarus, Vol. 17, pp. 289-327

Melosh, H.J., and A.M. Vickery, 1989, Impact erosion of the primordial Martian atmosphere, Nature, Vol. 338, pp. 487-489

Michaud, J., and S. Sorooshian, 1994, Comparison of simple versus complex distributed runoff models on a midsized semiarid watershed, Water Resources Research, Vol. 30, No. 3, pp. 593-605

Miller, V.C., 1953, A quantitative geomorphic study of drainage basin characteristics in the Clinch Mountain area, Virginia and Tennessee, Office of Naval Research, Project NR 389-042, Technical Report No. 3, 30 p.

Milton, L.E., 1966, The geomorphic irrelevance of some drainage net laws, Australian Geographical Studies, Vol. 4, No. 2, pp. 89-95

NASA, 2008a, Phoenix Mars Mission press release, August 4th, http://phoenix.lpl.arizona.edu/

NASA, 2008b, Phoenix Mars Mission press release, August 5th, http://phoenix.lpl.arizona.edu/

Nunnally, J.C., 1978, Psychometric Theory, 2nd edition, New York: McGraw Hill, 701 p.

O'Callaghan, J.F., and D.M. Mark, 1984, The extraction of drainage networks from digital elevation data, Computer Vision, Graphics and Image Processing, Vol. 28, pp. 323-344

Osborne, J.W., and A. Costello, 2004, Sample size and subject to item ratio in principal components analysis, Practical Assessment, Research & Evaluation, Vol. 9, No. 11

Pestova, O.N., Myund, L.A., Khripun, M.K., and A.V. Prigaro, 2005, Polythermal Study of the Systems $M(ClO_4)_2$-H_2O (M^{2+} = Mg^{2+}, Ca^{2+}, Sr^{2+}, Ba^{2+}), Russian Journal of Applied Chemistry, Vol. 78, No. 3, pp. 409-413

Renard, K.G., Lane, L.J., Simanton, J.R., Emmerich, W.E., Stone, J.J., Weltz, M.A., Goodrich, D.C., and D.S. Yakowitz, 1993, Agricultural impacts in an arid environment: walnut gulch studies, hydrological science and technology, Vol. 9, pp. 145-190

Rodriguez-Iturbe, I., Rinaldo, A., 1997, Fractal river basins: Chance and self-organization, New York: Cambridge University Press, 565 p.

R Project for statistical computing, 2008, R v2.6.2, www.r-project.org

Osinski, G.R., 2005, Geological Map: Haughton Impact Structure, Devon Island, Nunavut, Canada, Scale 1:25000, Supplement to Meteoritic and Planetary Science, Vol. 40, Issue 12

Ruiz-Jimenez, J., Priego-Capote, F., Gracia-Olmo, J., and M.D. Luque de Castro, 2004, Use of chemometrics and mid infrared spectroscopy for the selection of extraction alternatives to reference analytical methods for total fat isolation, Analytica Chimica Acta, Vol. 525, pp. 159-169

Scholz, M., 2006, Wetland systems to control urban runoff, Elsevier, 360 p.

Schumm, S.A., 1956, Evolution of drainage systems and slopes in badlands at Perth Amboy, New Jersey, Geological Society of America Bulletin, Col. 67, pp. 597-646

Schumm, S.A., Boyd, K.F., Wolff, C.G., and W.J. Spitz, 1995, A ground-water sapping landscape in the Florida Panhandle, Geomorphology, Vol. 12, pp. 281-297

Scott, D.H., and M.G. Chapman, 1991, Geologic map of science study area 6, Memnonia region of Mars, scale 1:500,000, U.S. Geological Survey Miscellaneous Investigations Series Map, 1-2084

Sommer, D., and M. Golz, 2005, Studies in the classification, data analysis, and knowledge engineering, Proceedings of the 29th Annual Conference of the Gesellschaft für Klassifikation e.v. University of Magderburg, March 9-11

Southeast Regional Climate Centre, 2008, Climate Normals (1971-200), Niceville, Florida, http://www.sercc.com/

Stearns, H.T., 1966, Geology of the state of Hawaii, Palo Alto, California: Pacific Books, 266 p.

Stearns, H.T., and G.A. MacDonald, 1946, Geology and ground-water resources of the island of Hawaii, Hawaii Division of Hydrography Bulletin 9, 363 p.

Stepinski, T.F., and M.L. Collier, 2004, Extraction of Martian valley networks from digital topography, Journal of Geophysical Research, Vol. 109, E11005, doi: 10.1029/2004JE002269

Stepinski, T.F., and S. Coradetti, 2004, Comparing morphologies of drainage basins on Mars and Earth using integral-geometry and neural maps, Geophysical Research Letters, Vol. 31, L15604, doi: 10.1029/2004GL020359

Stepinski, T.F., and A.P. Stepinski, 2005, Morphology of drainage basins as an indicator of climate on early Mars, Journal of Geophysical Research, Vol. 110, E12S12, doi: 10.1029/2005JE002448

Strahler, A.N., 1952, Hypsometric (area-altitude) analysis of erosional topography, Geological Society of America Bulletin, Vol. 63, pp. 1117-1142

Squyres, S.W., and J.F. Kasting, 1994, Early Mars: How warm and how wet?, Science, Vol. 265, pp. 744-749

Tabachnick, B.G., and L.S. Fidell, 1996, Using multivariate Statistics, 3rd edition, New York: Harper Collins College Publishers

Tanaka, K.L., 1986, The stratigraphy of Mars, Proceedings of the 17th Lunar Planetary Science Conference, Journal of Geophysical Research, Vol. 91, pp. E139-E158

Van Liew, M.W., and J. Garbrecht, 2003, Hydrologic simulation of the Little Washita River Experimental Watershed using SWAT, Journal of the American Water Resources Association, Vol. 39, No. 2, pp. 413-426

Weigert, A., Wenk, G., Ollesch, G., and H. Fritz, 2003, Short Communication: Simulation of snowmelt erosion using the EROSION 3D model, Journal of Plant Nutrition and Soil Science, Vol. 166, Issue 1, pp. 128-130

Western Regional Climate Centre, 2008, Climate Normals (1971-200), Bullfrog Basin, Utah, http://www.wrcc.dri.edu

Willgoose, G., and G. Hancock, 1998, Revisiting the hypsometric curve as an indicator of form and process in transport-limited catchment, Earth Surface Processes and Landforms, Vol. 23, No. 7, pp. 611-623

Williams, R.M.E., and R.J. Phillips, 2001, Morphometric measurements of Martian valley networks from Mars Orbiter Laser Altimeter (MOLA) data, Journal of Geophysical Research, Vol. 106, No. E10, pp. 23,737-23,751

Wilppu, R., 1997, The visualization capability of self-organizing maps to detect deviation in distribution control. TUCS Technical Report No. 153, Turku Centre for Computer Science, Finland

Appendix A

This appendix presents the results of the t-Test on the bifurcation ratio and stream length ratio of 5 surface runoff basins (3 from Utah, 1 from Arizona and 1 from Oklahoma) and 6 groundwater sapping basins (4 from Utah and 2 from Florida). The Welch Modified two-sample t-Test used here assumes the distribution is normal, but does not assume equal variances. Table A.1 presents the bifurcation ratios of the drainage basins and Table A.2 presents the stream length ratios.

Table A.1: Bifurcation ratio of selected drainage basins

Surface Runoff	Groundwater Sapping
3.01	7.94
3.44	3.74
2.88	3.38
4.41	2.82
4.12	3.88
	4.13

Table A.2: Stream length ratio of selected drainage basins

Surface Runoff	Groundwater Sapping
2.09	6.07
2.24	4.61
2.49	2.54
2.50	2.19
2.57	3.16
	2.99

The results of the Welch Modified two-sample t-Test for the bifurcation ratio were as follows: $t = 0.92$, $df = 6.54$, p-value = 0.39. Similarly, the results of the Welch Modified two-sample t-Test for the bifurcation ratio were as follows: $t = 1.97$, $df = 5.20$, p-value = 0.10. As such, based on t-Test tables, at the 95% confidence level, there is insufficient evidence to reject the null hypothesis.

Appendix B

As presented in Chorley et al. (1957), this appendix presents the derivation of the perimeter of a lemniscate loop, *P*, and the elliptic integral, *E(K)*, used to compute the perimeter's value.

The expression for a lemniscate loop (Figure B.1) is given by:

$$\rho = l\cos(k\theta) \qquad \text{(B.1)}$$

where:

θ lies between $-\pi/2k$ and $\pi/2k$

l is the longest diameter of the loop and is analogous to the basin length

k, the lemniscate index, is a constant, greater than or equal to unity, upon which the relationship between the maximum width of the loop depends, through its control of the angle α (Figure B.1).

The area of the loop, (A), is obtained through integration:

$$A = \frac{1}{2}\int_{-\pi/2k}^{\pi/2k} l\cos(k\theta)^2\, d\theta$$
$$A = \frac{l^2\pi}{4k} \qquad \text{(B.2)}$$

Therefore the lemniscate index is given by:

$$k = \frac{l^2\pi}{4A} \qquad \text{(B.3)}$$

Similarly, the perimeter of the loop is obtained by:

$$P = \int_{-\pi/2k}^{\pi/2k} \sqrt{l^2\cos^2(k\theta) + l^2k^2\sin^2(k\theta)}\, d\theta \qquad \text{(B.4)}$$

which may be simplified to:

$$P = 2l\int_0^{\pi/2} \sqrt{1 - K^2\sin^2\Psi}\, d\Psi$$
$$P = 2lE(K) \qquad \text{(B.5)}$$

where $K = \frac{\sqrt{(k^2-1)}}{k}$ and *E(K)* is an elliptic integral of the second kind which may be solved for values of $K^2 < 1$ by:

$$E(k)=\frac{\pi}{2}\left[1-\left(\frac{1}{2}\right)^2 K^2-\left(\frac{1}{2}\cdot\frac{3}{4}\right)^2\frac{K^4}{3}-\left(\frac{1}{2}\cdot\frac{3}{4}\cdot\frac{5}{6}\right)^2\frac{K^6}{5}-\ldots\right] \qquad \text{(B.6)}$$

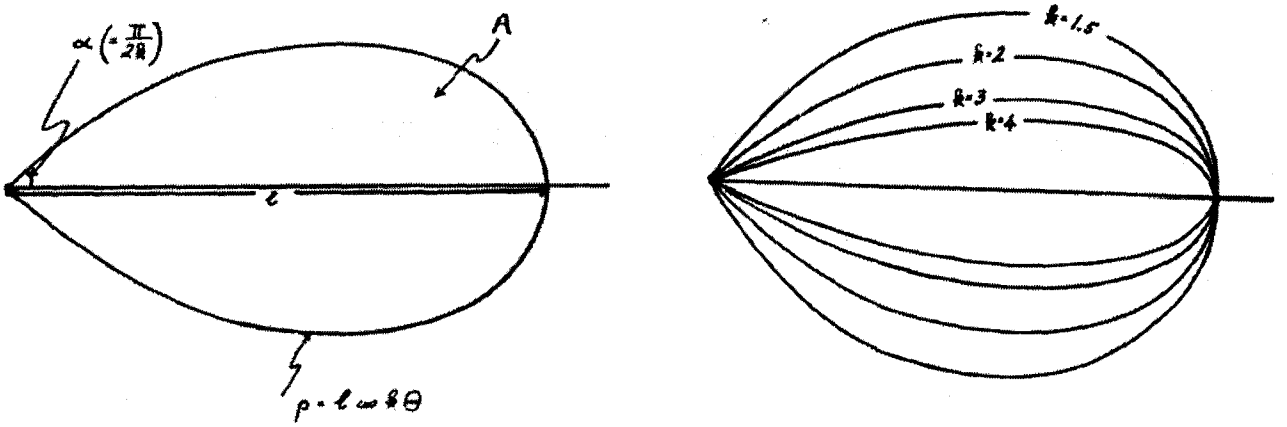

Figure B.1: Parameters used to describe a lemniscate loop. (From Chorley, 1957)

Appendix C

This appendix provides the raw circularity, elongation, lemniscate index and lemniscate ratio data for the 39 terrestrial basins and 23 Martian valley networks used in this study. Tables C.1 and C.2 enumerate the ID numbers associated with the basins in the subsequent tables. Table C.3 presents the circularity data of the terrestrial basins. Table C.4 presents the circularity data of the Martian valley networks. Table C.5 presents the elongation data of the terrestrial basins. Table C.6 presents the elongation data of the Martian valley networks. Table C.7 presents the lemniscate index data of the terrestrial basins. Table C.8 presents the lemniscate index data of the Martian valley networks. Table C.9 presents the lemniscate ratio data of the terrestrial basins. Table C.10 presents the lemniscate ratio data of the Martian valley networks.

Table C.1: ID numbers associated with the terrestrial basins. SR: surface runoff; GW: groundwater sapping; M: meltwater

ID	Terrestrial Basins	Formation Process
1	Colorado 1	SR
2	Colorado 2	SR
3	Colorado 3	SR
4	Colorado 4	SR
5	Colorado 5	SR
6	Colorado 6	SR
7	Colorado 7	SR
8	Colorado 8	GW
9	Colorado 9	GW
10	Colorado 10	GW
11	Colorado 11	GW
12	Devon 1	M
13	Devon 2	M
14	Devon 3	M
15	Devon 4	M
16	Florida 1	GW
17	Florida 2	GW
18	Chile 1	GW
19	Chile 2	GW
20	Chile 3	GW
21	Chile 4	GW
22	Chile 5	GW
23	Arizona 1	SR
24	Arizona 2	SR
25	Arizona 3	SR
26	Arizona 4	SR
27	Oklahoma 1	SR
28	Oklahoma 2	SR
29	Oklahoma 3	SR
30	Oklahoma 4	SR
31	Hawaii 1	GW
32	Hawaii 2	GW
33	Hawaii 3	SR
34	Hawaii 4	SR
35	Hawaii 5	SR
36	Hawaii 6	GW
37	Hawaii 7	SR
38	Hawaii 8	SR
39	Hawaii 9	GW

Table C.2: ID numbers associated with the Martian valley networks

ID	Martian Valley Networks
1	Arda Valles
2	Dawes East
3	Douglass
4	Evros Vallis North_1
5	Evros Vallis North_2
6	Evros Vallis West
7	Locras_1
8	Locras_2
9	Millochau South
10	Millochau West
11	Millochau East
12	Naktong Vallis
13	Schiaparelli
14	Unnamed 1_1
15	Unnamed 1_2
16	Unnamed 2
17	Unnamed 3
18	Unnamed 4
19	Unnamed 5_1
20	Unnamed 5_2
21	Unnamed 6
22	Warrego Valles_1
23	Warrego Valles_2

Table C.3: Circularity data of the terrestrial basins

	C1	C2	C3	C4	C5	C6	C7	C8	C9	C10	C11	C12	C13	C14	C15	C16	C17	C18	C19	C20	C21	C22	C23	C24	C25
1	0.157	0.104	0.054	0.059	0.051	0.044	0.039	0.036	0.040	0.041	0.034	0.041	0.047	0.060	0.077	0.099	0.122	0.151	0.185	0.245	0.300	0.299	0.300	0.337	0.333
2	0.032	0.037	0.042	0.034	0.035	0.034	0.035	0.035	0.034	0.047	0.059	0.092	0.104	0.120	0.131	0.158	0.148	0.150	0.184	0.222	0.290	0.370	0.412	0.445	0.452
3	0.065	0.059	0.037	0.031	0.035	0.032	0.036	0.035	0.042	0.054	0.072	0.080	0.106	0.121	0.153	0.173	0.180	0.205	0.230	0.257	0.286	0.331	0.343	0.377	0.380
4	0.018	0.026	0.031	0.036	0.041	0.045	0.045	0.040	0.039	0.046	0.056	0.055	0.060	0.056	0.073	0.105	0.112	0.145	0.185	0.337	0.370	0.376	0.374	0.372	0.372
5	0.052	0.040	0.045	0.058	0.082	0.155	0.219	0.268	0.247	0.219	0.189	0.188	0.237	0.285	0.294	0.285	0.338	0.335	0.348	0.359	0.403	0.475	0.492	0.493	0.488
6	0.056	0.080	0.118	0.132	0.174	0.238	0.317	0.311	0.335	0.363	0.342	0.324	0.354	0.346	0.319	0.305	0.331	0.363	0.383	0.390	0.411	0.460	0.486	0.547	0.547
7	0.094	0.204	0.209	0.150	0.284	0.410	0.426	0.412	0.429	0.458	0.478	0.461	0.453	0.428	0.386	0.383	0.370	0.344	0.420	0.443	0.500	0.550	0.548	0.543	0.548
8	0.037	0.037	0.056	0.106	0.149	0.187	0.269	0.378	0.394	0.385	0.407	0.445	0.460	0.450	0.439	0.395	0.361	0.346	0.390	0.414	0.467	0.477	0.497	0.490	0.488
9	0.047	0.038	0.032	0.036	0.066	0.104	0.134	0.165	0.268	0.335	0.345	0.377	0.397	0.414	0.434	0.442	0.444	0.422	0.396	0.362	0.397	0.441	0.450	0.493	0.545
10	0.061	0.048	0.045	0.074	0.143	0.264	0.435	0.429	0.422	0.477	0.519	0.528	0.536	0.522	0.527	0.486	0.431	0.394	0.526	0.554	0.546	0.567	0.587	0.571	0.597
11	0.065	0.051	0.044	0.057	0.101	0.167	0.239	0.266	0.268	0.276	0.283	0.302	0.298	0.314	0.320	0.326	0.329	0.313	0.314	0.324	0.336	0.356	0.384	0.411	0.421
12	0.122	0.100	0.075	0.085	0.071	0.064	0.059	0.062	0.044	0.040	0.034	0.035	0.041	0.043	0.042	0.058	0.075	0.090	0.147	0.227	0.311	0.385	0.451	0.464	0.538
13	0.141	0.094	0.076	0.066	0.056	0.053	0.049	0.043	0.040	0.035	0.033	0.028	0.033	0.039	0.042	0.042	0.046	0.051	0.064	0.097	0.176	0.258	0.339	0.372	0.408
14	0.401	0.211	0.242	0.204	0.242	0.229	0.250	0.272	0.218	0.199	0.173	0.154	0.131	0.075	0.059	0.061	0.065	0.061	0.080	0.117	0.154	0.316	0.425	0.516	0.536
15	0.173	0.099	0.108	0.114	0.127	0.127	0.118	0.120	0.125	0.127	0.118	0.116	0.107	0.092	0.073	0.049	0.035	0.031	0.037	0.053	0.080	0.141	0.300	0.488	0.525
16	0.003	0.001	0.001	0.002	0.003	0.004	0.004	0.004	0.005	0.006	0.007	0.008	0.010	0.013	0.017	0.032	0.051	0.059	0.087	0.144	0.210	0.223	0.271	0.303	0.320
17	0.002	0.001	0.001	0.002	0.003	0.003	0.003	0.003	0.005	0.006	0.008	0.010	0.015	0.019	0.026	0.034	0.048	0.068	0.094	0.158	0.236	0.306	0.322	0.330	0.333
18	0.178	0.156	0.107	0.172	0.248	0.234	0.242	0.268	0.288	0.307	0.311	0.273	0.243	0.207	0.207	0.214	0.238	0.268	0.265	0.257	0.262	0.273	0.286	0.304	0.305
19	0.186	0.217	0.230	0.250	0.288	0.267	0.262	0.240	0.228	0.260	0.273	0.286	0.314	0.335	0.353	0.364	0.378	0.386	0.393	0.375	0.326	0.330	0.317	0.254	0.291
20	0.267	0.257	0.217	0.170	0.138	0.134	0.151	0.162	0.178	0.178	0.191	0.195	0.210	0.230	0.254	0.255	0.260	0.269	0.263	0.269	0.266	0.243	0.237	0.214	0.233
21	0.314	0.371	0.254	0.265	0.210	0.222	0.190	0.234	0.227	0.212	0.213	0.248	0.240	0.284	0.256	0.266	0.275	0.289	0.292	0.337	0.400	0.407	0.427	0.452	0.453
22	0.194	0.281	0.360	0.368	0.301	0.315	0.297	0.244	0.273	0.284	0.329	0.299	0.308	0.353	0.352	0.394	0.358	0.365	0.388	0.399	0.402	0.373	0.388	0.413	0.426
23	0.064	0.109	0.077	0.089	0.098	0.085	0.070	0.069	0.056	0.055	0.066	0.091	0.099	0.108	0.136	0.169	0.214	0.250	0.251	0.261	0.280	0.278	0.274	0.272	0.270
24	0.057	0.046	0.064	0.090	0.072	0.081	0.073	0.074	0.081	0.105	0.150	0.174	0.230	0.311	0.337	0.320	0.294	0.349	0.373	0.374	0.371	0.363	0.360	0.356	0.350
25	0.042	0.069	0.061	0.039	0.045	0.066	0.119	0.132	0.270	0.344	0.396	0.408	0.418	0.444	0.461	0.479	0.491	0.500	0.515	0.522	0.542	0.544	0.549	0.547	0.546
26	0.165	0.110	0.084	0.088	0.108	0.120	0.167	0.182	0.172	0.197	0.221	0.205	0.179	0.171	0.187	0.209	0.216	0.233	0.252	0.265	0.310	0.349	0.378	0.399	0.416
27	0.005	0.003	0.004	0.007	0.007	0.007	0.007	0.007	0.007	0.008	0.010	0.012	0.017	0.024	0.041	0.089	0.161	0.254	0.309	0.349	0.348	0.361	0.363	0.364	0.364
28	0.008	0.005	0.005	0.005	0.005	0.006	0.007	0.008	0.010	0.012	0.016	0.029	0.058	0.113	0.156	0.241	0.320	0.382	0.403	0.386	0.396	0.398	0.402	0.402	0.403
29	0.027	0.016	0.029	0.023	0.023	0.025	0.027	0.035	0.047	0.063	0.089	0.109	0.116	0.158	0.209	0.232	0.291	0.325	0.379	0.391	0.404	0.408	0.409	0.419	0.426
30	0.016	0.010	0.010	0.018	0.021	0.026	0.021	0.024	0.029	0.041	0.052	0.063	0.090	0.127	0.169	0.218	0.278	0.352	0.401	0.490	0.514	0.527	0.527	0.533	0.533
31	0.200	0.152	0.145	0.123	0.105	0.109	0.113	0.124	0.131	0.145	0.171	0.187	0.202	0.223	0.248	0.264	0.281	0.257	0.228	0.212	0.261	0.259	0.257	0.267	0.270
32	0.390	0.559	0.476	0.433	0.444	0.507	0.436	0.298	0.332	0.356	0.364	0.354	0.329	0.326	0.292	0.258	0.256	0.252	0.251	0.232	0.243	0.220	0.227	0.230	0.223
33	0.730	0.757	0.427	0.522	0.349	0.536	0.377	0.369	0.326	0.303	0.280	0.260	0.287	0.281	0.258	0.246	0.245	0.217	0.226	0.219	0.214	0.196	0.190	0.191	0.172
34	0.730	0.757	0.427	0.522	0.349	0.536	0.377	0.369	0.326	0.303	0.280	0.260	0.287	0.281	0.258	0.246	0.245	0.217	0.226	0.219	0.214	0.196	0.190	0.191	0.172
35	0.472	0.613	0.695	0.715	0.739	0.558	0.490	0.384	0.384	0.340	0.326	0.328	0.300	0.275	0.293	0.293	0.286	0.301	0.317	0.315	0.310	0.300	0.271	0.255	0.226
36	0.130	0.152	0.180	0.204	0.228	0.263	0.294	0.324	0.358	0.390	0.414	0.416	0.440	0.412	0.445	0.438	0.391	0.413	0.473	0.509	0.509	0.516	0.512	0.508	0.481
37	0.686	0.606	0.435	0.556	0.322	0.399	0.508	0.439	0.444	0.351	0.319	0.363	0.439	0.420	0.462	0.496	0.479	0.470	0.520	0.561	0.500	0.567	0.602	0.626	0.602
38	0.052	0.040	0.045	0.058	0.082	0.155	0.219	0.268	0.247	0.219	0.189	0.188	0.237	0.285	0.294	0.285	0.338	0.335	0.348	0.359	0.403	0.475	0.492	0.493	0.488
39	0.056	0.080	0.118	0.132	0.174	0.238	0.317	0.311	0.335	0.363	0.342	0.324	0.354	0.346	0.319	0.305	0.331	0.363	0.383	0.390	0.411	0.460	0.486	0.547	0.547

Table C.4: Circularity data of the Martian basins

	C1	C2	C3	C4	C5	C6	C7	C8	C9	C10	C11	C12	C13	C14	C15	C16	C17	C18	C19	C20	C21	C22	C23	C24	C25
1	0.353	0.274	0.368	0.289	0.266	0.209	0.243	0.231	0.233	0.324	0.386	0.361	0.312	0.286	0.439	0.427	0.425	0.429	0.434	0.428	0.430	0.443	0.447	0.452	0.455
2	0.286	0.285	0.286	0.278	0.269	0.248	0.229	0.216	0.202	0.195	0.175	0.176	0.156	0.176	0.165	0.171	0.139	0.090	0.097	0.102	0.087	0.110	0.054	0.079	0.283
3	0.375	0.287	0.245	0.288	0.278	0.177	0.169	0.172	0.180	0.117	0.084	0.123	0.162	0.171	0.202	0.270	0.278	0.300	0.319	0.341	0.350	0.348	0.346	0.350	0.353
4	0.347	0.342	0.340	0.323	0.325	0.305	0.277	0.291	0.293	0.271	0.244	0.285	0.311	0.263	0.249	0.230	0.169	0.162	0.159	0.098	0.089	0.279	0.512	0.489	0.344
5	0.149	0.203	0.190	0.394	0.378	0.330	0.236	0.197	0.214	0.175	0.241	0.198	0.186	0.196	0.168	0.199	0.184	0.208	0.208	0.251	0.271	0.277	0.284	0.289	0.288
6	0.192	0.079	0.067	0.075	0.112	0.117	0.108	0.122	0.090	0.088	0.053	0.069	0.114	0.149	0.220	0.269	0.303	0.308	0.312	0.318	0.317	0.317	0.315	0.315	0.316
7	0.383	0.061	0.066	0.111	0.197	0.209	0.265	0.272	0.232	0.297	0.245	0.233	0.334	0.333	0.446	0.451	0.469	0.469	0.481	0.477	0.480	0.477	0.477	0.477	0.478
8	0.195	0.212	0.289	0.150	0.117	0.169	0.207	0.148	0.198	0.255	0.117	0.165	0.194	0.219	0.260	0.277	0.272	0.288	0.306	0.301	0.303	0.306	0.307	0.309	0.309
9	0.248	0.182	0.174	0.191	0.185	0.327	0.364	0.440	0.366	0.310	0.433	0.433	0.417	0.512	0.565	0.567	0.564	0.575	0.548	0.542	0.548	0.539	0.525	0.528	0.526
10	0.268	0.200	0.228	0.137	0.281	0.203	0.115	0.097	0.104	0.155	0.104	0.150	0.143	0.190	0.300	0.363	0.359	0.322	0.392	0.389	0.410	0.415	0.417	0.416	0.421
11	0.716	0.654	0.770	0.772	0.763	0.739	0.735	0.694	0.721	0.704	0.505	0.559	0.569	0.555	0.526	0.560	0.574	0.570	0.529	0.454	0.364	0.449	0.485	0.509	0.511
12	0.169	0.106	0.080	0.090	0.086	0.032	0.043	0.058	0.092	0.110	0.099	0.064	0.071	0.087	0.115	0.134	0.171	0.206	0.229	0.235	0.330	0.352	0.366	0.374	0.374
13	0.155	0.180	0.227	0.199	0.203	0.265	0.213	0.192	0.218	0.212	0.200	0.202	0.178	0.276	0.349	0.326	0.326	0.342	0.384	0.393	0.390	0.398	0.397	0.401	0.402
14	0.188	0.244	0.384	0.415	0.365	0.178	0.172	0.333	0.294	0.335	0.364	0.363	0.357	0.320	0.330	0.360	0.408	0.438	0.459	0.449	0.450	0.448	0.446	0.443	0.442
15	0.348	0.308	0.479	0.309	0.271	0.484	0.418	0.328	0.310	0.360	0.297	0.345	0.352	0.336	0.359	0.350	0.353	0.354	0.353	0.355	0.354	0.356	0.357	0.357	0.366
16	0.047	0.113	0.156	0.233	0.200	0.257	0.280	0.236	0.281	0.344	0.356	0.205	0.237	0.241	0.254	0.282	0.294	0.275	0.288	0.289	0.289	0.288	0.289	0.291	0.291
17	0.163	0.257	0.106	0.110	0.176	0.140	0.220	0.217	0.178	0.206	0.177	0.194	0.187	0.203	0.180	0.169	0.258	0.299	0.434	0.448	0.460	0.467	0.467	0.466	0.468
18	0.564	0.320	0.244	0.139	0.151	0.281	0.277	0.227	0.153	0.152	0.283	0.333	0.294	0.241	0.236	0.268	0.320	0.369	0.384	0.390	0.387	0.369	0.357	0.375	0.374
19	0.630	0.338	0.244	0.274	0.295	0.263	0.268	0.243	0.243	0.235	0.294	0.212	0.190	0.221	0.237	0.210	0.253	0.296	0.352	0.383	0.419	0.406	0.401	0.393	0.391
20	0.486	0.296	0.254	0.254	0.280	0.306	0.360	0.293	0.318	0.349	0.358	0.472	0.501	0.528	0.555	0.510	0.574	0.564	0.497	0.552	0.521	0.514	0.503	0.477	0.482
21	0.405	0.495	0.378	0.232	0.190	0.147	0.165	0.218	0.138	0.115	0.122	0.111	0.158	0.173	0.189	0.183	0.164	0.171	0.186	0.261	0.288	0.367	0.420	0.432	0.441
22	0.637	0.552	0.591	0.630	0.554	0.447	0.258	0.233	0.254	0.296	0.336	0.349	0.338	0.340	0.313	0.326	0.360	0.371	0.344	0.361	0.364	0.350	0.337	0.344	0.349
23	0.678	0.726	0.641	0.546	0.515	0.639	0.598	0.490	0.450	0.561	0.529	0.518	0.522	0.509	0.548	0.580	0.467	0.597	0.635	0.638	0.627	0.600	0.583	0.570	0.578

Table C.5: Elongation data of the terrestrial basins

	C1	C2	C3	C4	C5	C6	C7	C8	C9	C10	C11	C12	C13	C14	C15	C16	C17	C18	C19	C20	C21	C22	C23	C24	C25
1	0.189	0.275	0.400	0.477	0.555	0.624	0.657	0.652	0.638	0.631	0.630	0.626	0.637	0.647	0.653	0.656	0.660	0.660	0.659	0.661	0.662	0.668	0.660	0.661	0.661
2	0.296	0.352	0.485	0.561	0.608	0.619	0.648	0.643	0.646	0.645	0.636	0.633	0.638	0.630	0.623	0.616	0.614	0.614	0.621	0.624	0.625	0.629	0.633	0.638	0.638
3	0.234	0.366	0.471	0.554	0.673	0.700	0.710	0.707	0.707	0.702	0.701	0.691	0.681	0.672	0.654	0.640	0.642	0.644	0.648	0.651	0.654	0.656	0.654	0.653	0.652
4	0.181	0.247	0.370	0.470	0.571	0.648	0.682	0.677	0.668	0.656	0.657	0.658	0.657	0.652	0.647	0.629	0.622	0.619	0.620	0.619	0.622	0.623	0.624	0.622	0.622
5	0.197	0.228	0.246	0.352	0.503	0.600	0.653	0.716	0.742	0.737	0.736	0.733	0.729	0.729	0.729	0.730	0.731	0.731	0.729	0.733	0.734	0.735	0.733	0.734	0.740
6	0.245	0.247	0.286	0.467	0.654	0.721	0.724	0.711	0.706	0.707	0.710	0.713	0.717	0.718	0.716	0.707	0.694	0.680	0.681	0.672	0.666	0.666	0.665	0.659	0.649
7	0.278	0.241	0.298	0.394	0.527	0.602	0.622	0.625	0.619	0.615	0.613	0.617	0.619	0.622	0.623	0.624	0.621	0.624	0.626	0.625	0.616	0.610	0.611	0.607	0.606
8	0.411	0.400	0.284	0.299	0.285	0.300	0.329	0.341	0.362	0.363	0.370	0.411	0.453	0.483	0.503	0.528	0.532	0.542	0.554	0.564	0.566	0.557	0.555	0.552	0.551
9	0.235	0.245	0.264	0.250	0.248	0.237	0.241	0.260	0.287	0.328	0.377	0.426	0.462	0.493	0.522	0.549	0.550	0.561	0.568	0.564	0.562	0.559	0.552	0.544	0.545
10	0.351	0.379	0.363	0.372	0.384	0.407	0.420	0.439	0.474	0.510	0.541	0.511	0.543	0.576	0.609	0.637	0.653	0.638	0.603	0.611	0.595	0.612	0.602	0.600	0.597
11	0.237	0.285	0.308	0.329	0.347	0.362	0.380	0.414	0.481	0.545	0.583	0.592	0.607	0.629	0.682	0.720	0.759	0.792	0.807	0.831	0.828	0.825	0.820	0.814	0.810
12	0.305	0.297	0.288	0.283	0.289	0.306	0.314	0.345	0.318	0.322	0.347	0.388	0.433	0.459	0.503	0.559	0.619	0.648	0.685	0.735	0.775	0.807	0.837	0.849	0.860
13	0.335	0.281	0.246	0.219	0.203	0.203	0.223	0.229	0.239	0.272	0.320	0.360	0.400	0.446	0.508	0.583	0.646	0.683	0.734	0.755	0.797	0.806	0.806	0.810	0.817
14	0.469	0.308	0.358	0.331	0.343	0.340	0.354	0.372	0.335	0.321	0.293	0.291	0.293	0.315	0.323	0.338	0.389	0.410	0.457	0.525	0.569	0.613	0.647	0.663	0.681
15	0.321	0.245	0.262	0.280	0.305	0.334	0.320	0.336	0.351	0.364	0.377	0.380	0.368	0.368	0.391	0.406	0.445	0.459	0.499	0.566	0.642	0.715	0.743	0.773	0.763
16	0.111	0.112	0.111	0.145	0.198	0.232	0.265	0.302	0.338	0.382	0.412	0.457	0.493	0.547	0.605	0.675	0.728	0.790	0.819	0.851	0.869	0.868	0.876	0.880	0.880
17	0.116	0.092	0.117	0.152	0.203	0.232	0.264	0.303	0.364	0.399	0.436	0.470	0.491	0.506	0.529	0.544	0.575	0.608	0.641	0.664	0.674	0.673	0.674	0.674	0.674
18	0.378	0.408	0.448	0.554	0.649	0.700	0.701	0.745	0.737	0.719	0.705	0.674	0.649	0.627	0.616	0.609	0.610	0.603	0.583	0.571	0.567	0.555	0.545	0.546	0.548
19	0.480	0.527	0.606	0.695	0.693	0.677	0.670	0.656	0.656	0.671	0.672	0.670	0.661	0.658	0.655	0.639	0.638	0.632	0.623	0.599	0.583	0.579	0.555	0.518	0.517
20	0.469	0.416	0.371	0.332	0.302	0.312	0.341	0.366	0.384	0.396	0.410	0.430	0.436	0.446	0.449	0.450	0.454	0.453	0.452	0.450	0.444	0.441	0.434	0.408	0.403
21	0.636	0.609	0.623	0.616	0.600	0.584	0.562	0.552	0.538	0.534	0.524	0.531	0.535	0.541	0.548	0.552	0.556	0.560	0.565	0.567	0.570	0.575	0.579	0.580	0.580
22	0.784	0.817	0.823	0.781	0.753	0.735	0.684	0.651	0.639	0.626	0.619	0.611	0.603	0.593	0.594	0.589	0.585	0.578	0.572	0.567	0.562	0.559	0.559	0.557	0.557
23	0.236	0.341	0.335	0.370	0.391	0.404	0.386	0.410	0.434	0.454	0.472	0.492	0.500	0.506	0.508	0.517	0.518	0.504	0.493	0.486	0.479	0.475	0.471	0.470	0.468
24	0.192	0.273	0.364	0.428	0.416	0.472	0.468	0.528	0.543	0.559	0.585	0.599	0.595	0.589	0.553	0.542	0.528	0.519	0.513	0.508	0.505	0.498	0.497	0.494	0.491
25	0.151	0.215	0.241	0.252	0.322	0.433	0.513	0.622	0.703	0.745	0.794	0.830	0.856	0.870	0.878	0.883	0.886	0.888	0.887	0.888	0.889	0.889	0.889	0.890	0.890
26	0.298	0.257	0.268	0.307	0.364	0.370	0.436	0.488	0.500	0.523	0.527	0.534	0.537	0.554	0.557	0.565	0.565	0.570	0.575	0.578	0.582	0.583	0.582	0.580	0.576
27	0.095	0.087	0.136	0.196	0.258	0.297	0.329	0.382	0.413	0.463	0.513	0.553	0.585	0.618	0.648	0.674	0.689	0.693	0.697	0.698	0.699	0.699	0.699	0.699	0.699
28	0.097	0.106	0.121	0.158	0.183	0.247	0.306	0.368	0.432	0.482	0.541	0.595	0.658	0.695	0.720	0.729	0.739	0.744	0.746	0.746	0.746	0.746	0.746	0.746	0.746
29	0.129	0.109	0.160	0.150	0.162	0.198	0.238	0.277	0.328	0.368	0.409	0.446	0.460	0.490	0.515	0.533	0.544	0.546	0.545	0.549	0.551	0.552	0.552	0.553	0.553
30	0.108	0.103	0.119	0.185	0.235	0.292	0.334	0.399	0.463	0.517	0.570	0.613	0.655	0.688	0.710	0.724	0.734	0.744	0.751	0.757	0.760	0.761	0.761	0.761	0.761
31	0.463	0.530	0.559	0.551	0.539	0.528	0.508	0.498	0.501	0.517	0.536	0.551	0.565	0.578	0.591	0.585	0.555	0.521	0.516	0.491	0.466	0.447	0.435	0.436	0.437
32	0.338	0.281	0.275	0.265	0.273	0.279	0.291	0.304	0.321	0.341	0.356	0.371	0.386	0.399	0.409	0.417	0.427	0.446	0.449	0.455	0.472	0.474	0.467	0.463	0.461
33	0.679	0.619	0.507	0.477	0.507	0.511	0.490	0.439	0.453	0.438	0.428	0.421	0.410	0.406	0.389	0.371	0.362	0.363	0.361	0.355	0.357	0.344	0.339	0.334	0.326
34	0.854	0.859	0.658	0.591	0.542	0.568	0.451	0.443	0.419	0.395	0.393	0.390	0.394	0.383	0.361	0.352	0.347	0.338	0.341	0.335	0.328	0.314	0.306	0.303	0.285
35	0.686	0.810	0.943	1.037	1.063	0.756	0.605	0.514	0.506	0.474	0.436	0.441	0.465	0.456	0.461	0.456	0.454	0.443	0.425	0.415	0.403	0.387	0.363	0.350	0.329
36	0.372	0.385	0.405	0.418	0.436	0.455	0.472	0.490	0.509	0.529	0.545	0.561	0.580	0.598	0.618	0.638	0.656	0.684	0.720	0.754	0.781	0.756	0.711	0.683	0.648
37	0.835	0.901	0.627	0.747	0.633	0.661	0.604	0.555	0.552	0.497	0.474	0.518	0.564	0.571	0.597	0.648	0.677	0.664	0.663	0.647	0.613	0.602	0.597	0.588	0.568
38	0.189	0.275	0.400	0.477	0.555	0.624	0.657	0.652	0.638	0.631	0.630	0.626	0.637	0.647	0.653	0.656	0.660	0.660	0.659	0.661	0.662	0.668	0.660	0.661	0.661
39	0.296	0.352	0.485	0.561	0.608	0.619	0.648	0.643	0.646	0.645	0.636	0.633	0.638	0.630	0.623	0.616	0.614	0.614	0.621	0.624	0.625	0.629	0.633	0.638	0.638

Table C.6: Elongation data of the Martian basins

	C1	C2	C3	C4	C5	C6	C7	C8	C9	C10	C11	C12	C13	C14	C15	C16	C17	C18	C19	C20	C21	C22	C23	C24	C25
1	0.585	0.693	0.800	0.894	0.890	0.875	0.872	0.830	0.806	0.814	0.824	0.836	0.809	0.781	0.815	0.821	0.825	0.829	0.832	0.834	0.837	0.838	0.839	0.839	0.839
2	0.789	0.789	0.789	0.789	0.787	0.784	0.778	0.768	0.774	0.774	0.786	0.837	0.861	0.855	0.828	0.828	0.887	0.834	0.773	0.768	0.743	0.762	0.627	0.459	0.789
3	0.719	0.624	0.539	0.625	0.674	0.660	0.689	0.676	0.640	0.572	0.504	0.545	0.574	0.598	0.609	0.618	0.613	0.605	0.601	0.603	0.600	0.594	0.592	0.591	0.591
4	0.684	0.683	0.682	0.680	0.679	0.679	0.682	0.709	0.744	0.742	0.739	0.744	0.749	0.741	0.719	0.750	0.726	0.667	0.658	0.571	0.606	0.690	0.856	0.822	0.679
5	0.533	0.718	0.714	0.757	0.718	0.726	0.703	0.663	0.639	0.567	0.579	0.577	0.584	0.599	0.587	0.582	0.582	0.585	0.592	0.593	0.597	0.599	0.600	0.600	0.601
6	0.571	0.532	0.470	0.620	0.663	0.759	0.782	0.706	0.681	0.669	0.669	0.667	0.700	0.720	0.735	0.741	0.744	0.746	0.747	0.748	0.748	0.748	0.748	0.748	0.748
7	0.783	0.505	0.724	0.799	0.790	0.730	0.762	0.770	0.771	0.749	0.709	0.736	0.740	0.751	0.756	0.759	0.760	0.755	0.752	0.751	0.750	0.746	0.743	0.742	0.740
8	0.633	0.654	0.769	0.746	0.734	0.792	0.842	0.798	0.832	0.861	0.767	0.728	0.704	0.730	0.722	0.721	0.724	0.728	0.730	0.731	0.732	0.734	0.734	0.734	0.734
9	0.578	0.607	0.608	0.647	0.737	0.768	0.761	0.778	0.793	0.811	0.841	0.818	0.818	0.819	0.813	0.793	0.794	0.799	0.803	0.806	0.786	0.787	0.788	0.787	0.786
10	0.527	0.561	0.601	0.661	0.717	0.663	0.604	0.664	0.743	0.779	0.735	0.743	0.767	0.772	0.789	0.798	0.803	0.806	0.805	0.801	0.795	0.796	0.796	0.796	0.796
11	0.829	0.714	0.782	0.765	0.795	0.798	0.782	0.793	0.790	0.790	0.737	0.730	0.718	0.712	0.743	0.720	0.714	0.729	0.667	0.655	0.658	0.625	0.625	0.613	0.599
12	0.630	0.506	0.529	0.688	0.791	0.483	0.571	0.643	0.685	0.721	0.758	0.742	0.773	0.795	0.778	0.776	0.792	0.804	0.792	0.801	0.806	0.809	0.809	0.809	0.809
13	0.604	0.688	0.658	0.670	0.698	0.700	0.719	0.746	0.746	0.743	0.720	0.703	0.690	0.708	0.710	0.695	0.680	0.672	0.670	0.670	0.670	0.671	0.671	0.671	0.671
14	0.475	0.684	0.690	0.675	0.651	0.696	0.701	0.685	0.657	0.661	0.666	0.677	0.688	0.691	0.702	0.717	0.729	0.736	0.738	0.741	0.742	0.742	0.742	0.742	0.742
15	0.857	1.009	1.141	0.921	0.904	0.907	0.891	0.733	0.697	0.655	0.652	0.649	0.655	0.660	0.664	0.668	0.669	0.670	0.670	0.671	0.669	0.670	0.668	0.667	0.668
16	0.547	0.714	0.883	0.945	0.866	0.896	0.829	0.815	0.740	0.754	0.769	0.621	0.629	0.607	0.600	0.605	0.607	0.610	0.608	0.609	0.609	0.609	0.610	0.610	0.610
17	0.648	0.750	0.624	0.775	0.864	0.862	0.848	0.823	0.817	0.826	0.792	0.801	0.828	0.856	0.901	0.820	0.796	0.805	0.810	0.813	0.815	0.816	0.816	0.817	0.817
18	0.898	0.636	0.669	0.721	0.765	0.860	0.805	0.770	0.700	0.755	0.748	0.753	0.756	0.763	0.753	0.752	0.759	0.757	0.759	0.762	0.765	0.767	0.771	0.772	0.772
19	0.659	0.668	0.568	0.595	0.636	0.572	0.554	0.562	0.592	0.555	0.580	0.581	0.553	0.552	0.572	0.608	0.630	0.602	0.612	0.624	0.633	0.639	0.642	0.645	0.646
20	0.765	0.917	0.882	0.929	0.857	0.785	0.750	0.769	0.774	0.816	0.839	0.853	0.852	0.820	0.797	0.768	0.770	0.755	0.715	0.700	0.683	0.670	0.652	0.628	0.627
21	0.847	0.721	0.677	0.688	0.637	0.560	0.610	0.606	0.615	0.626	0.664	0.602	0.625	0.652	0.670	0.675	0.694	0.705	0.720	0.741	0.758	0.769	0.771	0.772	0.772
22	0.736	0.722	0.726	0.767	0.697	0.601	0.478	0.472	0.512	0.524	0.557	0.581	0.607	0.629	0.654	0.668	0.674	0.682	0.674	0.678	0.679	0.676	0.679	0.683	0.684
23	1.007	1.010	0.797	0.706	0.713	0.726	0.733	0.696	0.698	0.716	0.695	0.713	0.748	0.751	0.761	0.769	0.814	0.810	0.798	0.781	0.753	0.733	0.716	0.704	0.704

Table C.7: Lemniscate index data of the terrestrial basins

	C1	C2	C3	C4	C5	C6	C7	C8	C9	C10	C11	C12	C13	C14	C15	C16	C17	C18	C19	C20	C21	C22	C23	C24	C25
1	27.981	13.212	6.259	4.399	3.242	2.565	2.318	2.351	2.456	2.512	2.523	2.555	2.463	2.388	2.345	2.326	2.296	2.294	2.306	2.287	2.280	2.244	2.294	2.290	2.286
2	11.391	8.089	4.247	3.178	2.704	2.613	2.382	2.416	2.399	2.402	2.470	2.492	2.460	2.521	2.578	2.634	2.656	2.649	2.596	2.569	2.559	2.528	2.493	2.459	2.460
3	18.225	7.459	4.513	3.262	2.209	2.042	1.984	1.999	2.001	2.029	2.033	2.095	2.157	2.216	2.338	2.440	2.429	2.415	2.384	2.363	2.341	2.323	2.340	2.345	2.352
4	30.628	16.399	7.313	4.520	3.069	2.383	2.152	2.180	2.239	2.327	2.320	2.311	2.317	2.351	2.390	2.526	2.589	2.608	2.602	2.610	2.588	2.574	2.567	2.582	2.581
5	25.808	19.320	16.494	8.086	3.947	2.780	2.342	1.953	1.817	1.843	1.847	1.862	1.882	1.882	1.881	1.878	1.873	1.871	1.880	1.862	1.857	1.850	1.862	1.855	1.826
6	16.712	16.399	12.219	4.588	2.341	1.922	1.910	1.979	2.004	1.999	1.984	1.968	1.944	1.938	1.948	1.999	2.075	2.161	2.154	2.218	2.253	2.256	2.260	2.304	2.374
7	12.912	17.214	11.224	6.439	3.594	2.764	2.586	2.559	2.613	2.642	2.665	2.629	2.610	2.589	2.576	2.569	2.590	2.572	2.553	2.563	2.633	2.687	2.676	2.716	2.719
8	5.923	6.247	12.389	11.158	12.311	11.120	9.256	8.579	7.620	7.570	7.320	5.917	4.873	4.285	3.960	3.581	3.535	3.399	3.254	3.147	3.120	3.223	3.249	3.287	3.299
9	18.108	16.627	14.345	15.987	16.218	17.773	17.223	14.761	12.154	9.277	7.043	5.509	4.691	4.108	3.669	3.321	3.304	3.182	3.103	3.147	3.161	3.197	3.276	3.373	3.364
10	8.139	6.944	7.599	7.234	6.774	6.040	5.680	5.185	4.446	3.847	3.415	3.837	3.394	3.014	2.695	2.462	2.348	2.454	2.750	2.678	2.824	2.674	2.757	2.778	2.803
11	17.835	12.282	10.519	9.225	8.296	7.612	6.913	5.831	4.318	3.362	2.940	2.854	2.717	2.531	2.150	1.929	1.736	1.596	1.535	1.449	1.457	1.471	1.485	1.509	1.524
12	10.755	11.302	12.053	12.500	11.955	10.654	10.124	8.425	9.899	9.633	8.308	6.628	5.330	4.751	3.952	3.199	2.610	2.382	2.129	1.852	1.666	1.535	1.429	1.388	1.353
13	8.895	12.675	16.495	20.908	24.233	24.261	20.116	19.059	17.442	13.500	9.769	7.700	6.264	5.026	3.867	2.946	2.397	2.142	1.858	1.755	1.574	1.539	1.539	1.522	1.497
14	4.546	10.527	7.809	9.125	8.525	8.668	7.970	7.232	8.901	9.720	11.663	11.833	11.673	10.089	9.598	8.748	6.621	5.953	4.792	3.630	3.086	2.658	2.389	2.275	2.153
15	9.715	16.623	14.554	12.741	10.771	8.971	9.763	8.849	8.130	7.543	7.027	6.927	7.393	7.397	6.544	6.072	5.054	4.743	4.018	3.122	2.423	1.958	1.811	1.674	1.718
16	80.801	79.851	80.737	47.758	25.479	18.625	14.288	10.991	8.749	6.868	5.889	4.785	4.120	3.342	2.728	2.196	1.887	1.603	1.490	1.381	1.324	1.327	1.303	1.292	1.291
17	74.104	118.873	73.324	43.547	24.235	18.500	14.327	10.863	7.544	6.292	5.258	4.520	4.152	3.904	3.572	3.374	3.022	2.706	2.436	2.268	2.203	2.208	2.203	2.202	2.201
18	7.008	6.003	4.974	3.253	2.373	2.043	2.033	1.801	1.841	1.933	2.011	2.199	2.373	2.540	2.636	2.693	2.686	2.749	2.945	3.062	3.111	3.242	3.367	3.352	3.332
19	4.336	3.594	2.723	2.070	2.083	2.183	2.228	2.325	2.326	2.219	2.212	2.229	2.287	2.313	2.329	2.447	2.454	2.500	2.574	2.789	2.938	2.981	3.246	3.729	3.742
20	4.539	5.777	7.259	9.049	10.945	10.252	8.600	7.475	6.775	6.378	5.951	5.411	5.259	5.029	4.959	4.928	4.858	4.868	4.903	4.935	5.070	5.132	5.305	5.993	6.169
21	2.473	2.692	2.574	2.634	2.778	2.937	3.169	3.278	3.454	3.504	3.647	3.549	3.495	3.419	3.331	3.287	3.234	3.191	3.132	3.108	3.082	3.020	2.985	2.976	2.975
22	1.626	1.498	1.475	1.638	1.764	1.850	2.135	2.356	2.448	2.551	2.614	2.675	2.750	2.844	2.837	2.883	2.918	2.994	3.058	3.108	3.164	3.197	3.202	3.225	3.222
23	17.928	8.595	8.903	7.305	6.537	6.134	6.710	5.936	5.312	4.860	4.486	4.129	4.004	3.903	3.871	3.742	3.727	3.937	4.111	4.240	4.351	4.424	4.504	4.528	4.575
24	27.236	13.461	7.564	5.466	5.778	4.497	4.571	3.585	3.394	3.205	2.919	2.788	2.825	2.883	3.269	3.405	3.582	3.716	3.795	3.873	3.928	4.028	4.051	4.099	4.143
25	43.655	21.649	17.287	15.724	9.673	5.336	3.801	2.582	2.024	1.804	1.585	1.451	1.365	1.321	1.298	1.283	1.275	1.269	1.271	1.268	1.266	1.264	1.264	1.264	1.264
26	11.275	15.188	13.902	10.594	7.528	7.291	5.268	4.205	3.996	3.651	3.607	3.513	3.467	3.259	3.223	3.131	3.135	3.081	3.022	2.997	2.949	2.942	2.953	2.968	3.017
27	109.670	132.367	53.955	26.042	15.030	11.302	9.222	6.865	5.858	4.665	3.803	3.270	2.924	2.621	2.382	2.198	2.109	2.084	2.058	2.050	2.048	2.047	2.047	2.047	2.047
28	106.378	89.839	67.817	40.073	29.776	16.350	10.701	7.379	5.360	4.313	3.412	2.821	2.313	2.073	1.929	1.884	1.832	1.809	1.799	1.796	1.795	1.795	1.795	1.795	1.795
29	60.514	84.872	39.043	44.170	37.931	25.539	17.588	13.021	9.307	7.385	5.978	5.038	4.735	4.171	3.771	3.520	3.380	3.354	3.369	3.322	3.289	3.280	3.277	3.274	3.273
30	85.459	93.673	71.063	29.240	18.131	11.732	8.957	6.293	4.671	3.747	3.076	2.659	2.334	2.111	1.983	1.907	1.854	1.808	1.773	1.745	1.732	1.728	1.727	1.727	1.727
31	4.671	3.566	3.200	3.288	3.442	3.591	3.877	4.037	3.977	3.748	3.475	3.297	3.138	2.993	2.859	2.920	3.252	3.679	3.759	4.152	4.597	5.008	5.274	5.258	5.241
32	8.751	12.643	13.261	14.257	13.459	12.841	11.783	10.795	9.727	8.625	7.890	7.250	6.700	6.289	5.970	5.744	5.473	5.016	4.967	4.828	4.488	4.460	4.593	4.671	4.704
33	2.170	2.610	3.895	4.392	3.896	3.824	4.167	5.183	4.869	5.217	5.465	5.634	5.946	6.074	6.613	7.268	7.638	7.597	7.656	7.942	7.841	8.467	8.691	8.953	9.411
34	1.371	1.355	2.307	2.866	3.402	3.102	4.923	5.096	5.709	6.396	6.478	6.584	6.434	6.819	7.665	8.076	8.320	8.776	8.614	8.890	9.294	10.167	10.645	10.899	12.275
35	2.123	1.526	1.124	0.929	0.884	1.751	2.729	3.781	3.906	4.451	5.252	5.148	4.634	4.799	4.715	4.818	4.862	5.102	5.524	5.796	6.171	6.661	7.587	8.177	9.245
36	7.224	6.735	6.107	5.731	5.252	4.826	4.491	4.165	3.853	3.580	3.372	3.182	2.973	2.794	2.616	2.458	2.322	2.135	1.931	1.757	1.641	1.750	1.977	2.145	2.383
37	1.433	1.233	2.543	1.790	2.494	2.285	2.737	3.248	3.277	4.056	4.458	3.729	3.141	3.072	2.808	2.383	2.179	2.269	2.277	2.391	2.661	2.758	2.804	2.895	3.103
38	27.981	13.212	6.259	4.399	3.242	2.565	2.318	2.351	2.456	2.512	2.523	2.555	2.463	2.388	2.345	2.326	2.296	2.294	2.306	2.287	2.280	2.244	2.294	2.290	2.286
39	11.391	8.089	4.247	3.178	2.704	2.613	2.382	2.416	2.399	2.402	2.470	2.492	2.460	2.521	2.578	2.634	2.656	2.649	2.596	2.569	2.559	2.528	2.493	2.459	2.460

Table C.8: Lemniscate index data of the Martian basins

	C1	C2	C3	C4	C5	C6	C7	C8	C9	C10	C11	C12	C13	C14	C15	C16	C17	C18	C19	C20	C21	C22	C23	C24	C25
1	2.919	2.084	1.561	1.251	1.262	1.307	1.314	1.450	1.540	1.508	1.472	1.430	1.527	1.641	1.506	1.485	1.470	1.454	1.445	1.436	1.427	1.423	1.422	1.421	1.420
2	1.606	1.606	1.606	1.608	1.613	1.626	1.651	1.696	1.671	1.669	1.620	1.428	1.350	1.367	1.460	1.457	1.272	1.439	1.674	1.696	1.814	1.721	2.543	4.752	1.606
3	1.932	2.571	3.443	2.558	2.199	2.296	2.105	2.187	2.444	3.062	3.940	3.371	3.032	2.796	2.695	2.617	2.660	2.732	2.770	2.753	2.778	2.834	2.853	2.860	2.864
4	2.139	2.141	2.150	2.162	2.171	2.168	2.152	1.988	1.805	1.818	1.833	1.804	1.782	1.824	1.933	1.779	1.896	2.245	2.308	3.064	2.725	2.103	1.366	1.482	2.170
5	3.518	1.940	1.964	1.746	1.938	1.899	2.023	2.276	2.448	3.108	2.988	3.005	2.927	2.785	2.905	2.951	2.955	2.921	2.857	2.845	2.805	2.786	2.779	2.774	2.769
6	3.066	3.529	4.527	2.598	2.276	1.735	1.634	2.005	2.156	2.233	2.236	2.245	2.040	1.927	1.849	1.820	1.806	1.796	1.791	1.789	1.788	1.787	1.787	1.787	1.787
7	1.633	3.922	1.906	1.566	1.604	1.877	1.721	1.686	1.681	1.782	1.990	1.845	1.828	1.774	1.748	1.736	1.730	1.753	1.767	1.771	1.780	1.797	1.809	1.817	1.825
8	2.497	2.339	1.691	1.797	1.854	1.595	1.411	1.570	1.446	1.349	1.700	1.885	2.018	1.878	1.919	1.924	1.908	1.885	1.879	1.872	1.865	1.858	1.858	1.858	1.858
9	2.989	2.714	2.704	2.392	1.839	1.694	1.728	1.653	1.589	1.522	1.415	1.496	1.494	1.492	1.514	1.592	1.586	1.566	1.550	1.538	1.617	1.613	1.612	1.615	1.617
10	3.598	3.174	2.767	2.291	1.947	2.272	2.739	2.267	1.812	1.648	1.851	1.813	1.698	1.676	1.605	1.570	1.552	1.539	1.543	1.558	1.581	1.580	1.579	1.579	1.580
11	1.456	1.959	1.633	1.710	1.580	1.571	1.636	1.591	1.601	1.604	1.843	1.875	1.942	1.972	1.813	1.929	1.960	1.882	2.246	2.331	2.310	2.558	2.562	2.663	2.784
12	2.522	3.900	3.568	2.114	1.600	4.281	3.070	2.422	2.133	1.923	1.738	1.817	1.674	1.581	1.652	1.661	1.595	1.549	1.593	1.558	1.539	1.530	1.529	1.528	1.528
13	2.745	2.115	2.310	2.228	2.052	2.038	1.936	1.797	1.795	1.813	1.931	2.023	2.103	1.994	1.982	2.068	2.164	2.217	2.231	2.225	2.225	2.222	2.220	2.219	2.219
14	4.426	2.135	2.100	2.197	2.363	2.065	2.035	2.132	2.314	2.290	2.252	2.181	2.114	2.093	2.027	1.944	1.884	1.847	1.836	1.822	1.816	1.816	1.815	1.815	1.815
15	1.360	0.982	0.768	1.179	1.223	1.217	1.259	1.861	2.056	2.328	2.355	2.371	2.333	2.296	2.266	2.241	2.231	2.227	2.226	2.222	2.233	2.226	2.238	2.246	2.244
16	3.343	1.961	1.282	1.120	1.335	1.246	1.456	1.507	1.826	1.759	1.689	2.593	2.524	2.715	2.780	2.735	2.717	2.690	2.701	2.700	2.695	2.694	2.692	2.691	2.690
17	2.379	1.777	2.567	1.664	1.340	1.344	1.392	1.475	1.498	1.465	1.596	1.557	1.460	1.363	1.232	1.488	1.577	1.545	1.524	1.514	1.505	1.502	1.500	1.499	1.499
18	1.240	2.474	2.237	1.924	1.710	1.352	1.543	1.687	2.040	1.754	1.790	1.765	1.747	1.718	1.764	1.769	1.737	1.746	1.734	1.721	1.710	1.698	1.684	1.676	1.676
19	2.300	2.241	3.097	2.824	2.470	3.056	3.260	3.163	2.854	3.252	2.973	2.961	3.266	3.285	3.062	2.705	2.522	2.763	2.674	2.564	2.496	2.449	2.425	2.403	2.393
20	1.709	1.190	1.287	1.159	1.363	1.624	1.778	1.693	1.669	1.502	1.419	1.375	1.378	1.488	1.576	1.696	1.689	1.755	1.956	2.041	2.141	2.229	2.352	2.535	2.544
21	1.395	1.922	2.181	2.113	2.467	3.185	2.689	2.723	2.642	2.554	2.265	2.764	2.562	2.349	2.225	2.194	2.078	2.009	1.930	1.819	1.739	1.693	1.682	1.677	1.676
22	1.846	1.917	1.897	1.702	2.060	2.765	4.380	4.493	3.808	3.642	3.219	2.967	2.714	2.528	2.341	2.244	2.204	2.153	2.200	2.175	2.169	2.191	2.167	2.142	2.138
23	0.987	0.980	1.575	2.007	1.967	1.898	1.860	2.065	2.054	1.949	2.071	1.970	1.789	1.774	1.727	1.692	1.507	1.526	1.570	1.639	1.765	1.859	1.951	2.018	2.018

Table C.9: Lemniscate ratio data of the terrestrial basins

	C1	C2	C3	C4	C5	C6	C7	C8	C9	C10	C11	C12	C13	C14	C15	C16	C17	C18	C19	C20	C21	C22	C23	C24	C25
1	0.826	0.498	0.370	0.356	0.371	0.467	0.538	0.598	0.583	0.552	0.514	0.515	0.571	0.620	0.626	0.615	0.666	0.663	0.677	0.685	0.726	0.784	0.803	0.804	0.800
2	0.550	0.556	0.499	0.468	0.505	0.584	0.653	0.649	0.673	0.701	0.686	0.670	0.697	0.695	0.673	0.663	0.693	0.725	0.738	0.743	0.762	0.802	0.821	0.866	0.867
3	0.895	0.852	0.683	0.503	0.603	0.708	0.716	0.706	0.721	0.747	0.764	0.757	0.756	0.742	0.716	0.724	0.710	0.683	0.752	0.770	0.816	0.853	0.854	0.850	0.855
4	0.726	0.530	0.443	0.487	0.490	0.502	0.582	0.693	0.713	0.714	0.734	0.766	0.779	0.774	0.769	0.743	0.717	0.703	0.747	0.770	0.815	0.822	0.839	0.834	0.833
5	0.756	0.590	0.495	0.370	0.362	0.395	0.423	0.444	0.556	0.623	0.633	0.663	0.682	0.697	0.713	0.719	0.721	0.703	0.681	0.650	0.680	0.716	0.724	0.758	0.793
6	0.694	0.607	0.510	0.409	0.436	0.559	0.716	0.718	0.715	0.760	0.791	0.796	0.799	0.788	0.793	0.767	0.729	0.706	0.815	0.843	0.842	0.858	0.873	0.867	0.895
7	0.629	0.640	0.485	0.419	0.430	0.500	0.583	0.613	0.619	0.631	0.641	0.659	0.653	0.669	0.673	0.679	0.685	0.665	0.665	0.677	0.695	0.721	0.748	0.778	0.788
8	0.669	0.559	0.563	0.555	0.544	0.480	0.411	0.384	0.380	0.382	0.345	0.341	0.336	0.357	0.391	0.424	0.470	0.515	0.559	0.634	0.700	0.708	0.711	0.757	0.754
9	0.520	0.534	0.531	0.508	0.515	0.534	0.533	0.494	0.442	0.456	0.445	0.496	0.490	0.496	0.495	0.521	0.504	0.499	0.548	0.604	0.692	0.785	0.837	0.880	0.885
10	0.502	0.443	0.364	0.328	0.335	0.304	0.315	0.298	0.302	0.324	0.356	0.393	0.430	0.439	0.474	0.488	0.490	0.530	0.585	0.612	0.658	0.694	0.714	0.751	0.757
11	0.384	0.386	0.390	0.395	0.404	0.403	0.385	0.336	0.289	0.283	0.296	0.289	0.297	0.280	0.303	0.353	0.355	0.398	0.446	0.596	0.625	0.632	0.630	0.631	0.631
12	0.786	0.731	0.653	0.706	0.631	0.569	0.530	0.500	0.454	0.428	0.366	0.335	0.325	0.317	0.287	0.312	0.328	0.348	0.429	0.514	0.587	0.643	0.688	0.695	0.746
13	0.772	0.750	0.765	0.807	0.796	0.776	0.677	0.621	0.570	0.472	0.388	0.319	0.317	0.308	0.286	0.255	0.250	0.253	0.273	0.332	0.436	0.526	0.604	0.631	0.659
14	0.949	1.024	0.949	0.940	0.990	0.970	0.974	0.970	0.959	0.956	0.974	0.926	0.850	0.597	0.516	0.504	0.454	0.420	0.433	0.465	0.499	0.676	0.756	0.821	0.823
15	0.893	0.878	0.859	0.825	0.804	0.735	0.738	0.711	0.696	0.677	0.629	0.619	0.614	0.569	0.480	0.380	0.295	0.270	0.272	0.293	0.330	0.411	0.588	0.736	0.768
16	0.311	0.235	0.221	0.196	0.176	0.178	0.166	0.152	0.144	0.139	0.137	0.139	0.147	0.150	0.161	0.204	0.244	0.253	0.304	0.387	0.465	0.480	0.528	0.558	0.573
17	0.275	0.241	0.216	0.179	0.171	0.163	0.145	0.133	0.131	0.138	0.141	0.153	0.176	0.192	0.219	0.245	0.275	0.317	0.358	0.454	0.550	0.626	0.642	0.650	0.652
18	0.773	0.673	0.510	0.539	0.576	0.535	0.544	0.554	0.578	0.604	0.615	0.591	0.571	0.539	0.546	0.560	0.589	0.631	0.643	0.644	0.653	0.678	0.705	0.725	0.725
19	0.634	0.631	0.583	0.555	0.597	0.583	0.581	0.564	0.550	0.578	0.592	0.607	0.642	0.665	0.684	0.706	0.720	0.733	0.746	0.750	0.713	0.722	0.731	0.693	0.743
20	0.773	0.848	0.868	0.854	0.843	0.805	0.786	0.761	0.760	0.740	0.741	0.716	0.734	0.753	0.785	0.785	0.788	0.801	0.795	0.806	0.811	0.780	0.783	0.786	0.832
21	0.659	0.736	0.600	0.618	0.560	0.589	0.561	0.631	0.634	0.617	0.629	0.671	0.655	0.707	0.664	0.673	0.680	0.693	0.691	0.741	0.805	0.806	0.821	0.844	0.845
22	0.461	0.547	0.618	0.636	0.585	0.605	0.611	0.571	0.611	0.633	0.686	0.659	0.676	0.733	0.732	0.779	0.745	0.760	0.790	0.806	0.815	0.788	0.805	0.833	0.845
23	0.731	0.666	0.571	0.558	0.553	0.501	0.475	0.444	0.380	0.361	0.382	0.434	0.447	0.460	0.515	0.566	0.635	0.703	0.718	0.743	0.778	0.780	0.781	0.781	0.780
24	0.849	0.540	0.482	0.489	0.449	0.425	0.406	0.368	0.376	0.419	0.482	0.511	0.591	0.692	0.756	0.749	0.734	0.811	0.846	0.854	0.856	0.856	0.855	0.854	0.851
25	0.925	0.838	0.703	0.539	0.455	0.414	0.478	0.433	0.574	0.628	0.656	0.657	0.659	0.677	0.688	0.701	0.709	0.715	0.725	0.730	0.744	0.745	0.749	0.748	0.747
26	0.938	0.887	0.740	0.664	0.622	0.646	0.655	0.617	0.588	0.605	0.638	0.607	0.565	0.538	0.560	0.586	0.596	0.615	0.634	0.648	0.696	0.738	0.770	0.793	0.814
27	0.486	0.430	0.333	0.294	0.225	0.192	0.178	0.153	0.139	0.133	0.138	0.143	0.160	0.184	0.235	0.337	0.448	0.561	0.617	0.654	0.653	0.665	0.667	0.668	0.668
28	0.637	0.459	0.388	0.304	0.260	0.210	0.191	0.166	0.160	0.160	0.167	0.210	0.276	0.374	0.431	0.532	0.609	0.663	0.680	0.665	0.674	0.675	0.678	0.678	0.679
29	0.880	0.804	0.733	0.691	0.640	0.544	0.468	0.463	0.457	0.470	0.505	0.517	0.521	0.573	0.631	0.647	0.712	0.750	0.812	0.819	0.829	0.833	0.834	0.844	0.851
30	0.794	0.652	0.581	0.493	0.424	0.376	0.296	0.271	0.260	0.278	0.289	0.302	0.345	0.397	0.452	0.508	0.569	0.636	0.676	0.744	0.761	0.770	0.770	0.774	0.775
31	0.580	0.577	0.626	0.666	0.675	0.683	0.697	0.687	0.695	0.694	0.719	0.735	0.754	0.778	0.782	0.793	0.791	0.812	0.809	0.813	0.808	0.841	0.848	0.849	0.845
32	0.911	0.952	0.950	0.909	0.815	0.813	0.792	0.794	0.776	0.772	0.801	0.804	0.806	0.821	0.846	0.856	0.864	0.794	0.744	0.709	0.762	0.756	0.763	0.783	0.791
33	0.703	0.895	0.966	0.971	0.933	0.989	0.953	0.868	0.890	0.952	0.983	0.984	0.971	0.977	0.962	0.946	0.965	0.956	0.958	0.937	0.952	0.941	0.967	0.988	0.996
34	0.871	0.886	0.750	0.894	0.782	0.934	0.953	0.958	0.949	0.966	0.934	0.906	0.943	0.958	0.972	0.973	0.985	0.950	0.962	0.960	0.970	0.969	0.977	0.991	0.998
35	0.768	0.811	0.836	0.836	0.795	0.795	0.851	0.857	0.869	0.866	0.914	0.907	0.828	0.805	0.825	0.833	0.826	0.866	0.922	0.939	0.960	0.979	0.990	0.997	0.995
36	0.669	0.702	0.729	0.752	0.764	0.789	0.808	0.821	0.834	0.844	0.848	0.831	0.832	0.787	0.799	0.776	0.719	0.720	0.750	0.760	0.749	0.764	0.785	0.800	0.804
37	0.849	0.785	0.782	0.798	0.668	0.723	0.868	0.861	0.868	0.844	0.839	0.829	0.849	0.823	0.835	0.817	0.780	0.782	0.824	0.870	0.852	0.919	0.952	0.983	0.990
38	0.826	0.498	0.370	0.356	0.371	0.467	0.538	0.598	0.583	0.552	0.514	0.515	0.571	0.620	0.626	0.615	0.666	0.663	0.677	0.685	0.726	0.784	0.803	0.804	0.800
39	0.550	0.556	0.499	0.468	0.505	0.584	0.653	0.649	0.673	0.701	0.686	0.670	0.697	0.695	0.673	0.663	0.693	0.725	0.738	0.743	0.762	0.802	0.821	0.866	0.867

Table C.10: Lemniscate ratio data of the Martian basins

	C1	C2	C3	C4	C5	C6	C7	C8	C9	C10	C11	C12	C13	C14	C15	C16	C17	C18	C19	C20	C21	C22	C23	C24	C25
1	0.740	0.583	0.631	0.543	0.521	0.464	0.500	0.494	0.501	0.588	0.640	0.616	0.579	0.561	0.684	0.674	0.671	0.673	0.677	0.671	0.672	0.682	0.685	0.689	0.691
2	0.559	0.558	0.559	0.552	0.543	0.521	0.502	0.491	0.474	0.465	0.438	0.430	0.402	0.428	0.418	0.425	0.377	0.307	0.328	0.337	0.316	0.352	0.275	0.430	0.556
3	0.668	0.638	0.658	0.637	0.596	0.483	0.458	0.468	0.496	0.434	0.408	0.462	0.509	0.508	0.544	0.622	0.634	0.666	0.690	0.712	0.724	0.727	0.727	0.732	0.735
4	0.660	0.656	0.655	0.640	0.642	0.622	0.591	0.593	0.580	0.559	0.531	0.573	0.596	0.551	0.544	0.513	0.445	0.458	0.458	0.398	0.363	0.590	0.729	0.721	0.660
5	0.517	0.491	0.477	0.667	0.670	0.623	0.536	0.508	0.541	0.534	0.618	0.561	0.539	0.542	0.510	0.559	0.537	0.569	0.564	0.618	0.639	0.645	0.652	0.657	0.656
6	0.556	0.377	0.388	0.326	0.382	0.364	0.345	0.385	0.337	0.336	0.262	0.300	0.373	0.421	0.506	0.557	0.590	0.594	0.597	0.603	0.602	0.602	0.600	0.600	0.601
7	0.649	0.348	0.280	0.347	0.464	0.495	0.546	0.550	0.508	0.582	0.544	0.520	0.622	0.616	0.710	0.713	0.727	0.729	0.739	0.737	0.740	0.740	0.741	0.741	0.743
8	0.520	0.531	0.567	0.414	0.369	0.429	0.465	0.400	0.457	0.513	0.362	0.440	0.485	0.506	0.555	0.573	0.567	0.582	0.599	0.593	0.594	0.597	0.598	0.600	0.600
9	0.627	0.517	0.505	0.507	0.463	0.604	0.641	0.697	0.631	0.576	0.674	0.679	0.667	0.738	0.777	0.786	0.783	0.789	0.769	0.764	0.775	0.768	0.758	0.760	0.759
10	0.701	0.576	0.584	0.424	0.579	0.515	0.412	0.355	0.346	0.413	0.347	0.416	0.399	0.459	0.572	0.627	0.622	0.588	0.650	0.648	0.667	0.671	0.673	0.672	0.676
11	0.870	0.885	0.920	0.930	0.911	0.895	0.900	0.869	0.887	0.877	0.765	0.809	0.823	0.816	0.778	0.815	0.829	0.817	0.828	0.776	0.693	0.795	0.828	0.859	0.875
12	0.486	0.456	0.383	0.335	0.306	0.260	0.264	0.281	0.339	0.361	0.334	0.271	0.280	0.307	0.357	0.385	0.432	0.471	0.499	0.504	0.595	0.614	0.627	0.633	0.634
13	0.480	0.475	0.547	0.507	0.499	0.570	0.503	0.469	0.500	0.493	0.487	0.496	0.470	0.578	0.648	0.634	0.643	0.663	0.704	0.711	0.708	0.715	0.714	0.718	0.719
14	0.641	0.554	0.691	0.728	0.699	0.469	0.458	0.647	0.623	0.662	0.687	0.679	0.668	0.630	0.634	0.655	0.691	0.714	0.729	0.719	0.720	0.718	0.716	0.714	0.713
15	0.601	0.601	0.559	0.559	0.524	0.701	0.653	0.618	0.618	0.691	0.629	0.680	0.683	0.664	0.683	0.673	0.675	0.675	0.675	0.676	0.676	0.677	0.679	0.680	0.689
16	0.286	0.369	0.400	0.483	0.455	0.511	0.544	0.502	0.570	0.624	0.630	0.541	0.576	0.595	0.616	0.646	0.658	0.634	0.649	0.651	0.650	0.649	0.650	0.652	0.653
17	0.468	0.542	0.387	0.348	0.427	0.380	0.480	0.479	0.436	0.466	0.439	0.457	0.445	0.459	0.428	0.425	0.529	0.567	0.682	0.693	0.701	0.706	0.706	0.705	0.706
18	0.757	0.664	0.561	0.405	0.412	0.539	0.547	0.503	0.433	0.415	0.569	0.615	0.577	0.520	0.518	0.552	0.601	0.646	0.658	0.662	0.659	0.642	0.631	0.646	0.645
19	0.910	0.661	0.629	0.645	0.637	0.651	0.673	0.634	0.609	0.630	0.681	0.577	0.567	0.614	0.618	0.555	0.595	0.664	0.716	0.736	0.763	0.746	0.738	0.729	0.726
20	0.738	0.547	0.510	0.506	0.539	0.580	0.641	0.572	0.594	0.610	0.613	0.701	0.722	0.750	0.776	0.755	0.800	0.800	0.771	0.822	0.809	0.814	0.819	0.818	0.823
21	0.651	0.766	0.693	0.538	0.512	0.494	0.491	0.568	0.446	0.402	0.398	0.407	0.472	0.480	0.493	0.483	0.451	0.455	0.470	0.549	0.571	0.640	0.683	0.693	0.700
22	0.860	0.808	0.834	0.839	0.826	0.816	0.748	0.719	0.700	0.741	0.750	0.741	0.705	0.690	0.645	0.650	0.679	0.684	0.663	0.677	0.680	0.668	0.654	0.658	0.662
23	0.834	0.834	0.834	0.814	0.786	0.868	0.835	0.777	0.743	0.818	0.808	0.789	0.773	0.762	0.785	0.804	0.706	0.800	0.830	0.838	0.844	0.836	0.834	0.833	0.839